

**Characterization of the long non-coding RNA encoded
by the *At4g14548* gene from *Arabidopsis thaliana***

Dissertation

zur Erlangung des
Doktorgrades der Naturwissenschaften (Dr. rer. nat.)
der
Naturwissenschaftlichen Fakultät I – Biowissenschaften –
der Martin-Luther-Universität
Halle-Wittenberg,

vorgelegt
von Frau Susanne Engelmann (M. Sc.)
geb. am 16.05.1990 in Karl-Marx-Stadt

Gutachter:
Prof. Dr. Sven-Erik Behrens
Prof. Dr. Steffen Abel
Prof. Dr. Dorothee Staiger

Tag der Verteidigung: Halle (Saale), 21.01.2022

Table of contents

Table of contents	I
1 Abbreviations	V
2 Abstract.....	1
3 Introduction	2
3.1 Types and functions of RNA molecules.....	2
3.2 Properties and classification of long non-coding RNAs.....	2
3.3 lncRNAs as ‘riboregulators’	4
3.4 Role of lncRNAs in plant stress response.....	6
3.5 lncNATs in <i>A. thaliana</i>	8
3.6 Auxin signaling pathway.....	9
3.7 The <i>AUX/IAA</i> multigene family	10
3.8 <i>AUXIN/INDOLE-3-ACETIC ACID 14 (IAA14)</i>	12
3.9 Regulation of <i>IAA14</i> expression and <i>IAA14</i> stability	14
4 Objectives	17
5 Materials and methods.....	20
5.1 Materials	20
5.1.1 Chemicals and supplies.....	20
5.1.2 Bacterial strains and plasmid vectors	20
5.2 Culture media.....	21
5.3 Plant materials and growth conditions	22
5.3.1 Plant lines.....	22
5.3.2 Plant cultivation	22
5.3.3 Arabidopsis transformation by floral dip method	22
5.3.4 Selection of transformed Arabidopsis plants.....	23
5.3.5 <i>N. benthamiana</i> infiltration with <i>A. tumefaciens</i>	23
5.3.6 Gene response to different treatments and stresses	23

5.3.6.1	Salt treatment.....	24
5.3.6.2	High light stress.....	24
5.3.6.3	Deoxynivalenol treatment.....	24
5.3.6.4	Auxin treatment.....	24
5.4	Bacterial general protocols.....	24
5.4.1	<i>E. coli</i> and <i>A. tumefaciens</i> cultivation.....	24
5.4.2	Transformation of chemically competent <i>E. coli</i>	25
5.4.3	Transformation of electrocompetent <i>A. tumefaciens</i>	25
5.4.4	Plasmid DNA isolation from <i>E. coli</i>	25
5.4.5	Colony PCR.....	25
5.5	Molecular biology methods.....	26
5.5.1	RNA extraction.....	26
5.5.2	Nuclear RNA extraction.....	26
5.5.3	RNA and DNA concentration measurement.....	27
5.5.4	Reverse transcription Polymerase chain reaction (RT-PCR).....	27
5.5.5	qRT-PCR.....	28
5.5.6	Gel electrophoresis of DNA molecules.....	29
5.5.7	DNA extraction from gels.....	29
5.5.8	Gateway cloning.....	30
5.5.9	Golden Gate assembly.....	30
5.5.10	CRISPR/Cas9 genome editing.....	31
5.5.11	DAPI staining.....	33
5.6	Biochemical methods.....	33
5.6.1	RNA stability measurements.....	33
5.6.2	Radioactive <i>in vitro</i> transcription.....	33
5.6.3	RNase protection assay.....	34
5.6.4	Circular RACE.....	34
5.6.4.1	5'RACE.....	34
5.6.4.2	3'RACE.....	35
5.6.5	Northern Blot.....	35

5.6.6	Production of capped and polyadenylated transcripts.....	36
5.6.7	Silver staining of nucleic acids.....	37
6	Results.....	38
6.1	Molecular analysis of the lncRNA <i>NAT-IAA14</i>	38
6.1.1	Determination of <i>NAT-IAA14</i> 5' and 3'ends.....	38
6.1.1.1	<i>NAT-IAA14</i> detection by RNase protection assay.....	38
6.1.1.2	<i>NAT-IAA14</i> RNA starts 15 nt downstream of the reported 5' end.....	40
6.1.2	<i>NAT-IAA14</i> is a stable transcript.....	42
6.1.3	<i>NAT-IAA14</i> is localized in the cytosol.....	43
6.1.4	<i>NAT-IAA14</i> expression is reduced by cycloheximide treatment.....	44
6.2	<i>NAT-IAA14</i> and <i>IAA14</i> transcript levels undergo changes during plant development.....	46
6.3	<i>NAT-IAA14</i> expression shows a variable response to light.....	47
6.4	<i>NAT-IAA14</i> transcript levels remain unaffected in response to auxin.....	48
6.5	<i>NAT-IAA14</i> and <i>IAA14</i> can be transiently co-expressed in the same <i>N. benthamiana</i> cell.....	49
6.6	Induction of <i>NAT-IAA14</i> transcription has no influence on <i>IAA14</i> expression in <i>N. benthamiana</i>	50
6.7	<i>NAT-IAA14</i> and <i>IAA14</i> response to different abiotic and biotic stresses.....	53
6.8	Effects of <i>NAT-IAA14</i> expression alteration in Col-0 plants.....	54
6.8.1	<i>NAT-IAA14</i> overexpression slightly alters <i>IAA14</i> transcript levels.....	54
6.8.2	<i>NAT-IAA14</i> knockdown slightly reduces <i>IAA14</i> transcript levels.....	57
6.8.2.1	<i>NAT-IAA14</i> knockdown in DNA-insertion lines.....	57
6.8.2.2	<i>NAT-IAA14</i> knockdown by artificial mircoRNAs.....	58
6.8.3	<i>IAA14</i> levels are not affected by <i>NAT-IAA14</i> knockout.....	60
6.9	Alteration of <i>IAA14</i> levels results in changes of the <i>NAT-IAA14</i> transcript abundance.....	63
6.9.1	Overexpression of <i>IAA14</i> slightly reduces <i>NAT-IAA14</i> levels and increases root growth.....	63
6.9.2	<i>NAT-IAA14</i> expression alteration in CRISPR/Cas9-edited <i>IAA14</i> lines.....	65

6.10	<i>NAT-IAA14</i> decreases the <i>in vitro</i> translation of the annotated <i>IAA14</i> transcript.....	67
7	Discussion.....	70
7.1	<i>NAT-IAA14</i> is autonomously expressed in <i>A. thaliana</i>	70
7.2	<i>NAT-IAA14</i> expression is modulated by external stimuli.....	72
7.3	<i>NAT-IAA14</i> and <i>IAA14</i> regulatory network	73
7.4	Potential regulatory mechanism of <i>NAT-IAA14</i> on <i>IAA14</i> translation.....	76
7.5	Concluding remarks	77
8	References.....	80
9	List of figures.....	88
10	List of tables.....	91
11	Appendix	92
11.1	Supplementary Figures	92
11.2	Supplementary Tables	115
12	Acknowledgements	118
13	Curriculum vitae	119
14	Statutory Declaration.....	120

1 Abbreviations

aa	amino acid
<i>ABA</i>	<i>abscisic acid</i>
AFB	AUXIN-SIGNALING F-BOX
amiRNA	artificial mircoRNA
<i>amiRNA</i>	<i>artifical microRNA</i>
AP2	APETALA 2
<i>APX2</i>	<i>ASCORBATE PEROXIDASE 2</i>
ARF	AUXIN RESPONSE FACTOR
<i>asCBF1</i>	<i>antisense CBF1</i>
ASCO-lncRNA	<i>AS competitor long noncoding RNA</i>
<i>asDOG1</i>	<i>antisense DOG1</i>
<i>asHSFB2a</i>	<i>antisense HSFB2a</i>
attL	<i>attachment</i> site left
attR	<i>attachment</i> site right
AUX/IAA	AUXIN/INDOLE-3-ACETIC ACID
<i>AuxRE</i>	Auxin-Responsive Element
<i>axr2</i>	<i>auxin-resistant 2</i>
<i>axr3</i>	<i>auxin-resistant 3</i>
<i>axr5</i>	<i>auxin-resistant 5</i>
<i>bdl</i>	<i>bodenlos</i>
BY-2	Bright Yellow-2
CaMV	Cauliflower mosaic virus
<i>CBF1</i>	<i>C-REPEAT/DRE BINDING FACTOR 1</i>
<i>CCA1</i>	<i>CIRCADIAN CLOCK ASSOCIATED 1</i>
<i>CDF5</i>	<i>CYCLING DOF FACTOR 5 CDF5</i>
cDNA	complementary DNA
ceRNA	competitive endogenous RNA
circRNA	circular RNA
<i>CKM</i>	Mediator's dissociable CDK8 kinase module
Col-0	<i>Columbia 0</i>
<i>COLDAIR</i>	<i>COLD ASSISTED INTRONIC NONCODING RNA</i>
<i>COLDWRAP</i>	<i>COLD OF WINTER-INDUCED NONCODING RNA FROM THE PROMOTER</i>

cordycepin	3'-deoxyadenosine
CRISPR/Cas9	clustered regularly interspaced short palindromic repeats associated Protein9
CstF64	CLEAVAGE STIMULATING FACTOR 64
CstF77	CLEAVAGE STIMULATING FACTOR 77
C _t	threshold cycle
dag	day after germination
<i>DAO2</i>	<i>DIOXYGENASE FOR AUXIN OXIDATION 2</i>
<i>DAPI</i>	4',6-Diamidin-2-phenylindol
DGDG	digalactosyldiacylglycerol
Di19-3	DROUGHT-INDUCED-19
DMSO	diemethylsulfat
<i>DOG1</i>	<i>DELAY OF GERMINATION 1</i>
DON	deoxynivalenol
dpi	day post infection
DREB	DEHYDRATION RESPONSIVE ELEMENT-BINDING PROTEIN
dsRNA	double-stranded RNA
<i>DTT</i>	dithiothreitol
<i>E. coli</i>	<i>Escherichia coli</i>
<i>EIF4A1</i>	<i>EUKARYOTIC TRANSLATION INITIATION FACTOR 4A-I</i>
<i>ELENA1</i>	<i>ELF18-INDUCED LONG-NONCODING RNA1</i>
<i>ENOD40</i>	<i>EARLY NODULIN 40</i>
<i>Expansin L1</i>	<i>EXPANSIN-LIKE1</i>
<i>FLC</i>	<i>FLOWERING LOCUS C</i>
<i>FLORE</i>	<i>CDF5 LONG NONCODING RNA</i>
Fluc	firefly luciferase
<i>GAPDH</i>	<i>GLYCERALDEHYDE 3-PHOSPHATE DEHYDROGENASE</i>
<i>GFP</i>	<i>GREEN FLUORESCENT PROTEIN</i>
gRNA	guide RNA
GUS	<i>β-glucuronidase</i>
HAR	hypocotyl adventitious root
HRB	high red and blue light
<i>HSFB2a</i>	<i>HEAT SHOCK TRANSCRIPTION FACTOR B2A</i>
HY5	LONG HYPOCOTYL 5
IAA	indole-3-acetic acid
<i>IAA14</i>	<i>AUXIN/INDOLE-3-ACETIC ACID 14</i>

<i>IPS1</i>	<i>Induced by Phosphate Starvation 1</i>
<i>LAIR</i>	<i>LRK Antisense Intergenic RNA</i>
<i>LB</i>	lysogeny broth
lincRNA	long intergenic non-coding RNA
lncNAT	long non-coding natural antisense transcripts
lncRNA	long non-coding RNA
<i>LRK</i>	<i>LEUCINE-RICH REPEAT RECEPTOR KINASE</i>
<i>MAF4</i>	<i>MADS AFFECTING FLOWERING 4</i>
MED19a	Mediator subunit 19a
<i>MES</i>	2-(N-morpholino)ethanesulfonic acid
miRNA	microRNA
mRNA	messenger RNA
MS	Murashige and Skoog
<i>msg2</i>	<i>massugu2</i>
NAA	1-naphthaleneacetic acid
NASC	Nottingham Arabidopsis Stock Centre
<i>NAT-IAA14</i>	<i>natural antisense transcript of IAA14</i>
nat-siRNA	natural antisense siRNA
Nluc	NanoLuc luciferase
NMD	nonsense mediated decay
<i>npc521</i>	<i>non-protein-coding RNA 521</i>
<i>npc83</i>	<i>non-protein-coding RNA 83</i>
NSR	nuclear speckle RNA-binding protein
<i>OLE1</i>	<i>OLEOSIN 1</i>
<i>PAGE</i>	polyacrylamide gel electrophoresis
Pgs	gene-specific primer
<i>PHO2</i>	<i>PHOSPHATE 2</i>
PHYB	Phytochrome B
PKL	PICKLE
poly(A)	polyadenylation
pORF	potential open-reading frame
PRC2	polycomb repressive complex 2
PU.1	transcription factor
qRT-PCR	quantitative real-time PCR
qRT-PCR	quantitative real-time PCR
RACE	rapid amplification of cDNA ends

RBP	RNA-binding protein
RBP1	RETINOL BINDING PROTEIN 1
RdDM	RNA directed DNA methylation
RISC	RNA-induced silencing complex
RNA pol II	DNA-dependent RNA polymerase II
RPA	RNase protection assay
<i>RPS5A</i>	<i>RIBOSOMAL PROTEIN 5A</i>
RRGD	rapid recovery gene downregulation
rRNA	ribosomal RNA
RT	room temperature
RT-PCR	<i>reverse transcription polymerase chain reaction</i>
SC	ARABIDOPSIS SKP1 HOMOLOGUE (ASK1) and CULLIN 1
<i>shy1</i>	<i>suppressor of hy2 1</i>
<i>shy2</i>	<i>suppressor of hy2 2</i>
siRNA	small interfering RNA
<i>slr-1</i>	<i>solitary-root-1</i>
smFISH	single-molecule fluorescence <i>in situ</i> hybridization
<i>SMG7</i>	<i>SUPPRESSOR OF MORPHOLOGICAL DEFECTS ON GENITALIA PROTEIN 7</i>
SOC	Super Optimal broth with Catabolite repression
sORF	short open-reading frame
SQDG	sulfoquinovosyldiacylglycerol
SVK	SVALKA
TAIR10	The Arabidopsis Information Resource 10
TAP	tobacco acid pyrophosphatase
TIR1	TRANSPORT INHIBITOR RESPONSE 1
<i>TOC1</i>	<i>TIMING OF CAB EXPRESSION 1</i>
TPL	TOPLESS
TSS	transcriptional start site
TYLCV	Tomato yellow leaf curl virus
Ub	ubiquitylation
uORF	upstream open-reading frame
<i>upf1-1</i>	<i>upstream frame shift protein 1-1</i>
<i>upf3-1</i>	<i>upstream frame shift protein 3-1</i>
UTR	untranslated region
UV-light	ultraviolet light

WDR5a	WD40 containing repeat 5a
<i>X-Gal</i>	5-bromo-4-chloro-3-indolyl- β -D-galactopyranoside

2 Abstract

Since their discovery by the first genome-wide studies in the early 2000s, the functional relevance of long non-coding RNAs (lncRNAs) has been debated. They were initially classified as 'transcriptional noise' without biological function, but research in the last decade has shown that they are important modulators of gene expression in eukaryotes. In plants, lncRNAs are involved in the regulation of a variety of biological processes, including flowering and germination time, root development, and response to abiotic and biotic stress. This thesis focuses on a lncRNA referred to as *NAT-IAA14* (*natural antisense transcript of IAA14*) encoded by the *At4g14548* gene from the model plant *Arabidopsis thaliana*. *NAT-IAA14* belongs to a particular subtype of lncRNAs, the long non-coding natural antisense transcripts (lncNATs), which are transcribed from genes located on the opposite DNA strand of a protein-coding gene. *At4g14548* is in close proximity to the *AUXIN/INDOLE-3-ACETIC ACID 14* (*IAA14*) gene, which encodes the IAA14 protein that regulates lateral root formation in response to auxin. IAA14 achieves its function by interacting with two auxin response factors, ARF7 and ARF19. Phenotypic analysis of transgenic *Arabidopsis* variants differing in the IAA14 degradation rate recently described that the timing of lateral root initiation is fine-tuned by the IAA14 turnover rate.

Molecular analysis of *NAT-IAA14* showed that the transcript is stable and localized in the cytosol and that, despite not containing introns or undergoing splicing, it is not a typical NMD target. Analysis of its expression pattern showed that *NAT-IAA14* levels increase during plant ageing. In *Nicotiana benthamiana*, co-expression of *IAA14* and *NAT-IAA14* was detected in the same cell by a transient assay indicating that both transcripts can co-exist in the same cell at least in this host. Overexpression, downregulation or knockout of *NAT-IAA14* did not significantly affect *IAA14* expression, and no phenotypic effect on root development was observed. The presence of a stabilized IAA14 protein in the *solitary-root-1* (*slr-1*) gain-of-function mutant resulted in a significant increase of *NAT-IAA14* levels. In contrast, overexpression of *IAA14* decreased *NAT-IAA14* levels and the *IAA14* knockout resulted in unaltered or slightly reduced *NAT-IAA14* abundance in most of the lines. While *NAT-IAA14* expression was affected in response to high salt, light stress and mycotoxin treatment, it remained unresponsive to auxin treatment, unlike *IAA14*, whose expression is induced by exposure to the hormone. Results from *in vitro* translation assays suggest an effect of *NAT-IAA14* on the translation of the transcript corresponding to the sequence variant of *IAA14* reported in the database. In these assays, the IAA14 protein levels were reduced in the presence of *NAT-IAA14*. These data suggest a possible role of *NAT-IAA14* in the regulation of IAA14 translation.

3 Introduction

3.1 Types and functions of RNA molecules

One of the most crucial molecules in the living organism is RNA that allows it to respond to various internal and external stimuli. Up to 90% of the eukaryotic genome is transcribed into RNA. In *Arabidopsis thaliana*, less than 50% of genome encodes for proteins (Ariel et al., 2015). Besides its role in protein biosynthesis, following the dogma DNA → RNA → protein, RNA is also involved in the regulation of gene expression. Many different classes of RNA molecules are required to achieve accurate and precise coordination of these events. In general, RNA is divided into two categories: protein coding messenger (m) RNAs and non-protein coding RNAs. Non-coding RNAs are a heterogeneous group and have been classified into different categories according to their length and function. The majority of non-protein coding transcripts, including ribosomal RNAs (rRNAs), transfer RNAs (tRNAs), small nuclear RNAs (snRNAs) and small nucleolar RNAs (snoRNAs), are involved in the protein synthesis process, while microRNAs (miRNAs), small interfering RNAs (siRNAs), circular RNAs (circRNAs) and long non-coding RNAs (lncRNAs) act in gene expression regulation (Bazin et al., 2017, Ghildiyal & Zamore, 2009, Karlik et al., 2019).

3.2 Properties and classification of long non-coding RNAs

Long non-coding RNAs (lncRNAs) have emerged as important regulators of gene expression in eukaryotes in the past few years, although they were initially considered as transcriptional byproducts or 'transcriptional noise' of protein-coding genes (Hüttenhofer et al., 2005). Several recent studies in *A. thaliana* have shown that lncRNAs are dynamically regulated and are key players in various biological processes, e.g. in the regulation of flowering time, root organogenesis, seedling photomorphogenesis, sexual reproduction, crop yield, and stress response (Wang et al., 2014a, Sun et al., 2020, Wang et al., 2014b, Zhang et al., 2014b, Wang et al., 2018b, Zhang et al., 2019, Zaynab et al., 2018). To date, the molecular function of only a few plant lncRNAs has been studied, although between 6480 (Liu et al., 2012) and 6510 (Zhao et al., 2018) lncRNAs have already been previously identified in *Arabidopsis* by large-scale analyses.

lncRNAs are defined as RNA molecules longer than 200 nt with no protein-coding capacity (Ben Amor et al., 2009). Since lncRNAs most often have only short open reading frames (sORFs, <70 amino acids (aa)), there is a strong indication that their activity is based on the RNA molecule itself and/or on the oligopeptides encoded by the sORF

(Hirsch et al., 2006) that function as signals during plant development (Lindsey et al., 2002). Most lncRNAs are localized in the nucleus where they associate with chromatin, however, they can function in both *cis* and *trans* in either the nucleus or the cytoplasm (Wang & Chekanova, 2017). lncRNAs are typically transcribed by DNA-dependent RNA polymerase II, therefore possess mRNA-like features such as 5'cap, introns and 3'poly(A) tail (Zhang et al., 2019). In addition, some plant lncRNAs are synthesized by RNA polymerases IV and V (Zhang et al., 2019). In contrast to mRNAs, lncRNAs are usually expressed in low levels and show only little sequence conservation (Wang & Chekanova, 2017), whereas the position in the genome might be conserved between plant species (Mohammadin et al., 2015).

Until now, only limited information is available on the (post)-transcriptional regulation and stability of lncRNAs. Depending on their mRNA-like properties, the half-lives of lncRNAs vary over a wide range. However, it is generally assumed that lncRNAs are relatively unstable, i.e. unspliced lncRNAs are less stable than spliced ones (Clark et al., 2012). Kurihara and collaborators showed that ~20% of the lncRNAs in Arabidopsis nonsense mediated decay (NMD) mutants *upstream frame shift protein 1-1 (upf1-1)* and *upstream frame shift protein 3-1 (upf3-1)* are upregulated, indicating NMD-dependent degradation (Kurihara et al., 2009). Furthermore, this study suggests that NMD might coordinate the quantity of small peptides that could be translated from lncRNAs with sORFs (Kurihara et al., 2009).

In plants, tens of thousands of lncRNAs are transcribed and are classified based on their localization relative to nearby protein-coding genes in intergenic, intronic, promoter or antisense lncRNA (Figure 3.1, (Wang & Chekanova, 2017)). Transcription of intergenic lncRNAs initiates at least 1 kb away from the transcriptional start site (TSS) of the nearest protein-coding genes (Bonasio & Shiekhattar, 2014), while transcription of intronic lncRNAs starts in the intron of a protein-coding gene. In both cases, the lncRNA can be produced in either direction and terminates without overlapping an exon. Promoter lncRNA transcription starts within the promoter region of a protein-coding gene in any direction. Long non-coding natural antisense transcripts (lncNATs) are synthesized from the opposite DNA strand of a protein-coding gene by initiating inside, 5' or 3' to this gene (Ariel et al., 2015). lncNATs can be further categorized into overlapping and non-overlapping transcripts, which can be expressed in divergent and convergent orientation to the protein-coding gene (Zhao et al., 2018).

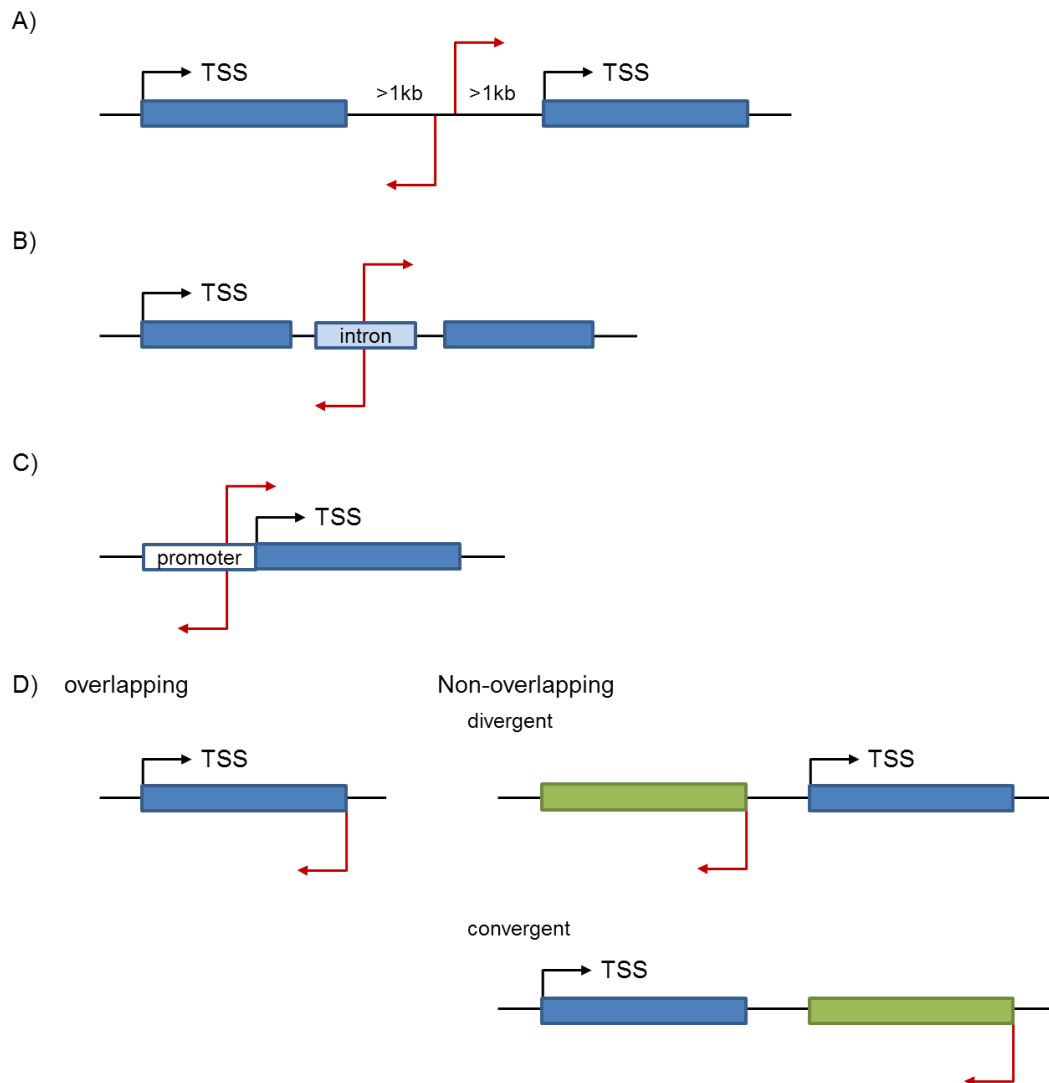


Figure 3.1: Classification of lncRNA according to their relationship to nearby protein-coding genes. (modified after Wang & Chekanova, 2017)

lncRNAs are classified in intergenic- (A), intronic- (B), and promoter lncRNAs (C) and natural antisense transcripts (D). Blue boxes and black lines correspond to the protein-coding genes, and green boxes and red lines indicate lncRNAs. Arrows show the direction of transcription from the transcriptional start site (TSS).

3.3 lncRNAs as 'riboregulators'

The mechanism of action of lncRNAs is complex and diverse, and they act at multiple levels including regulation of chromatin remodeling, RNA metabolism, and protein activity. By interaction with macromolecules such as DNA, RNA and proteins, lncRNAs can achieve their function as molecular scaffolds or decoys at transcriptional, post-transcriptional and epigenetic levels (Wu et al., 2020a). *EARLY NODULIN 40 (ENOD40)* was the first identified plant lncRNA (Crespi et al., 1994) and it has been shown to regulate the subcellular localization of RETINOL BINDING PROTEIN 1 (RBP1), a nuclear RNA-binding protein, in *Medicago truncatula* (Campalans et al., 2004). Since then, a variety of plant lncRNAs have

been reported to regulate miRNA activity (Franco-Zorrilla et al., 2007) and levels of epigenetic modifications (Swiezewski et al., 2009, Wu et al., 2020b), and to modulate chromatin structure (Ariel et al., 2014, Kim & Sung, 2017) and protein interactions (Wang et al., 2018b, Zhao et al., 2018).

The localization of a lncRNA is an important feature to predict its potential function in the subcellular context. While mRNAs are usually transported to the cytosol for translation, lncRNAs can remain in the nucleus or be exported to the cytoplasm, where they can be further transported to other subcellular locations and organelles to achieve their function (Carlevaro-Fita & Johnson, 2019). The potential function of lncRNAs in essential biological processes is summarized in Figure 3.2. Different studies have revealed that nuclear retained lncRNAs facilitate DNA methylation, histone modifications and chromatin conformational changes by recruiting or even sponging DNA-modifying and histone-modifying enzymes. Several nuclear lncRNAs activate or repress transcription in *cis* or in *trans* by regulating the expression of neighboring or distant genes, respectively, in some cases by modulating the activity of transcription factors (Sun et al., 2018). For example, in rice the *LRK Antisense Intergenic RNA (LAIR)* recruits chromatin-modifying complexes to the *LEUCINE-RICH REPEAT RECEPTOR KINASE (LRK)* genomic region to increase H3K4me3 and H4K16ac levels (Wang et al., 2018a). In Arabidopsis, *AS competitor long noncoding RNA (ASCO-lncRNA)* regulates plant root development by competing with alternative splicing targets of the splicing factors nuclear speckle RNA-binding proteins (NSRs) to alter alternative splicing by mimicking alternative spliced transcripts (Bardou et al., 2014).

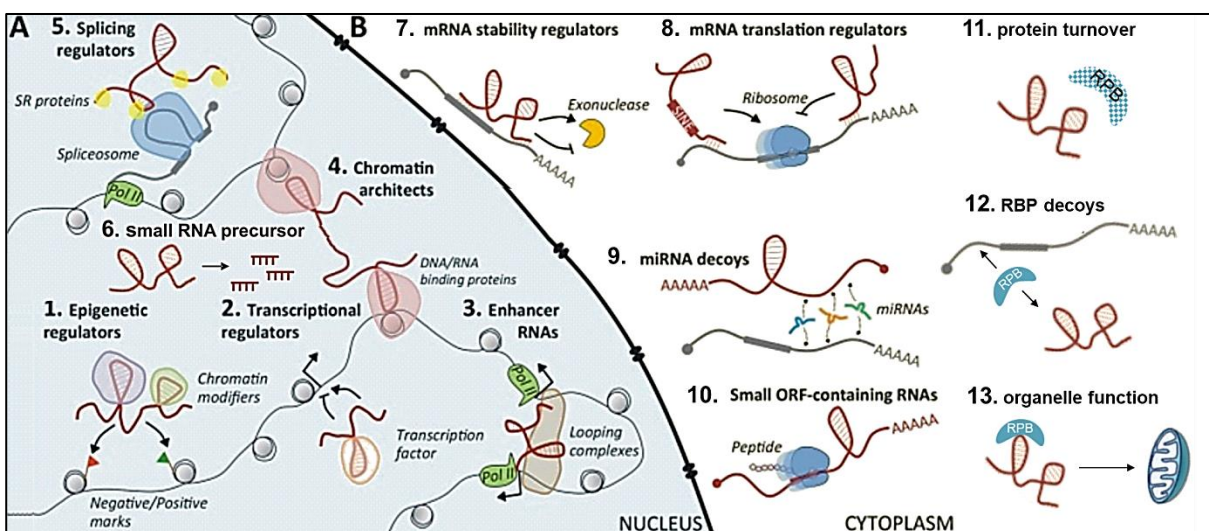


Figure 3.2: Cartoon showing various mechanisms of lncRNA action. (modified after Laneve et al., 2019 and Noh et al., 2018)

Nuclear (A) and cytosolic lncRNAs (B) can act by interacting with RNA-binding proteins (RBP) or with partially complementary mRNAs. Nuclear retained lncRNAs can regulate gene expression by recruiting epigenetic (1) or transcription (2) factors to specific loci, by acting as enhancers (3), by restructuring the conformation of chromatin (4), by guiding splicing factors (5), or by serving as small RNA precursors (6). Cytosolic lncRNAs can act by regulating mRNA stability (7) or translation (8) or by sequestering miRNAs (9) or RBPs (12), by encoding small peptides (10), by modulating protein turnover (11), or by altering organelle function (13).

At the posttranscriptional level, lncRNAs may affect mRNA stability, mask miRNA binding sites, sequester miRNAs, modulate protein translation or be precursors for endogenous small RNAs (Zhao et al., 2018, Laneve et al., 2019, Noh et al., 2018). It was shown in *Arabidopsis* that 34 lncRNAs are potential precursors of sRNAs, e.g. the miRNAs miR869a and miR160c mature from the lncRNAs *non-protein-coding RNA 83 (npc83)* and *non-protein-coding RNA 521 (npc521)*, respectively (Hirsch et al., 2006). Although lncRNAs by definition have small or no protein-coding capacity, some lncRNAs are translated into small peptides of less than 70 aa (Matsumoto & Nakayama, 2018). For example, the *ENOD40* lncRNA from soybean encodes for two small peptides of 12 and 24 aa, respectively. Both peptides regulate sucrose content in nodules and thereby contribute to root nodule organogenesis (Rohrig et al., 2002).

3.4 Role of lncRNAs in plant stress response

Plants, as immobile organisms, are exposed during their life cycle to changing environmental abiotic and biotic stresses, such as drought, salinity, extreme temperature, and pathogen infection. Therefore, they have evolved complex mechanisms that allow them to recognize stress factors, to transmit the signals and, accordingly, to reprogramme the expression of many genes at the transcriptional, post-transcriptional and epigenetic level (Jha et al., 2020).

Several lncRNAs act as competitive endogenous RNAs (ceRNAs) in response to abiotic stress and hijack miRNAs away from their target(s), in a mechanism known as target mimicry (Wang et al., 2017). For example, in *Arabidopsis*, the lncRNA *Induced by Phosphate Starvation 1 (IPS1)* was reported to mimic miRNA399 in response to low phosphate levels, thereby blocking its interaction with the target *PHOSPHATE 2 (PHO2)*. As a result, the miRNA399-mediated repression of *PHO2* is reduced (Franco-Zorrilla et al., 2007). Similar mechanisms of lncRNA action by target mimicry have been shown in rice (Xu et al., 2016) and *Populus* (Shuai et al., 2014) in response to phosphate deficiency and drought stress, respectively.

Plant lncRNAs can participate in abiotic stress response as precursors for small RNAs (Waititu et al., 2020). In *Populus*, for example, 14 long intergenic non-coding RNAs (lincRNAs) were identified to function as precursors for 25 miRNAs in response to nitrogen starvation (Chen et al., 2016). Under cold and heat stress, 50 lncRNAs were reported to act as miRNA precursor in *Brassica rapa* (Song et al., 2016). In *Zea mays* (Zhang et al., 2014a) and wheat (Yao et al., 2010, Xin et al., 2011), several lncRNAs described as precursors for miRNA, siRNA, and short hairpin RNAs (shRNA) were induced in response to drought and

heat stress, respectively. A specific group of lncRNAs that are produced by RNA polymerase V in plants play an important role as scaffolding factors in the RNA-directed DNA methylation (RdDM) pathway during response to stresses (Chekanova, 2015).

Antisense lncRNAs interacting with sense mRNAs encoded on the opposite DNA strand can lead to the formation of double-stranded RNA duplexes, affecting the expression of the mRNA (Waititu et al., 2020). In poplar, 15 lncRNAs were found to be expressed in response to nitrogen starvation conditions (Chen et al., 2016). Similar results have been reported for maize in response to drought stress (Zhang et al., 2014a) and Arabidopsis in response to heat and light stress (Wunderlich et al., 2014, Wang et al., 2014a).

In addition, chromatin remodeling in response to abiotic stress can be achieved by lncRNAs activity. Wang and collaborators showed ~1400 lncRNAs in Arabidopsis that respond to light in a spatial and developmental pattern, and that half of the sense and antisense transcripts associated with H3K9ac and/or H3K27ac were coordinately expressed, while the other half are anticorrelated (Wang et al., 2014a). Furthermore, *COOLAIR*, *COLD ASSISTED INTRONIC NONCODING RNA (COLDAIR)* and the promoter derived lncRNA *COLD OF WINTER-INDUCED NONCODING RNA FROM THE PROMOTER (COLDWRAP)* expression have been described to repress *FLOWERING LOCUS C (FLC)* transcription by reducing the H3K36me3 or H3K4me2 levels (Csorba et al., 2014). These modifications are carried out by recruiting the polycomb repressive complex 2 (PRC2) to promote H3K27me3 accumulation at the *FLC* locus (Heo & Sung, 2011, Kim & Sung, 2017) and to activate flowering after prolonged low temperature.

Several plant-pathogen responsive lncRNAs have been identified in wheat (Xin et al., 2011, Zhang et al., 2013), Arabidopsis (Zhu et al., 2014), grapevine (Xing et al., 2019), *Hevea brasiliensis* (Yin et al., 2019), and tomato (Wang et al., 2015). For example, in tomato several lncRNAs were identified as target mimics for miRNAs involved in Tomato yellow leaf curl virus (TYLCV) infection (Wang et al., 2015). In Arabidopsis, *ELF18-INDUCED LONG-NONCODING RNA1 (ELENA1)* activates the expression of defense-related genes to enhance the resistance against bacterial pathogen *Pseudomonas syringae pv. tomato DC3000* by interacting with Mediator subunit 19a (MED19a, (Seo et al., 2017)).

To date, functional studies on plant stress-responsive lncRNAs are still in the early stages. Since plant lncRNAs expression is extremely stress-sensitive and evolve rapidly compared to protein-coding genes, they are appropriate candidates for plants to serve as environmental sensors or effectors to help them to adapt to changing environments.

3.5 lncNATs in *A. thaliana*

In *A. thaliana*, about 70% of the annotated mRNAs are associated to long non-coding natural antisense transcripts (lncNATs), which have an average length of 731 nt (Wang et al., 2014a). They and their cognate sense transcripts might show concordant or discordant expression patterns (Wang et al., 2014a). lncNATs can positively or negatively regulate the expression of their sense transcript by transcriptional or posttranscriptional mechanisms of the lncRNAs. Simultaneous transcription of the lncNAT and the sense gene can compete for RNA polymerase II (IV and V) or regulatory transcription factors, or even results in transcriptional interference (Zhao et al., 2018). The expression of lncNATs is tissue-specific and tightly regulated in response to abiotic and biotic stresses (section 3.4, (Chekanova, 2015)). By increasing and improving sequencing and tiling array data, more and more lncNATs are discovered in *A. thaliana*. However, the mechanism of action is known for only a few of them.

In several studies, the importance of lncNAT-dependent recognition of external conditions has been reported. The best-studied example of regulation by lncNATs in Arabidopsis is *COOLAIR* that together with the lncRNAs *COLDAIR* and *COLDWRAP* repress *FLC* expression (section 3.4). A set of antisense transcripts, collectively referred to as *COOLAIR*, are produced from the 3' end of *FLC* and are alternatively spliced and polyadenylated (Liu et al., 2010). During the early phase of cold exposure, *COOLAIR* physically interacts with the *FLC* locus and coordinates the switch from H3K36 methylation to H3K27me3 at the intragenic *FLC* nucleation site to repress *FLC* transcription (Csorba et al., 2014). The exact molecular mechanism is not yet determined, however, the RNA 3' end processing factors CLEAVAGE STIMULATING FACTOR 64 (CstF64) and CLEAVAGE STIMULATING FACTOR 77 (CstF77), which are responsible for the alternative polyadenylation of *COOLAIR*, have been reported to trigger the localized histone demethylase activity at the *FLC* locus (Liu et al., 2010). Furthermore, the lncNAT *MAS* was described to fine-tune flowering time in response to cold by transcriptional activation of *MADS AFFECTING FLOWERING 4 (MAF4)*. *MAS* acts in *cis* by recruiting the WD40 containing repeat 5a (WDR5a) protein, which is a core component of the COMPASS-like complexes, and enhances the H3K4me3 methylation at the *MAF4* locus to promote transcription (Zhao et al., 2018).

A recent study performed by Kindgren *et al.* showed the influence of the lncNAT *SVALKA (SVK)* in maximizing freezing tolerance at reduced fitness costs. Read-through transcription of *SVK* results in expression of *antisense CBF1* lncRNA (*asCBF1*) that leads to Pol II collision and the restriction of the expression of the full-length *C-REPEAT/DRE BINDING FACTOR 1 (CBF1)*, (Kindgren et al., 2018)).

The lncNAT *antisense DOG1 (asDOG1)* is reported to inhibit *DELAY OF GERMINATION (DOG1)* expression in *cis*, thereby promoting germination initiation (Fedak et al., 2016). In addition to this function, asDOG1 expression has been shown to be decreased by abscisic acid (ABA) treatment in 40d-old plants, resulting in constitutively high *DOG1* levels and increased drought tolerance (Yatusevich et al., 2017). Another lncNAT, *asHSFB2a*, is strictly heat inducible and is transcribed antisense to the *HEAT SHOCK TRANSCRIPTION FACTOR B2A (HSFB2a)* gene (Wunderlich et al., 2014). The expression of the members of this NAT pair is anticorrelated and inhibits the transcription of the other in a so-called "Yin-Yang" mode of gene expression regulation. The results from Wunderlich and collaborators suggest that the *asHSFB2a* buffers the *HSFB2a*-dependent heat shock response in leaves. An expression change at the *HSFB2a* locus by overexpression one of these genes influences vegetative and gametophytic development in Arabidopsis. Recently, the circadian clock regulated *CDF5 LONG NONCODING RNA (FLORE)*, which is a natural antisense transcript of *CYCLING DOF FACTOR 5 (CDF5)*, was identified (Henriques et al., 2017). The *CDF5/FLORE* NAT pair expression is antiphase, reflecting reciprocal inhibitory regulation that directly affects regulation of flowering time.

3.6 Auxin signaling pathway

The phytohormone auxin, primarily indole-3-acetic acid (IAA), is one of the master regulator of plant growth and development, and controls a variety of diverse responses in plants like root and shoot elongation (Perrot-Rechenmann, 2010), apical dominance (McSteen & Leyser, 2005), embryogenesis and vascular patterning (Weijers et al., 2006, Möller & Weijers, 2009, Scarpella et al., 2010), organ polarity establishment and tropic responses by modulating gene transcription (Wang & Estelle, 2014, Friml et al., 2002, Abas et al., 2006). Plants can sense and react to auxin signaling in a precise and rapid manner. This response involves a group of genes called the early auxin response genes (Weijers & Wagner, 2016).

Nuclear auxin signal perception and gene expression regulation are carried out by the F-Box proteins from the TRANSPORT INHIBITOR RESPONSE 1/AUXIN-SIGNALING F-BOX (TIR1/AFB) family, the AUXIN/INDOLE-3-ACETIC ACID (AUX/IAA) repressor proteins and the AUXIN RESPONSE FACTOR (ARF) transcription factors. In *A. thaliana*, these proteins are encoded by genes belonging to multigene families with six, 29 and 23 members, respectively (Powers & Strader, 2020).

A general scheme of auxin-dependent gene expression is depicted in Figure 3.3. AUX/IAA proteins bind to ARFs and prevent activation of auxin-responsive genes in the

absence of auxin (Figure 3.3 A). Increasing auxin levels lead to the formation of a co-receptor complex (SCF^{TIR1/AFB} E3 ubiquitin ligase complex) between the AUX/IAA and TIR1/AFB F-box protein with auxin acting as molecular glue (Figure 3.3 B). After ubiquitination the AUX/IAA repressor protein is degraded by the 26S proteasome. Released from AUX/IAA repression, ARF transcription factors bound to auxin-responsive elements (AuxREs) present in the promoter regions of auxin-responsive genes subsequently initiate auxin-dependent gene transcription (Powers & Strader, 2020, Wang & Estelle, 2014).

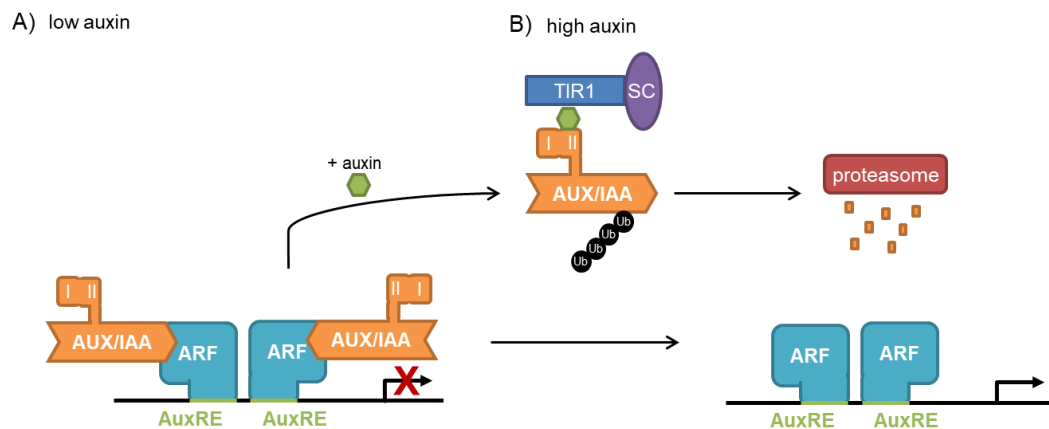


Figure 3.3: General scheme of auxin signaling through the SCF^{TIR1/AFB} pathway. (modified after Powers & Strader, 2020)

At low auxin concentrations AUX/IAA proteins block the transcription of auxin-responsive genes (A). Increasing auxin levels lead to the AUX/IAA degradation by the 26S proteasome and to transcription of the auxin-responsive genes (B).

AUX/IAA = AUXIN/INDOLE-3-ACETIC ACID, ARF = AUXIN RESPONSE FACTOR, AuxRE = Auxin-Responsive Element, TIR1 = TRANSPORT INHIBITOR RESPONSE 1, SC = ARABIDOPSIS SKP1 HOMOLOGUE (ASK1) and CULLIN 1, Ub =ubiquitylation

3.7 The AUX/IAA multigene family

AUX/IAA proteins are short-lived nuclear proteins (Abel et al., 1994). Most AUX/IAA proteins share a similar structure that consists of four conserved domains (Figure 3.4) separated by variable regions (Calderón Villalobos et al., 2012). The repression of the transcription factor activity of ARF by AUX/IAAs depends on the recruitment of co-repressor proteins, including TOPLESS (TPL), through interaction with domain I, located at the N-terminus. The domain II of AUX/IAAs contains a 13 aa degron motif that is required for auxin-triggered degradation through direct interaction with auxin and TIR1/AFB proteins (Gray et al., 2001, Ramos et al., 2001, Calderón Villalobos et al., 2012). Recently, flexible hotspots with specific lysine residues have been identified in the degron-flanking regions that are linked to AUX/IAA ubiquitylation mediated by TIR1 (Winkler et al., 2017). The C-terminal domain (also called DIII/IV, or separately as DIII and DIV) interacts with the ARF proteins to

suppress auxin-responsive transcription or is required for homodimerization and heterodimerization with other *AUX/IAA* gene family members (Kim et al., 1997). ARF proteins can be transcription activators or repressors, depending on the amino acid composition of the middle region (Ulmasov et al., 1999). Two *AUX/IAA* proteins in Arabidopsis, IAA29 and IAA33, are truncated and lack domain I and II.

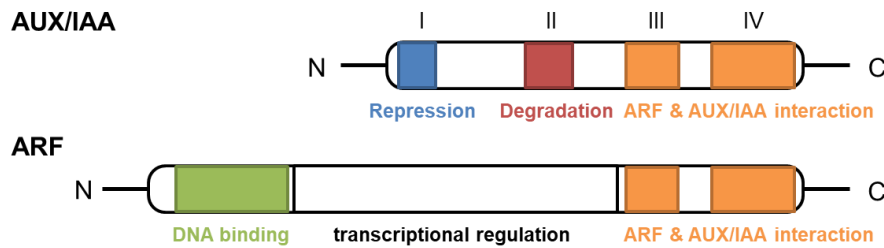


Figure 3.4: Schematic representation of the AUX/IAA and ARF domain structure. (modified after Powers & Strader, 2020)

The conserved domains of AUX/IAAs and ARFs are shown and their function in the auxin response regulation is displayed.

AUX/IAA = AUXIN/INDOLE-3-ACETIC ACID, ARF = AUXIN RESPONSE FACTOR, N = N-terminus, C = C-terminus

The variation in the domain structure of AUX/IAAs might contribute to the diverse functions in the auxin signaling pathway and facilitate multiple roles in response to environmental changes (Luo et al., 2018). Although 29 AUX/IAA proteins are identified in Arabidopsis, most mutations in the individual AUX/IAA proteins produce similar phenotypes *in planta*, indicating that they share redundant functions. AUX/IAA mutants show pleiotropic effects in plant developmental processes associated with decreased or increased auxin responses, such as altered embryo development, hypocotyl elongation, root growth, leaf and flower development, and tropism (Figure 3.5, (Luo et al., 2018)). To date, gain-of-function mutants with increased protein stability caused by the replacement of a single amino acid in domain II have been reported for 13 of the 29 Arabidopsis AUX/IAA proteins (Figure 3.5), including *iaa1* (*axr5/auxin-resistant 5*, (Yang et al., 2004)), *iaa3* (*shy2/suppressor of hy2 2*, (Kim et al., 1996, Tian & Reed, 1999, Goh et al., 2012)), *iaa6* (*shy1/suppressor of hy2 1*, (Kim et al., 1996)), *iaa7* (*axr2/auxin-resistant 2*, (Wilson et al., 1990, Nagpal et al., 2000, Gray, 2004)), *iaa8* (Wang et al., 2013), *iaa12* (*bdll/bodenlos*, (Hamann et al., 1999, Hamann et al., 2002)), *iaa14* (*slr/solitary-root*, (Fukaki et al., 2002)), *iaa15* (Kim et al., 2020), *iaa16* (Rinaldi et al., 2012), *iaa17* (*axr3/auxin-resistant 3*, (Leyser et al., 1996, Rouse et al., 1998, Tanimoto et al., 2007)), *iaa18* (*crane*, (Uehara et al., 2008, Reed, 2001)), *iaa19* (*msg2/massugu2*, (Tatematsu et al., 2004)), and *iaa28* (Rogg et al., 2001).

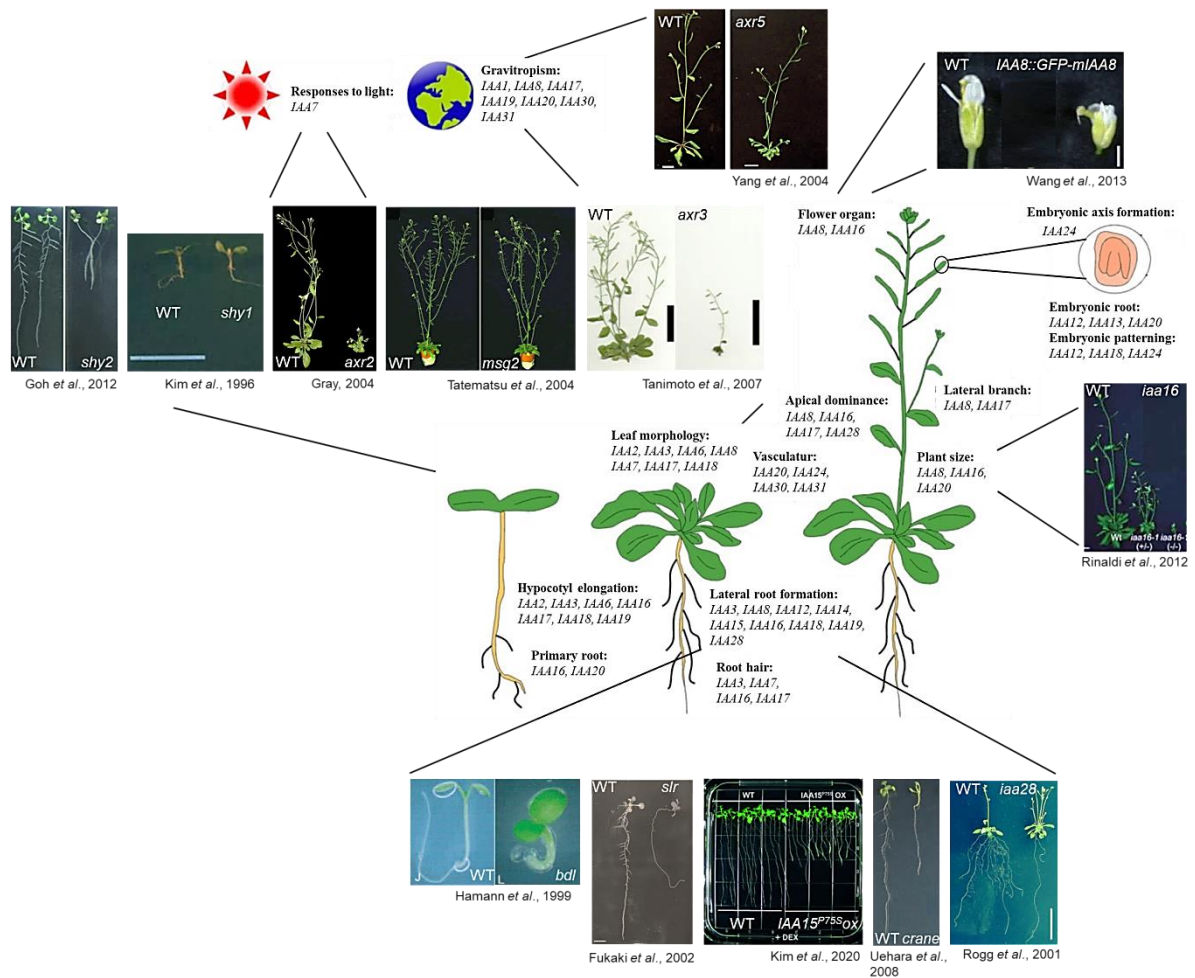


Figure 3.5: Functions of the AUX/IAA genes in developmental processes of *A. thaliana* and phenotypes of the gain-of-function mutants. (modified after Luo et al., 2018)

The 13 reported gain-of-function mutants of the Aux/IAA family are shown clockwise: *iaa1* (*axr5/auxin-resistant 5*), *iaa8*, *iaa16*, *iaa28*, *iaa18* (*crane*), *iaa15*, *iaa14* (*slr/solitary-root*), *iaa12* (*bdl/bodenlos*), *iaa3* (*shy2/suppressor of hy2 2*), *iaa6* (*shy1/suppressor of hy2 1*), *iaa7* (*axr2/auxin-resistant 2*), *iaa19* (*msq2/massugu2*), *iaa17* (*axr3/auxin-resistant 3*).

3.8 AUXIN/INDOLE-3-ACETIC ACID 14 (IAA14)

The focus of this work was on the possible regulation of the AUXIN/INDOLE-3-ACETIC ACID 14 (*IAA14*, *At4g14550*) gene expression by an uncharacterized lncRNA encoded by the *At4g14548* gene, which is located in close proximity and in antisense orientation. The *IAA14* transcript is composed by a short 5' untranslated region (UTR) of 96 nt, a coding region of 687 nt derived from the five exons present in the gene and by a 3'UTR of 699 nt, which is extremely long compared the average length of 3'UTRs in *A. thaliana* of 200 nt (Mignone et al., 2002). The *IAA14* mRNA is detectable in almost all organs except developing siliques (Abel et al., 1994). Upon exogenous application of auxin, *IAA14* levels are slightly increased and cycloheximide treatment induces *IAA14* expression (Abel et al., 1994).

The nuclear-localized IAA14 protein (Fukaki et al., 2002) comprises the typical four domains of the AUX/IAA proteins (section 3.6). In 2002, a gain-of-function mutant of *IAA14*, called *slr-1*, was isolated (Fukaki et al., 2002). *slr-1* has a point mutation (CCG to tCG) that results in a proline to serine change at position 82 within the conserved degron domain that blocks the interaction with the SCF^{TIR1} complex and leads to the generation of a stabilized IAA14 protein. This mutant shows a strong phenotype including the lack of lateral roots, deficiency of root hair formation and abnormal gravitropic responses of its root and hypocotyl (Figure 3.6). Furthermore, the mutant plant is auxin insensitive and the application of exogenous auxin cannot rescue the phenotype. The division of pericycle cells during lateral root initiation is blocked in *slr-1* (Fukaki et al., 2002). Moreover, reducing the auxin-dependent turnover of IAA14 by point mutations delayed lateral root emergency in proportion to the half-lives of the different IAA14 protein variants (Guseman et al., 2015).

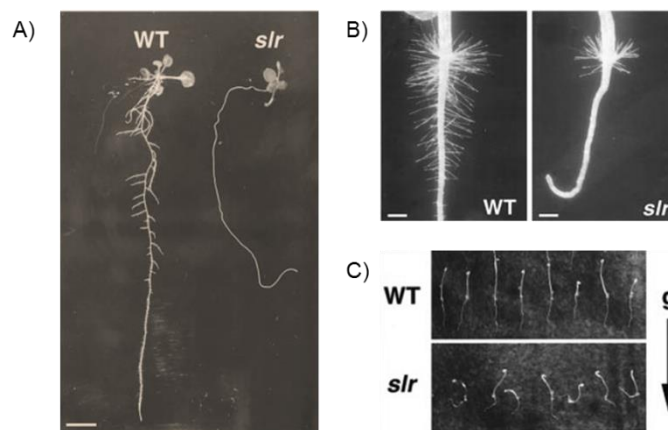


Figure 3.6: Phenotypes of the *slr-1* mutant. (Fukaki et al., 2002)

Shown is the morphology of 2-week-old seedlings (A, scale bar = 10 mm), the root hair density (B, scale bar = 0.5 mm), and the gravitropic response of 3d old etiolated seedlings (C, g arrow indicates direction of gravity).

IAA14 interacts in a yeast-two-hybrid system with several ARFs, including ARF7 and ARF19 that have redundant functions (Fukaki et al., 2005). Additionally, *ARF7* and *ARF19* are co-expressed with *IAA14* in root stele tissues, including the pericycle (Fukaki et al., 2002, Okushima et al., 2005, Wilmoth et al., 2005). While *arf7* and *arf19* single mutants lack an obvious phenotype, the *arf7 arf19* double mutant shows impaired lateral root formation and abnormal hypocotyl and root gravitropism, indicating a similar strong auxin-related phenotype as *slr-1* (Okushima et al., 2005). These data suggests that the stabilized IAA14 protein blocks lateral root formation by inactivating ARF7/ARF19 functions in the stele (Fukaki et al., 2005). However, *slr-1* completely lacks lateral roots and has only a few root hairs, suggesting that IAA14 also represses other ARFs. PICKLE (PKL), a chromatin-remodeling enzyme, is required for the IAA14-mediated inhibition of lateral root initiation through ARF7/19 by an yet

unknown regulatory mechanism (Fukaki et al., 2006). In addition, Ito and collaborators showed that IAA14 interacts through TPL with Mediator's dissociable CDK8 kinase module (CKM) that inhibits the recruitment of RNA polymerase II (Ito et al., 2016). Degradation of IAA14 by auxin results in the dissociation of the CKM component, while the other Mediator subunits bind to the promoter of the target genes together with ARF7/19 leading to an activation of transcription of the auxin-responsive genes.

3.9 Regulation of *IAA14* expression and IAA14 stability

IAA14 is a key player in auxin signaling and thus its expression has to be tightly regulated. In general, transcription of *Aux/IAA* genes is controlled by a negative feedback loop mediated by auxin-dependent release of ARFs (Salehin et al., 2015). In a previous study, basal *IAA14* levels were shown to be increased three-fold by treatment with 1 μ M 1-naphthaleneacetic acid (NAA), a synthetic auxin (Gao et al., 2015). In addition, auxin switches the polyadenylation site usage of *IAA14* (Hong et al., 2018). Increasing auxin levels resulted in an elevation of full-length *IAA14* transcripts by preferentially using the distal poly(A) site in the 3'UTR, while the percentage of *IAA14* transcripts with the proximal poly(A) site producing a truncated protein lacking domain II that functions in inhibiting downstream factors such as ARF7/19 (Dreher et al., 2006) remained unchanged (Hong et al., 2018). A recent study reported an *in silico* predicted upstream open-reading frame (uORF) in the 5'UTR of *IAA14* (Bazin et al., 2017), which could affect the expression of main ORFs on the same mRNA (Kurihara et al., 2020).

Almost every step of the auxin-signaling pathway, from the hormone synthesis to the auxin-responsive gene expression, is regulated by the circadian clock. Plant growth and metabolism is coordinated by the circadian clock to generate self-maintaining cycles of gene expression with a period of about 24 hours to adapt to the fluctuating environment (Covington & Harmer, 2007). Overall, more than 10% of expressed genes in Arabidopsis, including *IAA14* (Figure 3.7), displays circadian clock oscillation (Voß et al., 2015, Covington & Harmer, 2007, Harmer et al., 2000). Voß and collaborators concluded that the circadian clock is necessary to rephase auxin response in lateral root cells.

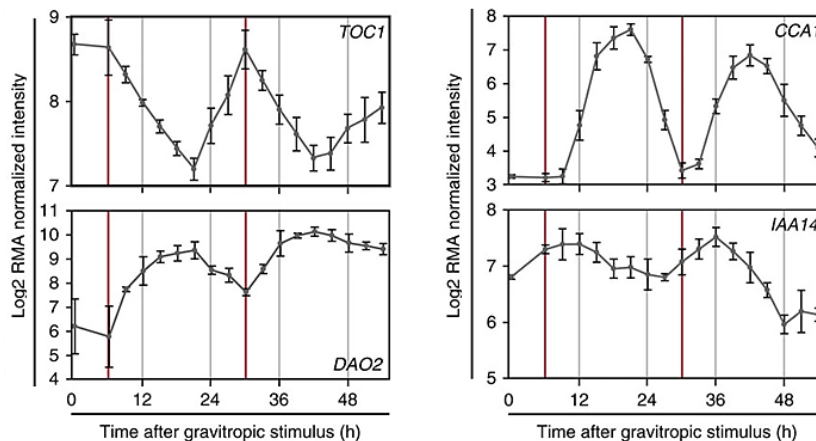


Figure 3.7: *IAA14* gene expression oscillates like circadian clock genes *CCA1* and *TOC1*. (Voß et al., 2015)

Voß and collaborators demonstrated the gating of auxin signaling genes like *IAA14* and *AtDAO2* by the circadian clock during lateral root primordium development. The mean of the gene expression is given by the solid line and the error bars show the mean \pm 2 s.e. N=4.

TOC1 = TIMING OF CAB EXPRESSION 1, *DAO2* = DIOXYGENASE FOR AUXIN OXIDATION 2, *CCA1* = CIRCADIAN CLOCK ASSOCIATED 1, *IAA14* = AUXIN/INDOLE-3-ACETIC ACID 14

Furthermore, *IAA14* transcription was shown to be modulated by light, a key factor in plant photomorphogenic development that controls auxin levels, transport and responsiveness. In *Arabidopsis*, *IAA14* expression is positively regulated by the transcription factor LONG HYPOCOTYL 5 (*HY5*), a negative regulator of the auxin signaling pathway, by directly affecting the transcription of light-induced genes. Concomitantly, the *hy5* mutant shows increased number of lateral roots caused by elevated auxin signaling (Cluis et al., 2004). A recent study showed that *IAA14* is regulated by photoreceptors to inhibit hypocotyl adventitious root (*HAR*) formation (Li et al., 2021). Phytochrome B (*PHYB*) interacts with the *IAA14*-*ARF7/ARF19* module, resulting in *IAA14* stabilization while repressing the transcriptional activities of *ARF7* and *ARF19*, leading to suppression of biogenesis of dark-induced *HARs*. In agreement with this, *slr-1* produces few *HARs* after 14 days of growth in darkness. The transcript level of *IAA14* was unchanged in *phyb* compared to *Col-0*, suggesting *IAA14* regulation by *PHYB* at the posttranscriptional level.

In addition, several studies showed that *IAA14* is regulated by various abiotic stresses. Shani and coworkers have reported that *IAA14* is downregulated by the transcription factors DEHYDRATION RESPONSIVE ELEMENT-BINDING PROTEIN (*DREB*) and APETALA 2 (*AP2*) in response to extreme drought stress (Shani et al., 2017). In addition, *IAA14* degradation rate was shown to be delayed by auxin in *di19-3* mutant seedlings, suggesting that DROUGHT-INDUCED-19 (*Di19-3*) protein interacts with *IAA14* to facilitate its degradation and to promote stress-induced plant responses such as lateral root formation. *slr-1* seed germination as well as cotyledon greening were increased in response to ABA, mannitol and NaCl, suggesting that *IAA14* might be involved in drought tolerance and ABA

sensitivity by interacting with Di19-3 (Maitra Majee et al., 2020). Furthermore, IAA14 and ARF7/19 have been reported to affect membrane lipid remodeling by increasing transcription of glycolipid synthase and phospholipase genes in response to phosphate deficiency. Phosphate starvation induces in higher plants the replacement of phospholipids with nonphosphorous glycolipids such as digalactosyldiacylglycerol (DGDG) and sulfoquinovosyldiacylglycerol (SQDG, (Narise et al., 2010)). In *slr-1*, the accumulation of DGDG and SQDG was suppressed (Narise et al., 2010), suggesting that regulation of IAA14 degradation is necessary for normal Pi homeostasis during Pi starvation. In addition, 20 microRNAs were recently reported to be differentially expressed in *slr-1*, the majority of which were downregulated. Therefore, *slr-1* was more susceptible to low temperatures during root elongation recovery, suggesting that IAA14 degradation is important for plant acclimation to cold by increasing the expression of cold-responsive miRNAs (Aslam et al., 2020).

IAA14 expression and protein levels are regulated by a variety of internal and external stimuli, but its regulatory network may not yet have been fully unravelled. In 2013, an antisense lncRNA was reported to be transcribed from the *At4g14548* gene, which is located in close proximity and on the opposite DNA strand to *IAA14* in *A. thaliana* (Obulareddy et al., 2013). The *IAA14/At4g14548* gene pair (Figure 3.8) is not a classic sense/antisense pair as, according to the annotation in the TAIR10 (The Arabidopsis Information Resource) database, they are separated by a 57 bp intergenic region. Nevertheless, the lncRNA encoded by *At4g14548*, hereafter referred as *NAT-IAA14*, could be involved in the regulation of *IAA14* expression in *cis* or *trans* or even at the protein level. Therefore, the characterization of *NAT-IAA14* itself and, in particular, the analysis of its potential role in the regulation of *IAA14* is of general interest to increase the understanding of the biological relevance and mechanisms of the action of lncRNAs.

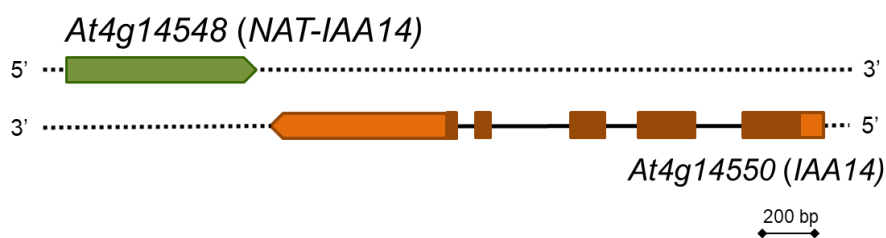


Figure 3.8: Schematic representation of *IAA14* and *NAT-IAA14* location on the chromosome 4 of *A. thaliana*.

The orange and green arrows represent the annotated *At4g14550* (*IAA14*, 1482 bp) and *At4g14548* (*NAT-IAA14*, 755 bp) genes, respectively. *IAA14* exons are indicated in brown and light orange areas depict the 5' and 3' UTRs. The black line displays *IAA14* introns and the dotted line DNA strands.

4 Objectives

As mentioned before the *NAT-IAA14* lncRNA was first reported in an RNA-Seq experiment from *A. thaliana* guard cells (Obulareddy et al., 2013). The *At4g14548* gene, which encodes *NAT-IAA14*, is located in close proximity to *IAA14* and transcribed in convergent orientation. According to the model proposed by Borsani et al., the main requirements for posttranscriptional regulation are co-expression and an overlap between complementary sequences present in the transcripts derived from a sense/antisense gene pair leading to the generation of natural antisense siRNAs (nat-siRNAs) (Borsani et al., 2005). To address this potential mode of action of *NAT-IAA14*, the expression pattern and the 3' end of the transcripts were analyzed in previous studies in the laboratory.

First, it was shown by RT-PCR that *IAA14* and *NAT-IAA14* are co-expressed in seedlings at the fully expanded cotyledons stage, in cauline and rosette leaves, and in flowers of *A. thaliana* (Seidel, 2014). To get a more detailed view on the expression in different developmental stages and organs, *promoter::GUS*-reporter lines including 2.5 kb of the promoter region of *NAT-IAA14* or *IAA14* upstream of the β -glucuronidase (*uidA*, *GUS*) gene were generated and analyzed in a time course experiment spanning the *A. thaliana* life cycle (Figure 4.1, (Pogoda, 2015)).

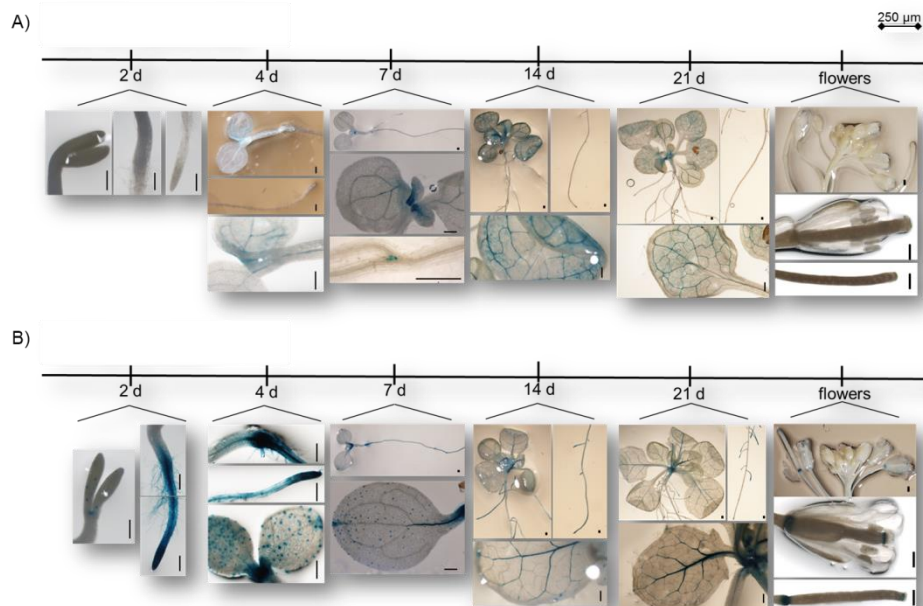


Figure 4.1: Pattern of GUS-staining of *NAT-IAA14*_{prom}::*GUS* and *IAA14*_{prom}::*GUS* reporter lines during the *A. thaliana* life cycle. (modified after Pogoda, 2015)

Representative stereomicroscope pictures of the time course experiment from *NAT-IAA14*_{prom}::*GUS* (A) and *IAA14*_{prom}::*GUS* (B) representative lines are shown. d indicates days after germination.

While *IAA14* shows promoter activity already two days after germination, the *NAT-IAA14* promoter becomes active four days after germination, suggesting a different regulation of gene expression at early developmental stages. At later time points, both genes are co-expressed in various tissues/organs, including petioles, guard cells of stomata and in the vasculature of true leaves, cotyledons, hypocotyl and root, suggesting a common regulation at later developmental stages.

Li and collaborators already predicted the *NAT-IAA14* and *IAA14* genes as a *cis*-NAT pair (Li et al., 2013). To elucidate the mechanism of action, 3'RACE (3' rapid amplification of cDNA ends) and Southern Blot were used in a previous study to investigate a potential overlap of the *NAT-IAA14* and *IAA14* transcripts. Interestingly, an additional *IAA14* variant that is 124 nt-longer than reported in TAIR10 was detected (Figure 4.2, (Seidel, 2014)). The alternative *IAA14* 3'end results in a 67 nt overlap with the *NAT-IAA14* transcript. In addition, an *IAA14* transcript with a 571 nt shorter 3'UTR caused by alternative splicing, in which only the first 45 nt and the last 87 nt of the UTR were included, was identified (Seidel, 2014, Pogoda, 2015).

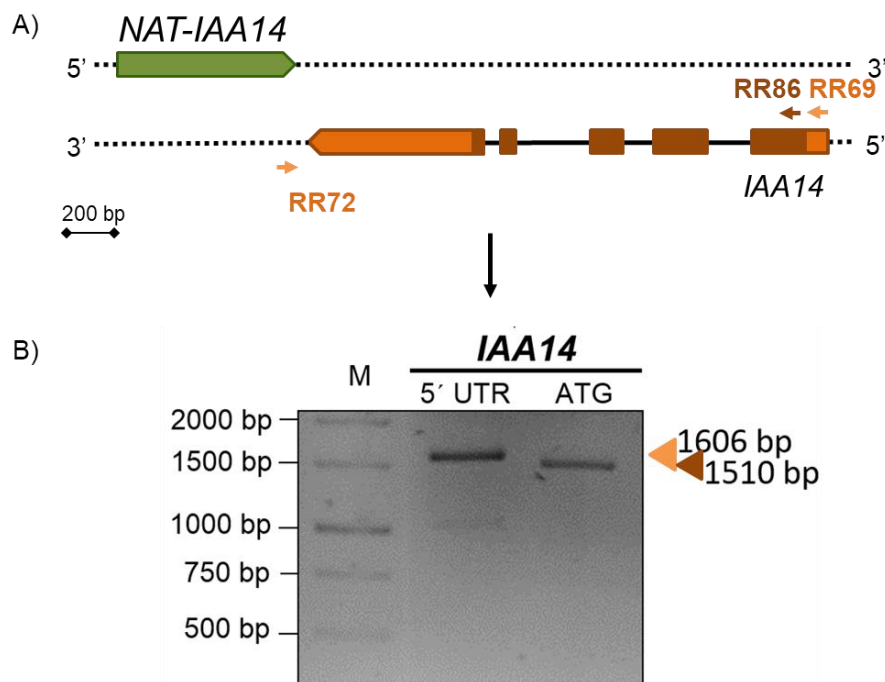


Figure 4.2: *IAA14* transcript variant with a longer 3' end. (modified after Seidel, 2014)

A schematic representation of *IAA14* (brown: exon; orange: UTR) and *NAT-IAA14* (green) genes including primers used for amplification by RT-PCR is shown in (A). Amplification products corresponding to the *IAA14* transcript with the longer 3'UTR are shown in (B). The reverse primer RR72, located in the *NAT-IAA14* gene region, was combined with RR69 or RR86 to obtain *IAA14* amplicons containing the 5'UTR or starting with the ATG codon, respectively. The length of the amplicons was determined by cloning and sequencing.

The few lncRNAs that have been functionally characterized so far have been shown to be involved in the regulation of essential developmental processes in *A. thaliana* (section 3.5). Nevertheless, studies to determine the biological role of lncRNAs in plants, particularly in multigene families, are still in the early stages. The co-expression of *IAA14* and *NAT-IAA14* during the life cycle of *A. thaliana* in combination with the identified overlap of the two transcripts suggests a concordant regulation of *IAA14* and *NAT-IAA14* gene expression. The aim of this doctoral thesis was to characterize *NAT-IAA14* at the molecular and functional level, to gain further insights into its role in *A. thaliana* and to evaluate its potential activity in the regulation of *IAA14* expression. To this end, the following objectives were addressed:

- (1) To characterize *NAT-IAA14* at the molecular level and to confirm its expression at different developmental stages of the *A. thaliana* life cycle.
- (2) To determine *NAT-IAA14* expression in response to various abiotic and biotic stresses.
- (3) To assess the phenotypic effects of altered *NAT-IAA14* expression.
- (4) To investigate the potential mechanism of action of *NAT-IAA14* on the transcription or translation of the sense gene *IAA14*.

5 Materials and methods

5.1 Materials

5.1.1 Chemicals and supplies

Unless otherwise indicated, chemicals and enzymes were obtained from the following suppliers: Ambion, Biozym, Bayer, Carl Roth, Duchefa Biochemie, GDR, Invitrogen, Merck, New England Biolabs, Roche Diagnostics, Sigma-Aldrich, Serva Electrophoresis and Thermo Scientific™. Molecular biology kits were obtained from Thermo Scientific™ and VWR. Primer synthesis as well as sequencing was performed by Eurofins Genomics.

5.1.2 Bacterial strains and plasmid vectors

The *Escherichia coli* (*E. coli*) TOP10 (Invitrogen) bacterial strain was used for molecular cloning. *Agrobacterium tumefaciens* (*A. tumefaciens*) GV3101 (Koncz & Schell, 1986) was used for transient expression in *Nicotiana benthamiana* and for plant transformation by floral dip in *A. thaliana* Col-0.

Plasmid vectors used in this work are listed in Table 5.1. Plasmid vector maps assembled by Golden gate cloning are shown in Supplemental Figure 11.3-11.7.

Table 5.1: Plasmid vectors.

plasmid	Purpose and features	reference
<i>modified pUC18</i> (<i>mpUC18</i>)	RPA and northern blot <ul style="list-style-type: none"> - T7 promoter sequence inserted - <i>lacZ</i>, <i>Amp^r</i>, <i>pBR322ori</i> 	(Carbonell et al., 2008)
<i>pENT^R_L1/L2_tRNA gRNA scaffold</i>	CRISPR/Cas9 editing <ul style="list-style-type: none"> - PCR template for gRNA synthesis 	provided by Dr. Mily Ron (University California, Davis)
<i>pENT^R_L1/L2_AtU6gRNA</i> (Supplemental Figure 11.1)	CRISPR/Cas9 editing <ul style="list-style-type: none"> - <i>U6</i> promoter in front of the inserted gRNA sequence - <i>Amp^r</i> 	
<i>pMR333_OLEp-OLE_GFP</i> (Supplemental Figure 11.2)	CRISPR/Cas9 editing <ul style="list-style-type: none"> - <i>Cas9</i> driven expression by <i>RPS5A</i> promoter - <i>GFP</i> driven expression by <i>OLE1</i> promoter - <i>Basta^r</i>, <i>Spec^r</i> 	
<i>pMDC32B-AtMIR390a-B/c</i> <i>pENTR™/D-TOPO™</i>	amiRNA cloning Gateway cloning <ul style="list-style-type: none"> - attL recombinationsites - M13 and T7 sequencing sites - <i>Kan^r</i>, <i>pUC ori</i> 	(Carbonell et al., 2014) Thermo Fisher™
<i>pZero®-2</i>	RACE <ul style="list-style-type: none"> - cloning of PCR products - <i>Kan^r</i> 	Invitrogen

pB7WG2	Gateway cloning - attR recombinationsites - 35S promoter driven gene of interest expression - Basta ^r , Spec ^r	(Karimi et al., 2002, Karimi et al., 2005)
pB7WGF2	Gateway cloning - attR recombinationsites - 35S promoter driven gene of interest expression - GFP for N-terminal fusion - Basta ^r , Spec ^r	

RPA = RNase protection assay, gRNA = guide RNA, RPS5A = RIBOSOMAL PROTEIN 5A, GFP = green fluorescent protein, *OLE1* = *OLEOSIN 1*, amiRNA = artificial microRNA, attL = attachment site left, RACE = rapid amplification of cDNA ends, attR = attachment site right

5.2 Culture media

Composition and optional supplements of the media used for cultivating *A. thaliana*, *A. tumefaciens* and *E. coli* are listed in Table 5.2. Culture media was sterilized at 120°C and 2 bar for 20 min.

For bacterial selection the corresponding antibiotics were added to LB media. In case of golden gate cloning, the Luria-Bertani (LB) media was additionally supplemented with 20 µM 5-bromo-4-chloro-3-indolyl-β-D-galactopyranoside (*X-Gal*).

Table 5.2: Culture media composition.

medium type	composition	supplements	Reference
½ MS (<i>A. thaliana</i>)	2.16 g/l Murashige & Skoog with salts and vitamins (Duchefa), 15 g/l sucrose, pH 5.6 (with KOH)	8-15 g/l phytoagar ^Z (Duchefa), 10 µg/ml BASTA [®] (200 g/l Glufosinat-ammonium; Bayer)	(Murashige & Skoog, 1962)
LB (Miller) (<i>E. coli</i> , <i>A. tumefaciens</i>)	20 g/l LB medium powder	1-1.5 g/l agar ^Z 50 µg/ml Kanamycin, 50 µg/ml Ampicillin, 10 µg/ml Rifampicin, 75 µg/ml Spectinomycin, 25 µg/ml Gentamycin	(Bertani, 1951)
SOC (<i>E. coli</i> , <i>A. tumefaciens</i>)	2% tryptone, 0.5% yeast extract, 10 mM NaCl, 2.5 mM KCl, 10 mM MgCl ₂ x 6H ₂ O, 10 mM MgSO ₄ x 6H ₂ O, 20 mM glucose		(Hanahan, 1983)

^Z supplemented in solid media plates

MS = Murashige and Skoog, LB = Luria-Bertani media, SOC = Super Optimal broth with Catabolite repression

5.3 Plant materials and growth conditions

5.3.1 Plant lines

All experiments were performed using *A. thaliana* ecotype *Columbia-0* (Col-0). Seeds from the mutant lines *slr-1* (Fukaki et al., 2002) were kindly provided by Dr. Luz Irina A. Calderón Villalobos. Seeds from the *SALK_113294* (referred to *nat-iaa14_1*), *SALK_012231* (referred to *nat-iaa14_2*) and *SALK_118398* (referred to *nat-iaa14_3*) lines were obtained from the Nottingham Arabidopsis Stock Centre (NASC). Lines expressing amiRNAs against *NAT-IAA14* or overexpressing *IAA14* or *NAT-IAA14* were previously generated in the laboratory (Seidel, 2014, Pogoda, 2015).

5.3.2 Plant cultivation

A. thaliana Col-0 seeds were surface sterilized twice for 5 min in sterilization solution (10% (v/v) sodium hypochlorite, 0.05% (v/v) Triton X-100), followed by three washes with sterile water and sowing on ½ Murashige and Skoog (MS) media plates. Seeds were stratified for at least two days at 4°C in dark. Plants were cultivated in growth chambers or cabinets in long day conditions (16 h light/8 h dark) with ca. 100-130 µmol/(m²s) light fluency at 20-22°C. For identification and selection of transformed plants seeds were sown on ½ MS plates supplied with 10 µg/ml BASTA[®] (Bayer) or 25 µg/ml hygromycin B (Carl Roth). Plants used for selection, transformation and propagation were grown in the greenhouse in long day conditions at 18-20°C on “Einheitserde Werkverband e.V” and 55–65% relative humidity. Specific changes in growth conditions are indicated in the individual experiments if necessary.

5.3.3 Arabidopsis transformation by floral dip method

Flowering *A. thaliana* Col-0 plants were stably transformed using floral dip method (Clough & Bent, 1998). *A. tumefaciens* carrying the vector for expression of the gene of interest were streaked out on two LB plates supplemented with the corresponding antibiotics and incubated at 28-30°C for 48 h. Bacteria were resuspended in liquid LB media and diluted to an OD₆₀₀ of two. Five percent sucrose (w/v) was added to the bacterial suspension in a 4:1 ratio and Silwet L-77 (Lehle seeds) was supplemented to a final concentration of 0.03% (v/v). Plants were dipped upside down and agitated for 15 seconds in the cell suspension to immerse all floral buds and finally covered with foil to keep wet and dark. The transformed plants were cultivated in the greenhouse as described in section 5.3.2.

5.3.4 Selection of transformed *Arabidopsis* plants

T₁ seeds from transformed plants were harvested, sown on soil, stratified for at least two days, and grown in the greenhouse. Circa ten days after germination the seedlings were sprayed with 80 mg/l BASTA® solution every two days until resistant plants were detectable. The BASTA®-resistant seedlings were transferred to individual pots and cultivated for seed setting. The used *Agrobacterium*-mediated transformation could cause multiple insertions of the transgene into the genome (Gelvin, 2003). Therefore, transformants that show a 3:1 segregation on ½ MS plates containing 10 µg/ml BASTA® in the T₂ generation were selected and 24 resistant T₂ seedlings were further cultivated until T₃ seed setting. To obtain homozygous lines the T₃ seeds were again sown on BASTA®-containing medium on plates. Homozygous T₃ lines were used for phenotypic analysis and qRT-PCR (section 5.5.5).

5.3.5 *N. benthamiana* infiltration with *A. tumefaciens*

Infiltration with *A. tumefaciens* strain GV3101 transformed with selected constructs was used to express transiently genes of interest in *N. benthamiana* following a previously described protocol (Carbonell et al., 2008). Individual colonies of recombinant bacteria were inoculated in 5 ml LB media supplemented with 10 µg/ml rifampicin, 25 µg/ml gentamicin and corresponding plasmid-selecting antibiotic (75 µg/ml Spectinomycin or 50 µg/ml Ampicillin) and grown at 30°C. Overnight cultures were diluted with fresh induction media (LB supplemented with 10 mM MES pH 5.6, 20 µM acetosyringone, 25 µg/ml gentamicin, 10 µg/ml rifampicin; plasmid-selecting antibiotic) and incubated overnight at 30°C until OD₆₀₀ of 0.5 (BioPhotometer plus, Eppendorf) was reached. Cells were harvested by centrifugation for 10 min at 4000 rpm and room temperature (RT) and resuspended to an OD₆₀₀ of one in infiltration media (LB supplemented with 10 mM MES pH 5.6, 10 mM MgCl₂ and 150 µM acetosyringone). After 3 h incubation at RT the bacterial suspension was infiltrated into *N. benthamiana* leaves using a needle-free syringe.

The ethanol induction of the *NAT-IAA14* expression (section 6.6) was performed two days after infiltration of the plants with the corresponding construct.

5.3.6 Gene response to different treatments and stresses

To evaluate the effect of the treatments described below, the expression of select genes was determined by qRT-PCR. In all cases, and after the treatments, the plant material was frozen in liquid nitrogen, total RNA was extracted according to the instructions of the peqGOLD Plant RNA Kit (VWR) and samples were incubated with dsDNase (Thermo Scientific™) prior to cDNA synthesis. PCR primers used for the subsequent qRT-PCR (section 5.5.5) are listed in the Supplementary Table 11.1.

5.3.6.1 Salt treatment

To monitor salt sensitivity, 10 day old *A. thaliana* Col-0 seedlings, grown in long day conditions on vertical plates containing ½ MS media, were transferred to a 6-well plate (Corning Incorporated) with liquid ½ MS containing 150 mM NaCl and incubated for 6 h at room temperature prior collection.

5.3.6.2 High light stress

A. thaliana plants were grown on soil (“Einheitserde Typ GS 90”) in high light (1300 $\mu\text{mol m}^{-2} \text{s}^{-1}$) or standard light conditions (mock (130 $\mu\text{mol m}^{-2} \text{s}^{-1}$)) and the rosettes were collected at 20 days. The light spectrum ranged from 230 to 1000 nm.

5.3.6.3 Deoxynivalenol treatment

To monitor the response of *NAT-IAA14* and *IAA14* to mycotoxin, 5 day old *A. thaliana* Col-0 seedlings, grown in long day conditions at 20°C on vertical ½ MS plates, were transferred to 6-well plates (Corning Incorporated) containing liquid ½ MS and incubated for 48 h on an orbital shaker (100 rpm) before adding 16.9 μM Deoxynivalenol (DON, Sigma Aldrich). After two rounds of 5 min vacuum infiltration, the plants were incubated for 4 h at 20°C on an orbital shaker (100 rpm) before collection.

5.3.6.4 Auxin treatment

To analyze auxin-induced gene expression, 5 day old *A. thaliana* Col-0 seedlings, grown on ½ MS plates, were transferred to a 6-well plate (Corning Incorporated) with 1.5 ml liquid ½ MS media per well, and incubated for two days at 20°C on an orbital shaker (100 rpm). 7 day old seedlings were treated with 1 μM IAA (Duchefa) for 30 min or 3 h before collection.

5.4 Bacterial general protocols

5.4.1 *E. coli* and *A. tumefaciens* cultivation

E. coli was cultivated overnight (16 h) at 37°C on LB containing plates or in liquid LB medium supplemented with the required antibiotics. Liquid cultures were shaken at 110 to 140 rpm.

A. tumefaciens was cultivated for 48 h at 30°C on LB plates containing appropriate antibiotics. Overnight cultures in liquid LB with corresponding antibiotics were incubated at 30°C and 110 to 140 rpm.

Stocks of either *E. coli* or *A. tumefaciens* were prepared from liquid overnight cultures mixed with sterile glycerol to a final concentration of 25% (v/v), flash-frozen in liquid nitrogen and stored at -80°C.

5.4.2 Transformation of chemically competent *E. coli*

Chemically competent *E. coli* TOP10 cells were transformed by using the heat shock method. Bacterial cells were thawed on ice, mixed with DNA (ligation products or purified plasmids) and incubated for 20 min on ice. After 1 min incubation at 42°C the heat shocked bacteria were chilled on ice before adding 400 µl SOC media (section 5.2). Next, bacterial suspension was incubated for 1 h at 37°C with agitation, plated on LB plates containing the appropriate antibiotics and incubated overnight (16 h) at 37 C.

5.4.3 Transformation of electrocompetent *A. tumefaciens*

Electrocompetent *A. tumefaciens* GV3101 cells were transformed by electroporation. Bacterial cells were thawed on ice, mixed with 10 to 50 ng DNA and pulsed in a 2 mm electroporation cuvette at 2.5 kV, 25 µFD and 400 Ω (BIO RAD MicroPulser Electroporator). Afterwards, 450 µl of SOC medium was added, cell suspension was incubated for 2 h at 30°C with agitation and then plated on LB plates containing Rifampicin and Gentamycin as well as antibiotics for selection of the plasmids used for transformation.

5.4.4 Plasmid DNA isolation from *E. coli*

After centrifugation at 4°C and 13000 rpm for 20 min plasmid DNA was isolated using GeneJET Plasmid Miniprep Kit (Thermo Scientific™) according to the manufacturers' protocol.

5.4.5 Colony PCR

Recombinant, positive *E. coli* and *A. tumefaciens* clones were identified by colony PCR. Used primers are listed in Supplementary Table 11.1. Samples for colony PCR were generated either from liquid cultures or from single colonies. In the first case, 500 µl of an overnight culture were centrifuged for 10 min at 14,000 rpm and room temperature and the bacterial pellet was resuspended in 50 µl of sterile ddH₂O. The suspension was incubated at 90°C for 10 min, kept on ice for 2 min and centrifuged for 10 min at 14,000 rpm at room temperature. In the second case, a single colony was transferred into 25 µl of ddH₂O, incubated at 90°C for 10 min, centrifuged for 10 min at 14,000 rpm. In both cases 1 µl of the

supernatant were used as template for a 10 µl colony PCR reaction. DreamTaq DNA Polymerase (Thermo Scientific™) was used for the PCR reaction as described in section 5.5.4.

5.5 Molecular biology methods

5.5.1 RNA extraction

For total RNA extraction, including small RNAs, the protocol described by Chomczynski and Sacchi was used with slight modifications (Chomczynski & Sacchi, 2006). After grinding the material, denaturing solution (4 M guanidinium thiocyanate, 25 mM sodium citrate (pH 7), 0.5% (w/v) N-laurylsarcosine, 0.1 M β-Mercaptoethanol), sodium acetate (pH 4), acidic phenol (Roti®- Aqua Phenol) and a mixture of chloroform/isoamyl alcohol (49:1) was added to extract the RNA, which was precipitated overnight with isopropanol. DNase I (RNase-free, Roche Diagnostics) treatment was followed by purification with the mini Quick spin RNA columns (Roche Diagnostics) to remove potential DNA contaminations.

Total RNA used as template for RT-PCR was extracted with the Plant RNA Kit (peqGOLD) according to manufactures' protocol.

5.5.2 Nuclear RNA extraction

Nuclear RNA extraction was performed like described in (Csorba et al., 2014). Briefly, 1 g of 7 d old *A. thaliana* Col-0 seedlings was grinded and resuspended in 5 ml ice-cold wash buffer (20 mM Tris-HCl pH7.5, 2.5 mM MgCl₂, 25% glycerol). The suspension was filtrated through two layers of Miracloth (Merck) and centrifuged at 1,500 g and 4°C during 5 min. To lyse the cells and organelles, but to keep the nuclei intact, the resuspension of the pellet was carefully performed with 5 ml ice-cold fractionation buffer (20 mM Tris-HCl pH7.5, 2.5 mM MgCl₂, 25% glycerol, 0.3% triton X-100) and the suspension centrifuged at 1,500 g and 4°C for 10 min. The process was repeated and the supernatants from the second centrifugation were retained as cytosolic fraction and the pellet containing the nuclei was resuspended in 500 µl lysis buffer (20 mM Tris-HCl pH7.5, 200 mM potassium chloride, 2 mM DTT, 1% triton X-100). Nuclear and cytosolic fractions were extracted with phenol/chloroform and RNAs were precipitated with 0.1 vol. of 3 M sodium acetate and 1 vol. isopropanol. 300-400 ng of nuclear and 1.5-2 µg of cytosolic RNAs were used for cDNA synthesis with gene-specific primers (section 5.5.4) and analyzed by qRT-PCR (section 5.5.5) with a threshold value of 0.2. Detection of nuclear *U6* RNA and cytoplasmic *GLYCERALDEHYDE 3-PHOSPHATE DEHYDROGENASE (GAPDH)* mRNAs was used to address the purity of the fractions.

5.5.3 RNA and DNA concentration measurement

Nucleic acid concentration and purity were determined by using the Infinite M200 NanoQuant (Tecan) measuring the absorbance of 2 μ l of a sample at 260 nm (A260) and 280 nm (A280). A260/280 value allowed the evaluation of the sample purity. Samples with an A260/280 ratio between 1.7 and 1.9 and between 1.8 and 2, for DNA and RNA preparations, respectively, were used for further studies.

5.5.4 Reverse transcription Polymerase chain reaction (RT-PCR)

Unless otherwise indicated, for cDNA synthesis, oligo(dT)-primer and SuperScript® II Reverse Transcriptase (Thermo Scientific™) were used according to the manufacture's instruction. PCRs were performed with Phusion High-Fidelity DNA Polymerase (Thermo Scientific™) or DreamTaq DNA Polymerase (Thermo Scientific™) using specific primers (Supplementary Table 11.1). Reagents included in the amplification reaction and their corresponding volumes are listed in Table 5.3. The synthesis time of the expected amplicon was calculated based on the polymerase synthesis velocity and on the length of the amplicon. The general thermal profile of both enzymes is depicted in Table 5.4. The PCR products were separated either on an agarose gel or by non-denaturing polyacrylamide gel electrophoresis and stained with SERVA DNA stain G.

Table 5.3: PCR components used for gene amplification with Phusion™ and DreamTaq™ DNA Polymerase.

Phusion High-Fidelity DNA Polymerase		DreamTaq DNA Polymerase	
component	volume	component	volume
Phusion High-Fidelity DNA Polymerase (2 units/ μ l)	0.2 μ l	DreamTaq DNA Polymerase (5 units/ μ l)	0.06 μ l
5 X Phusion buffer	4 μ l	10 X DreamTaq buffer	1 μ l
[10mM] dNTPs	0.4 μ l	[10mM] dNTPs	0.2 μ l
[10pmol/ μ l] forward primer	1 μ l	[10pmol/ μ l] forward primer	0.2 μ l
[10pmol/ μ l] reverse primer	1 μ l	[10pmol/ μ l] reverse primer	0.2 μ l
template (0.5 ng) – or sterile milliQ water	1 μ l	Template – or sterile milliQ water	1 μ l for Colony PCR / 0.5 μ l for RT-PCR
sterile milliQ water	up to a final volume of 20 μ l	Sterile milliQ water	up to a final volume of 10 μ l

Table 5.4: Thermal profiles of Phusion™ and DreamTaq™ PCR.

phase	cycle number	Phusion High-Fidelity DNA Polymerase		DreamTaq DNA Polymerase	
		temperature	duration	temperature	duration
initial denaturation/activation	1	98°C	30 sec	95°C	90 sec
denaturation	35	98°C	10 sec	95°C	30 sec
annealing		$T_m^z+3^\circ\text{C}$	30 sec	$T_m^z-5^\circ\text{C}$	30 sec
extension		72°C	30 sec/kb ^y	72° C	1 min/kb ^y
final extension	1	72°C	5 min	72°C	5 min

^z T_m: melting temperature of the primer with the lower T_m

^y velocity of the respective enzyme, the extension time was adjusted considering the length of the expected amplicon

5.5.5 qRT-PCR

Quantification of transcript levels was determined by qRT-PCR (Quantitative real-time PCR) using Fast SYBR® Green Master Mix (Applied Biosystems). Components and their corresponding volumes are listed in Table 5.5. The amplification reaction was carried out using specific primer listed in Supplementary Table 11.1. The analysis was performed with the 7500 Fast Real-Time PCR system (Applied Biosystems) using the PCR cycle listed in Table 5.6. All used primer pairs have a similar amplification efficiency of 2. The threshold was set to 0.4 unless otherwise specified. The following formula was used to calculate the fold enrichment:

$$\text{fold gene expression} = 2^{\Delta|C_t|} \quad (1)$$

Table 5.5: Components and volumes used for qRT-PCR.

component	volume
Fast SYBR® Green Master Mix	5 µl
[10pmol/µl] forward primer	0.1 µl
[10pmol/µl] reverse primer	0.1 µl
template	1 µl
sterile milliQ water	3.8 µl

Table 5.6: qRT-PCR thermal profile.

phase	cycle number	temperature	duration
initial denaturation/activation	1	95°C	20 sec
denaturation	40	95°C	3 sec
annealing/extension		60°C	30 sec
melting curve	1	95°C	15 sec
		60°C	60 sec
		95°C	15 sec
		60°C	15 sec

5.5.6 Gel electrophoresis of DNA molecules

PCR products and restriction fragments were separated, depending on size and abundance, by electrophoresis in 0.8-2% agarose gels or in 5-10% non-denaturing polyacrylamide gels. The agarose was dissolved by heating in 1x TAE (40 mM Tris-HCl (pH 8.4), 20 mM acetic acid, 1 mM EDTA). Stain G (Serva) for DNA staining was added (3 µl/100 ml) and poured into a gel tray. Samples were mixed with 6x DNA Loading Dye (30% glycerol; 0.25% (w/v) bromophenol blue; 0.25% xylene cyanol) to a final concentration of 1x before loading on the gel. As DNA markers, GeneRuler™ 1 kb DNA Ladder, GeneRuler™ 100 bp DNA Ladder and GeneRuler™ Ultra Low Range DNA Ladder (Thermo Scientific™) were used. Electrophoretic separation was performed in 1x TAE at 100-120 V. Non-denaturing polyacrylamide gels were stained in diluted Stain G (Serva) for 10 min followed by a washing step in 1x TAE or ddH₂O. Gels were analyzed by GeneGenius Bio Imaging System (Syngene).

5.5.7 DNA extraction from gels

DNA from agarose gel was purified by using the GeneJET Gel extraction kit (Thermo Scientific™) following manufacturers' instructions. To extract DNA from non-denaturing polyacrylamide gels the gel slice was incubated in PAGE-DNA extraction buffer (100 mM Tris-HCl pH8.9, 1 mM EDTA pH8, 0.5% SDS) at 37°C overnight. After centrifugation at 4°C and 13000 rpm for 20 min and re-extraction with the extraction buffer, the DNA was precipitated with ethanol and STE (10 mM Tris-HCl, 1 mM EDTA, 100 mM NaCl, pH 8.0). After centrifugation, the pellet was resuspended in ddH₂O. Purified DNA fragments were used for sequencing or cloning.

5.5.8 Gateway cloning

The Gateway system (Thermo Scientific™) was employed for molecular cloning to obtain gene, amiRNA or guide RNA expression in plants. For directional cloning of blunt-end PCR products corresponding to the different *IAA14* and *NAT-IAA14* constructs the pENTR™/D-TOPO™ (Thermo Scientific™, section 5.1.2) was used. The 5' end of the forward primers (Supplementary Table 11.1) included an additional CACC non-template sequence to mediate the directional amplicon insertion into the pENTR™/D-TOPO™ vector by topoisomerase I. The TOPO® cloning reaction of purified PCR products was performed according to manufacturer's instructions and the products were transformed in One Shot® Competent *E. coli* cells (Invitrogen) or into chemically competent *E. coli* as described in section 5.4.2. Positive clones were confirmed via colony PCR (section 5.4.5) using vector-specific primers or by restriction assays. Plasmid DNA of positive transformants was extracted with the GeneJET Plasmid Miniprep Kit (Thermo Scientific™) and the sequence was confirmed by the sequencing service (Eurofins Genomics).

To generate expression clones via the Gateway system, an LR reaction with Gateway® LR Clonase™ II enzyme Mix (Thermo Scientific™) including the entry clone and destination vector was prepared. 60 ng of DNA of entry clone was mixed with 60 ng of the destination vector in a total volume of 4 µl. 1 µl Gateway® LR Clonase™ II enzyme Mix was added and the reaction incubated at 25°C for one hour. After adding 1 µl proteinase K (Fermentas), the mixture was incubated at 37°C for 10 min to terminate the LR reaction. Typically, 1 µL of reaction mixture was used in subsequent transformation into chemically competent *E. coli* or One Shot® Competent *E. coli* cells (Invitrogen). Positive clones were confirmed via colony PCR (section 5.4.5) and sequenced with a suitable primer.

5.5.9 Golden Gate assembly

Golden-gate cloning (Engler et al., 2009) using type IIs restriction enzymes and T4 DNA ligase was performed to generate constructs to determine the influence of *NAT-IAA14*, whose expression was initiated by an ethanol-inducible promoter, on *IAA14* and to analyze the co-expression of *NAT-IAA14* and *IAA14* in *N. benthamiana*. The modules were amplified by PCR using primers with BsaI or BpiI recognition sites at the 5' end, cloned in an intermediate cloning vector with recombination sites overlapping BsaI/BpiI cleavage sites and sequenced. Ligation-digestion (Table 5.7) was performed with intermediate plasmids (20 fmol each plasmid) and acceptor plasmids in the presence of the BsaI/BpiI enzyme (New England Biolabs), T4 DNA Ligase (Thermo Scientific™), 1 mM ATP and 1x CutSmart buffer (50 mM potassium acetate, 20 mM Tris-acetate, 10 mM magnesium acetate, 100 µg/ml BSA).

Table 5.7: Thermal profile for ligation-digestion reaction.

temperature	time	
37 °C	4 min	} 50x
20 °C	2 min	
37 °C	5 min	
50 °C	5 min	
70 °C	5 min	

Each module can be ligated only to another module that contains the next consecutive homologous module sequence. In the Supplemental Figure 11.3-11.6 the vector maps are depicted. Constructs were infiltrated in *N. benthamiana* as described in section 5.3.5.

5.5.10 CRISPR/Cas9 genome editing

Used vectors were kindly provided by Dr. Mily Ron (University California, Davis, unpublished). The fragments including the guide RNA (gRNA) sequence (designed by CHOPCHOP website) were amplified by PCR (section 5.5.4) with primers listed in Table 5.8 using the *pENT^R_L1L2_tRNA gRNA scaffold* vector as template. PCR products were cloned into the *pENT^R_L1/L2_AtU6gRNA* vector (Supplemental Figure 11.1), which allows gRNA expression driven by the *A. thaliana U6* promoter, via digestion-ligation reaction (Table 5.7) using BbsI (Thermo Scientific™) and T4 DNA ligase (Fermentas). The obtained products were transformed into chemically competent TOP10 *E. coli* cells (section 5.4.2). Recombinant plasmids were purified from the resulting colonies and the identity of the inserts was confirmed by sequencing. The LR reaction was performed as described in section 5.5.8 with pMR333_OLEp-OLE_GFP (Supplemental Figure 11.2) as acceptor vector containing *RPS5A::Cas9* (*Cas9* gene under the control of the constitutively expressed ribosomal promoter) and *OLE1::GFP* (*GFP* gene under the control of a seed coat promoter, allowing GFP-selection of transformed seeds). The vector was transformed into *A. thaliana* using the floral dip method (section 5.3.3) and T₁ seeds expressing GFP were selected with a Leica MZ FLIII fluorescence stereomicroscope (Leica Fluo Combi™). Seedlings derived from the selected seeds were analyzed by PCR for the presence of deletions (section 5.5.5). T₂ seeds, obtained from selected T₁ plants carrying the desired deletions, were screened for negative GFP signal in the seed coat and genotyped to confirm deletion homozygosity and the absence of the *Cas9* gene. T₃ plants were analyzed by PCR to verify the homozygous deletions and the absence of the *Cas9* gene. Primers used for the PCR selection of deletion positive plants are listed in Supplementary Table 11.1.

Table 5.8: PCR primers for guide strand amplification used for CRISPR/Cas9 genome editing.

target	gRNA	F/R	primer sequence (5'-3')
<i>IAA14</i> (473 bp) ^z	TCAGAAGA GCGGCGA AGCAGAG	F	CACCGAAGACCTATTGAACAAAGCACCAGTGGTC
		R	ATATGAAGACCGCCGCTCTTCTGATGCACCAGCCG GGAATCG
	AGATATGA ACCTTAAG GAGA	F	TATAGAAGACGAGCGGCGAAGCAGGTTTTAGAGCT AGAAATA
		R	ATATGAAGACAGAACTCTCCTTAAGGTTTCATATCT TGCACCAGCCGGGAATCG
<i>NAT-IAA14</i> (305 bp) ^z	GTTATGCC AAGCATTT AGGG	F	CACCGAAGACCTATTGAACAAAGCACCAGTGGTC
		R	ATATGAAGACATGCTTGGCATAACTGCACCAGCCG GGAATCG
	AAACAAGT AATCTTAG GCAG	F	TATAGAAGACCCAAGCATTAGGGGTTTTAGAGCT AGAAATA
		R	ATATGAAGACAGAACTGCCTAAGATTACTTGTTT TGCACCAGCCGGGAATCG
<i>NAT-IAA14</i> (1538 bp) ^z	GGAACATG AGATGTAA TCAA	F	CACCGAAGACCTATTGAACAAAGCACCAGTGGTC
		R	ATATGAAGACACATCTCATGTTCTGCACCAGCCG GGAATCG
	AAACAAGT AATCTTAG GCAG	F	TATAGAAGACTGAGATGTAATCAAGTTTTAGAGCTA GAAATA
		R	ATATGAAGACAGAACTGCCTAAGATTACTTGTTT TGCACCAGCCGGGAATCG
<i>NAT-IAA14</i> (1923 bp) ^z	GGAACATG AGATGTAA TCAA	F	CACCGAAGACCTATTGAACAAAGCACCAGTGGTC
		R	ATATGAAGACACATCTCATGTTCTGCACCAGCCG GGAATCG
	ATTCTTCTT ACCGTAAA CGG	F	TATAGAAGACTGAGATGTAATCAAGTTTTAGAGCTA GAAATA
		R	ATATGAAGACAGAAACCCGTTTACGGTAAGAAGAA TTGCACCAGCCGGGAATCG
<i>NAT-IAA14</i> (2144 bp) ^z	GGAACATG AGATGTAA TCAA	F	CACCGAAGACCTATTGAACAAAGCACCAGTGGTC
		R	ATATGAAGACACATCTCATGTTCTGCACCAGCCG GGAATCG
	AACCAGTT CAGAAGTT AAGC	F	TATAGAAGACTGAGATGTAATCAAGTTTTAGAGCTA GAAATA
		R	ATATGAAGACAGAAACGCTTAAGTTCTGAACTGGTT TGCACCAGCCGGGAATCG

^z Size of the DNA fragment, which is theoretically removed by the gRNA-mediated cleavage.

5.5.11 DAPI staining

4',6-Diamidin-2-phenylindol (DAPI) is a fluorescent dye preferentially binding to AT-rich DNA (Andrade & Arismendi, 2013). To analyze the integrity of isolated nuclei (section 5.5.2) DAPI staining was performed. For nuclei staining 0.2% of the second resuspension in fractionation buffer was mixed with 0.5 µg/ml DAPI (diluted in 1x PBS) and analyzed by microscopy (Axioplan).

5.6 Biochemical methods

5.6.1 RNA stability measurements

RNA half-lives were determined as previously described (Fedak et al., 2016). *A. thaliana* Col-0 seedlings were grown on ½ MS plates and after 11 d transferred to a 6-well-plate containing incubation buffer (1 mM PIPES pH 6.25, 1 mM trisodium citrate, 1 mM KCl, 15 mM sucrose). After 30 min of incubation, 150 mg/l cordycepin (3'-deoxyadenosine, in DMSO) was added and vacuum-infiltrated (2x 5 min). Seedlings were collected at regular time-points every 15 min (0, 15, 30, 45, 60, 75, 90, 105 and 120 min) and frozen in liquid nitrogen. Total RNA was isolated with the peqGOLD Plant RNA Kit (VWR) following manufacturer's instruction and analyzed by qRT-PCR (sections 5.5.4, 5.5.5). *EXPANSIN-LIKE1* (*Expansin L1*), a short-lived transcript, and *EUKARYOTIC TRANSLATION INITIATION FACTOR 4A1* (*EIF4A1A*), a long-lived mRNA, were used as controls. For half-life calculation and statistical analysis, all samples were normalized to their respective C_t -value at time point 0 ($C_{t(0)}$, formula 2) and plotted as degradation curves. Slope of this curve was used to calculate RNA half-lives ($t_{1/2}$, formula 3).

$$C_{t(n)} = (\ln(C_t/C_{t(0)})*(-10)) \quad (2)$$

$$t_{1/2} = (\ln 2)/|\text{slop}| \quad (3)$$

5.6.2 Radioactive *in vitro* transcription

³²P-labeling by *in vitro* transcription was performed to generate probes for the RNase protection assay using [α ³²P]-UTP (Hartmann Analytic). Components and their corresponding volumes are listed in Table 5.9. After incubation for 2 h at 37°C, the reaction was stopped by adding 5 U DNase I (Roche Diagnostics) and by incubating the mixture at 37°C for 15 min. The *in-vitro* transcripts were purified using mini Quick Spin RNA Columns (Roche Diagnostics) following manufacturer's protocol. The labeling efficiency was measured with a Scintillation Counter and expressed as cpm/µl. The integrity and purity of the riboprobes was analyzed by a 5% denaturing PAGE following phosphorimaging.

Table 5.9: Components and volumes used for ³²P-labeling of *in vitro* synthesized transcripts.

component	volume
100 ng purified PCR product or 500 ng linearized plasmid	x µl
10x transcription buffer	2 µl
5 mM rATP, rCTP, rGTP 0.5 mM rUTP	2 µl
[α ³² P]-UTP	2 µl
RiboLock (Thermo Scientific™)	0.5 µl
T7-RNA-Polymerase (Roche Diagnostics)	1.5 µl
sterile milliQ water	up to 20 µl

5.6.3 RNase protection assay

The RNase protection assay was performed as described in the manufactures' protocol RPA III™ kit (Thermo Scientific™) to determine the ends of *NAT-IAA14*. 10 µg of total RNA extracted from 11 d old Col-0 seedlings were mixed with 4,000 cpm of the ³²P-labeled probe. For RNA precipitation 0.1 vol. of 5 M NH₄OAc and 2.5 vol. of 100% ethanol were added, incubated at -20°C for 15 min and centrifuged at RT for 15 min with 14,000 rpm. The pellet was air dried for 5 min and resuspended in 10 µl Hybridization Buffer III (provided in the kit). The samples were denatured at 90°C for 2 min and to hybridize the ³²P-probe with its complementary RNA incubated at 42°C overnight. RNase T1 was mixed 1:25 with RNase Digestion III Buffer (150 µl, provided in the kit) and 150 µl of this mixture were added to the samples. After 30 min incubation at 37°C the RNase T1 was inactivated by adding 225 µl RNase Inactivation/Precipitation III Solution (provided in the kit), and the RNAs recovered by precipitation at -20°C for 90 min and centrifugation at RT for 15 min with 14,000 rpm. The pellet was air dried for 5 min and resuspended in 5 µl Gel Loading Buffer II (provided in the kit). The samples were separated on a 5% PAGE after heat denaturation at 90°C for 2 min and signals detected by exposure to an x-ray film.

5.6.4 Circular RACE

Rapid amplification of cDNA ends (RACE) is a widely used PCR-based method to identify the 5' and 3' ends of transcripts by using cDNA as template.

5.6.4.1 5'RACE

The 5'RACE was performed as described in (Dallmeier & Neyts, 2013) with small modifications (Supplemental Figure 11.11 A). 5 µg of total *A. thaliana* Col-0 RNA was used for first strand cDNA synthesis performed with SuperScript III™ (Thermo Scientific™) according to the instruction manual. The gene-specific primer (1250 pmol) for cDNA

synthesis was phosphorylated using T4 Polynucleotide Kinase (NEB) according to manufacturer's instruction. After reverse transcription 1 U RNase H (Thermo Scientific™) was added and the mixture incubated at 37°C for 1 h. cDNA ends were ligated using T4 RNA Ligase (NEB) for approximately 16 h and precipitated at -20°C by adding 2.5x 100% ethanol and 0.5 µl GlycoBlue™ (Amersham). The circular cDNA was used, after resuspension, as template for nested PCR. Amplification products were separated on a 10% non-denaturing polyacrylamide gel, cut and purified from the gel by overnight incubation at 37°C with elution buffer (100 mM Tris-HCl pH 8.9, 1 mM EDTA pH 8, 0.5% SDS). After ethanol precipitation using STE (10 mM Tris-HCl, 1 mM EDTA, 100 mM NaCl, pH 8.0) the PCR products were cloned into pZero®-2 (Thermo Scientific™, section 5.4.2) and positive clones that carry the insert were identified by PCR analysis (section 5.4.5) and sequenced.

5.6.4.2 3'RACE

The 3'RACE (Supplemental Figure 11.11 B) follows the same principle as the 5'RACE. First steps were the removal of the potential cap-structure using *Tobacco acid pyrophosphatase* (Invitrogen, FirstChoice® RLM-RACE Kit), the ligation of 5' and 3' RNA ends using T4 RNA Ligase (NEB) and precipitation. The circularized transcripts were reverse transcribed using gene-specific primer and afterwards 1 U RNase H (Thermo Scientific™) was added and incubated at 37°C for 1 h. The amplicons generated after nested PCR were separated on a 10% non-denaturing polyacrylamide gel and purified from the gel by overnight incubation at 37°C with elution buffer (100 mM Tris-HCl pH 8.9, 1 mM EDTA pH 8, 0.5% SDS). PCR products were cloned into pZero®-2 (Thermo Scientific™, section 5.4.2) after ethanol precipitation using STE (10 mM Tris-HCl, 1 mM EDTA, 100 mM NaCl, pH 8.0). Positive clones carrying the inserts were identified by PCR analysis (section 5.4.5) and initial transcripts ends determined by sequencing.

5.6.5 Northern Blot

Northern Blot was performed for the detection of mature amiRNAs targeting *NAT-IAA14* RNA. Total RNA from fresh leaf material was extracted as described in section 5.5.1, denatured for 10 min at 65°C in loading solution (10 M urea, 1.5 mM EDTA (pH 8), 0.25% (w/v) bromophenol blue, 0.25% (w/v) xylencyanol) and separated by electrophoresis on a 17% denaturing PAGE containing 7 M urea and 0.5x TBE (45 mM Tris-HCl (pH 8.3), 45 mM boric acid, 1 mM EDTA). The RNAs were transferred to a nylon membrane (Roche Diagnostics) using a semi-dry blotting unit (BioRad®) and crosslinked twice with UV-light. For the detection of small RNAs, radiolabeled oligonucleotide probes were used, which were prepared using T4-polynucleotide kinase (Thermo Scientific™) and [$\gamma^{32}\text{P}$]-ATP (Hartmann

Analytic) according to manufacturer's instructions. Oligoprobes were purified by miniQuick spin oligo columns (Roche Diagnostics) and the integrity and concentration was checked by performing denaturing polyacrylamide gel electrophoresis and Scintillation Counter measurement (cpm/ μ l). Blotted membranes were pre-hybridized using Perfect Hyb™ Plus buffer (Sigma Aldrich) at 68°C for 30 min followed by a 16 h hybridization with appropriate oligoprobes (1,5 mil cpm) at 42°C (temperature depends on nucleotide composition of the oligo [$T(^{\circ}C) = (4(G+C) + 2(A+T)) - 20(^{\circ}C)$]). After an initial washing step with SSC buffer (1.5 M NaCl; 150 mM sodium citrate) for 5 min at room temperature, the membrane was incubated twice for 20 or 30 min each at 40°C with SSC buffer supplemented with 0.5% SDS solution and finally rinsed with 3x SSC. The signal on the membranes was detected by autoradiography or visualized by phosphor imaging using a Typhoon FLA 7000 phosphor imager. Oligoprobes used for the specific detection of amiRNAs are listed in Supplementary Table 11.1. *U6* snRNA was used as loading and hybridization control.

5.6.6 Production of capped and polyadenylated transcripts

Capped and polyadenylated transcripts were used for *in vitro* translation assay kindly performed by Dr. T. Gursinsky, MLU Halle (Saale). Components and their corresponding volumes are listed in Table 5.10. The *in vitro* transcription reaction was performed as described in section 5.6.2 including the m⁷G(5')ppp(5')G RNA cap structure analog to obtain capped molecules. After purification of the transcripts using the RNA cleanup kit (New England Biolabs) according the manufacturer's protocol, the RNA was polyadenylated (Table 5.11). The reaction was incubated for 30 min at 37°C and the RNA was purified with the RNA cleanup kit (New England Biolabs). The integrity and purity of the *in vitro* transcripts was analyzed on a 5% denaturing PAGE.

Table 5.10: Components and volumes used for *in vitro* synthesis of capped transcripts.

component	volume
250 ng PCR product (with T7 promoter)	x μ l
5x transcription buffer	4 μ l
10 mM rATP, rCTP, rGTP, rUTP	4 μ l
8 mM m ⁷ G(5')ppp(5')G	2 μ l
RiboLock (Thermo Scientific™)	0.5 μ l
T7-RNA-Polymerase	2 μ l
sterile milliQ water	up to 20 μ l

Table 5.11: Components and volumes of the polyadenylation reaction of *in vitro* synthesized transcripts.

component	volume
capped RNA	x μ l (as much as possible)
10x <i>E.coli</i> Poly(A) Polymerase Reaction Buffer	2 μ l
10 mM rATP	2 μ l
Poly(A) Polymerase (NEB)	1 μ l
RiboLock (Thermo Scientific™)	0.5 μ l
sterile milliQ water	up to 20 μ l

5.6.7 Silver staining of nucleic acids

Silver staining of non-denaturing and denaturing polyacrylamide gels was performed for detecting small amounts of nucleic acids. First, the gel was incubated in fixing solution (10% (v/v) ethanol, 0.5% (v/v) acetic acid in ddH₂O) for at least 5 min with agitation and then stained for 20 min in staining solution (0.2 (w/v) AgNO₃ (GDR) in ddH₂O). Afterwards, the gel was incubated in development solution (3% (w/v) NaOH, 0.5% (v/v) formaldehyde in ddH₂O) until the signals appeared and then stopped by washing the gel with fixing solution. The GeneGenius Bio Imaging System (Syngene) was used to document the gel.

6 Results

6.1 Molecular analysis of the lncRNA *NAT-IAA14*

6.1.1 Determination of *NAT-IAA14* 5' and 3' ends

6.1.1.1 *NAT-IAA14* detection by RNase protection assay

NAT-IAA14 is annotated as a 755 nt long RNA molecule in the TAIR10 database. To determine, whether *NAT-IAA14* is longer than annotated and has an overlap with *IAA14*, RNase protection assay (RPA) was used. Two radioactive labeled riboprobes complementary to the *NAT-IAA14* RNA were generated by *in vitro* transcription (Figure 6.1 A). Probe_1 is 493 nt long and targets the *NAT-IAA14* 5' end region by starting 68 nt upstream of the annotated 5' end, while probe_2 is 517 nt long and targets the *NAT-IAA14* 3' end region by ending 162 nt downstream of the annotated 3' end. *In vitro* transcribed RNAs that were complementary to the riboprobes (RNA_1 and RNA_2) were used as controls in the assay to ensure complete riboprobe protection.

The *NAT-IAA14* transcript was detected in total RNA extracts from 10 d old Col-0 seedlings using the ³²P-labeled probe_1 after 7 d of exposure (lane 3 in Figure 6.1 C and D). The identified transcript (indicated with a red asterisk) seems to have the same size as the transcript present in total RNA preparations from plants overexpressing the *NAT-IAA14* annotated sequence (*NAT-IAA14ox*, lane 2) that was included as control (section 6.8.1). This result indicates that the *NAT-IAA14* transcript contains the sequence reported in the TAIR10 database at its 5' end. The almost complete digestion of ³²P-labelled probe_1 is shown in lane 4, indicating that the incubation time of the assay was sufficient to digest all of the single-stranded, unprotected RNA by RNase T1.

The 3' end of *NAT-IAA14* was detected in total RNA preparations from 11 d old Col-0 seedlings using the ³²P-labeled probe_2 after 5 weeks of exposure (Figure 6.1 E and F). In addition to the undigested ³²P-labeled probe_2 signal, a second, smaller band (indicated with a red asterisk) was obtained in the total Col-0 RNA extracts (lane 2), showing that the endogenous *NAT-IAA14* 3' end is shorter than the riboprobe. However, the exact length of the detected *NAT-IAA14* 3' end remained undetermined as no size marker was included. The presence of a band of the same size as the ³²P-labeled probe_2 in the yeast RNA (lane 3) indicates that the digestion of unprotected RNA by RNase T1 was incomplete.

In conclusion, this assay showed that the *NAT-IAA14* RNA can be detected in total RNA extracts from Col-0 seedlings. The long exposure time required to detect the transcripts indicates that the abundance of the *NAT-IAA14* transcript is relatively low at the developmental stage analyzed. However, the precise *NAT-IAA14* transcript ends cannot be exactly defined by the performed assay.

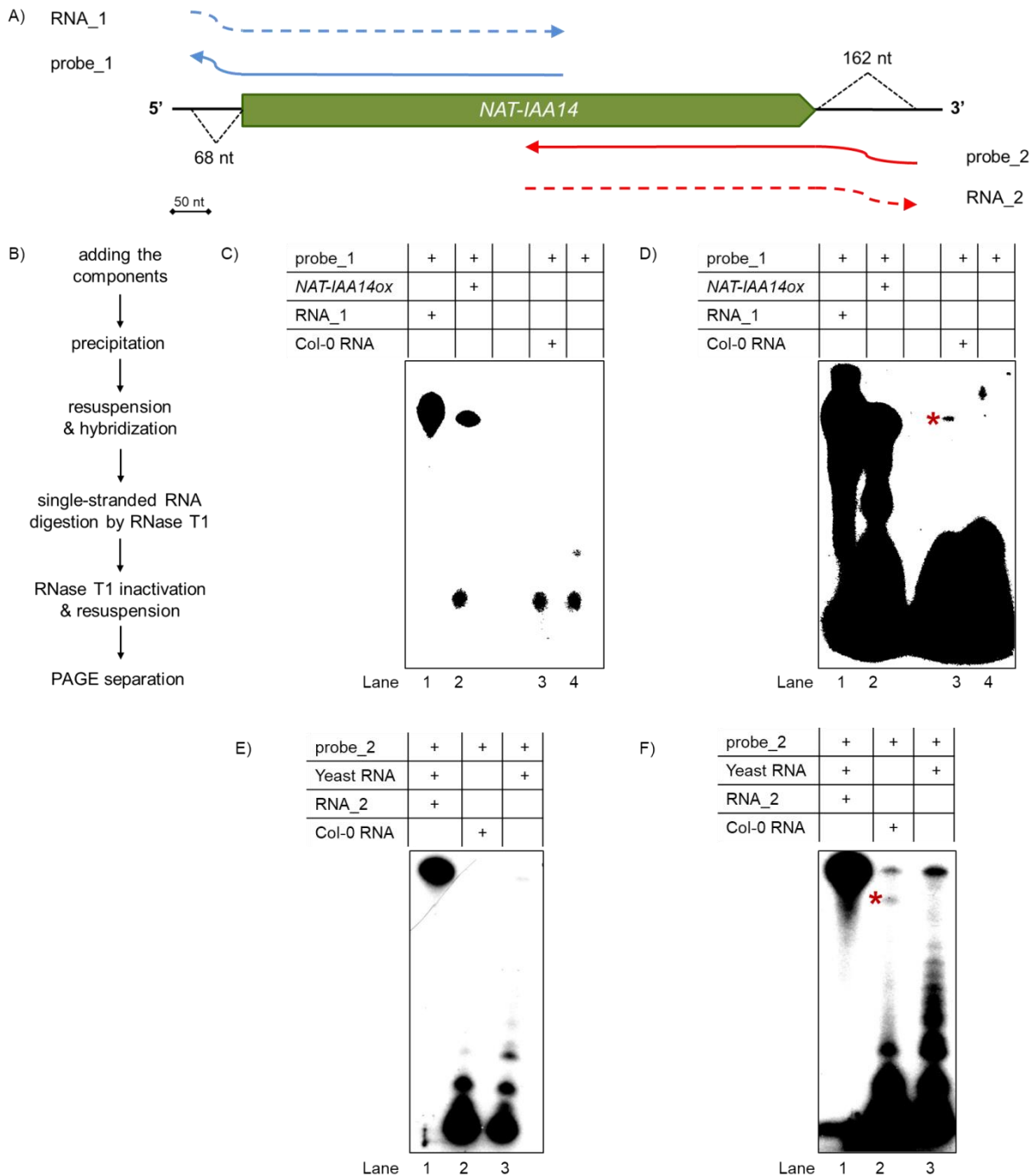


Figure 6.1: RPA-mediated detection of the *NAT-IAA14* transcript in total RNA extracts of Col-0.

Schematic representation of the 755 nt long *NAT-IAA14* transcript (green, arrow indicates transcription direction) and the probe regions (blue, red) for detecting *NAT-IAA14* (A). Probe_1 (blue) is 493 nt long and probe_2 (red) is 517 nt long and target the *NAT-IAA14* 5' or 3' end region, respectively. The RNA_1 (dotted blue) and the RNA_2 (dotted red) are complementary to 32 P-labeled probe_1 and probe_2, respectively, that were labeled with 32 P. Arrows indicate probe direction. The procedure of the RPA is shown in (B). Transcript end determination was performed using total RNA extracts from Col-0 seedlings or plants overexpressing the annotated *NAT-IAA14* transcript (*NAT-IAA14ox*) by RNase protection (B) with probe_1 (C and D) and probe_2 (E and F) followed by electrophoresis on denaturing polyacrylamide gels (PAGE). C) and D) shows the x-ray film of the same experiment that was exposed for 3 h or 7 d, respectively, while E) and F) from another experiment were exposed for 3 d or 5 weeks, respectively. Red asterisks highlight the corresponding 32 P-labeled probe protected by the *NAT-IAA14* transcript.

6.1.1.2 *NAT-IAA14* RNA starts 15 nt downstream of the reported 5' end

To confirm the results of the RNase protection assay (section 6.1.1.1) and to get more defined *NAT-IAA14* 5' and 3' transcript ends, circular RACE was used. By circular 5'RACE (Supplemental Figure 11.11 A) an expected PCR product of about 230 bp was detected after nested PCR using total RNA extracts of 11 d old Col-0 seedlings (Figure 6.2 A) and 37 d old Col-0 leaves (Figure 6.2 B) as templates. After sequencing ten clones, which showed the same sequence (Supplemental Figure 11.12), the *NAT-IAA14* 5' end was determined to start 15 nt downstream of the annotated TSS (Figure 6.2 C). The additional cytosine between the 5' and 3' end of the *NAT-IAA14* transcript was added by the SuperScript III reverse transcriptase as reported previously (Zajac et al., 2013).

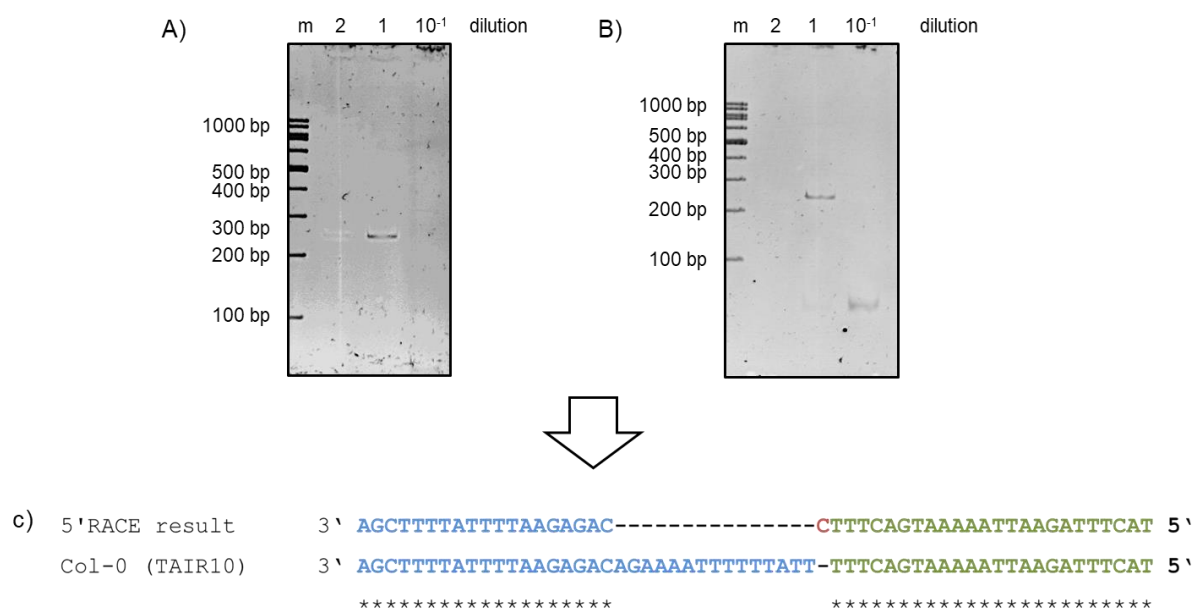


Figure 6.2: *NAT-IAA14* RNA starts 15 nt downstream of the annotated transcription start site.

Shown are amplicons from nested PCR (using 2 μ l, 1 μ l and 0.1 μ l of the first PCR as template) of total RNA extracts from 11 d old Col-0 seedlings (A) and 37 d old Col-0 leaves (B), separated in non-denaturing polyacrylamide gels. An alignment of the reported sequence and the *NAT-IAA14* 5'RACE sequence obtained after cloning in pZero[®]-2 and sequencing is depicted in (C). Blue nucleotides display the *NAT-IAA14* 5' end sequence, while green nucleotides highlight the 3' end sequence. The additional cytosine (red) accrues through the usage of SuperScript III.

To determine *NAT-IAA14* 3' end, circular 3'RACE (Supplemental Figure 11.11 B) was used. A PCR product of the expected size (about 233 bp) was detected (Figure 6.3 A). Sequencing confirmed the TAIR10 annotated 3' end of the *NAT-IAA14* transcript (Figure 6.3 B, Supplemental Figure 11.13). The six sequenced clones showed a stretch of thymines (ranging from 5 to 34) at the 3' end, indicating that the *NAT-IAA14* RNA is polyadenylated (Supplemental Figure 11.13). In addition, a deletion from 57 to 129 nucleotides of the 5' end was detected (Supplemental Figure 11.13) potentially caused by degradation during the preparation.

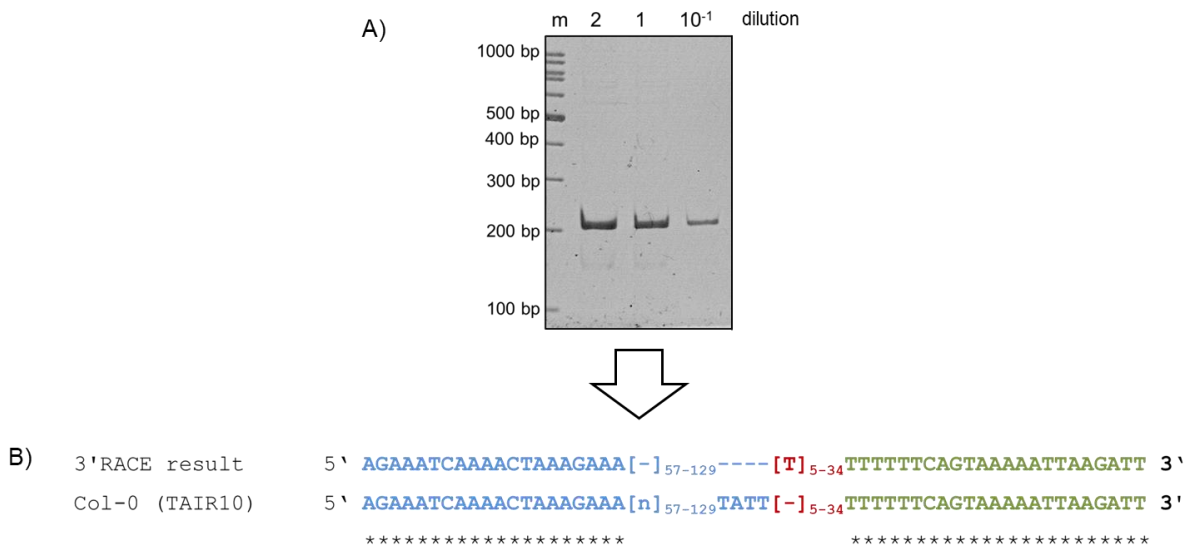


Figure 6.3: Determination of *NAT-IAA14* 3'end by circular 3'RACE.

Separation in non-denaturing polyacrylamide gels of the PCR products from the nested PCR (using 2 μ l, 1 μ l and 0.1 μ l of the first PCR as template) of total RNA preparations of 11 d old Col-0 seedlings are shown after 3'RACE (A). Cloning in pZero[®]-2 and sequencing of the amplicons resulted in the annotated *NAT-IAA14* 3'end after alignment with the reported Col-0 sequence (B). The sequence of the annotated *NAT-IAA14* 3'end is shown in green. A stretch of thymines present in the sequence of the 3'RACE amplicon is highlighted in red and the 5'end is shown in blue. n (A, T, G, C) represents the nucleotides missing from the reported *NAT-IAA14* 5'end (blue). A consensus sequence out of six clones is depicted.

In summary, the circular RACE showed that the 5'end of *NAT-IAA14* transcript starts 15 nt downstream of the annotated TSS. The 3'end corresponds to the annotated sequence in TAIR10 and no longer *NAT-IAA14* variants with an *IAA14* overlap were detected using this method. In addition to RPA and RACE, RT-PCR walking was performed to analyze the length of *NAT-IAA14* using different primer combinations targeting regions downstream the reported *NAT-IAA14* 3'end (Supplemental Figure 11.10 A). Two times, an amplicon covering the complete *IAA14* transcript was detected in Col-0 seedlings at the fully expanded cotyledon stage (Supplemental Figure 11.10 B and C). These results suggest that in particular conditions, longer *NAT-IAA14* molecules, which completely overlap *IAA14*, can be transcribed.

Furthermore, as already mentioned before (section 4) 3'RACE and Southern blot analysis has already shown in the laboratory that an *IAA14* transcript variant 124 nt-longer than the in TAIR10 annotated *IAA14* sequence is present in Col-0 plants (Seidel, 2014). The longer *IAA14* 3'UTR results in an overlap of 67 nt with the *NAT-IAA14* transcript (Figure 6.4 A). To estimate the ratio between both *IAA14* transcripts, cDNA synthesis was performed using the primers RR70 and RR72. The quantity of the annotated *IAA14* transcript was determined by subtracting the threshold cycle (C_t) value of the 124 nt-longer *IAA14*

transcript (RR72) from the one of the total *IAA14* transcripts (RR70). Based on this calculation, the 124 nt-longer *IAA14* transcript and the reported transcript were present in a 60%:40% ratio (Figure 6.4 B). Due to this overlap, the longer *IAA14* transcripts could be regulated by *NAT-IAA14*.

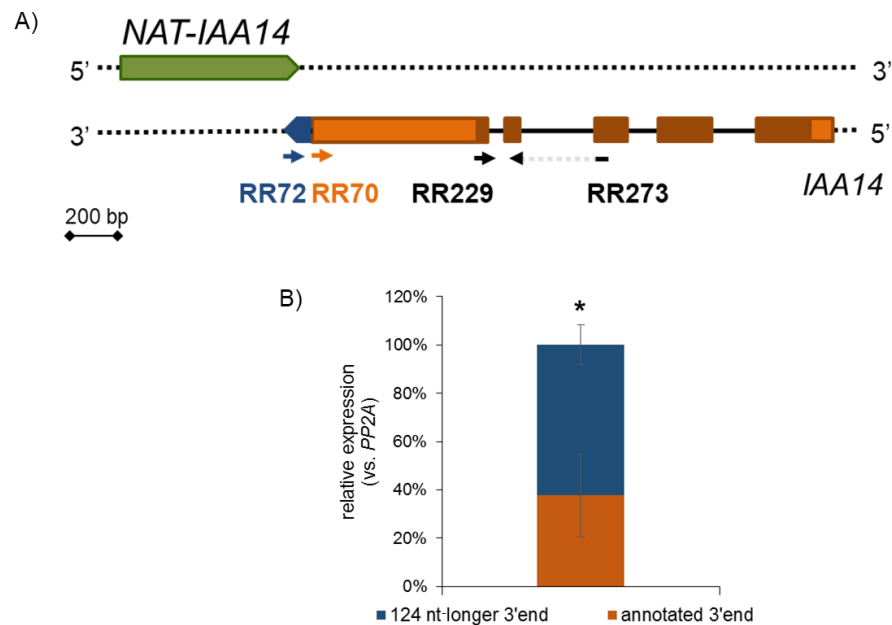


Figure 6.4: 60% of the *IAA14* transcripts have an overlap of 67 nt with *NAT-IAA14*.

Schematic representation of the genomic region of *NAT-IAA14* (green) and *IAA14* (brown: exon; orange: *UTR*, A). The 124 nt-longer *IAA14* 3'UTR region is indicated in dark-blue. Primers used for cDNA synthesis (RR70, RR72) and for qRT-PCR (RR273, RR229) are indicated. The proportion of annotated and 124 nt-longer *IAA14* transcripts was measured using total RNA extracts of 14 d old Col-0 seedlings (B). qRT-PCR results were normalized by *PP2A* and values correspond to averages with SD from three independent, biological experiments. (Student's t-test: * ≤ 0.05)

6.1.2 *NAT-IAA14* is a stable transcript

The stability of a transcript can give a hint on its subcellular localization and is therefore an important feature for the characterization of lncRNAs. It is assumed that short-lived transcripts act in the nucleus at the transcriptional level, whereas RNAs with a long half-life are transported to the cytosol to achieve their function (Fedak et al., 2016). The half-life of RNAs can be determined by using a cordycepin-dependent assay that blocks transcription elongation once cordycepin is incorporated into the nascent RNA. The slope of the resulting degradation curve allows RNA half-life calculation.

To compare the half-life of the lncRNA *NAT-IAA14* and the protein-coding mRNA *IAA14*, Col-0 seedlings were treated with 150 mg/l cordycepin and a degradation curve was plotted (Figure 6.5 A). This approach showed that *NAT-IAA14* has a half-life of about 99 min which is similar to that of the protein-coding transcript *IAA14* with a half-life of about 111 min (Figure 6.5 B). To validate the experimental conditions the half-lives of two previously

characterized mRNAs (Fedak et al., 2016), *Expansin L1* with a half-life of approximately 35 min and *EIF4A1* with a half-life of more than 120 min, were determined. The long half-life of the *NAT-IAA14* RNA indicates a cytosolic localization and suggests a function at the posttranscriptional level. This high stability of the *NAT-IAA14* transcript suggests a *trans*-acting function that requires the diffusion of an RNA molecule over a long distance.

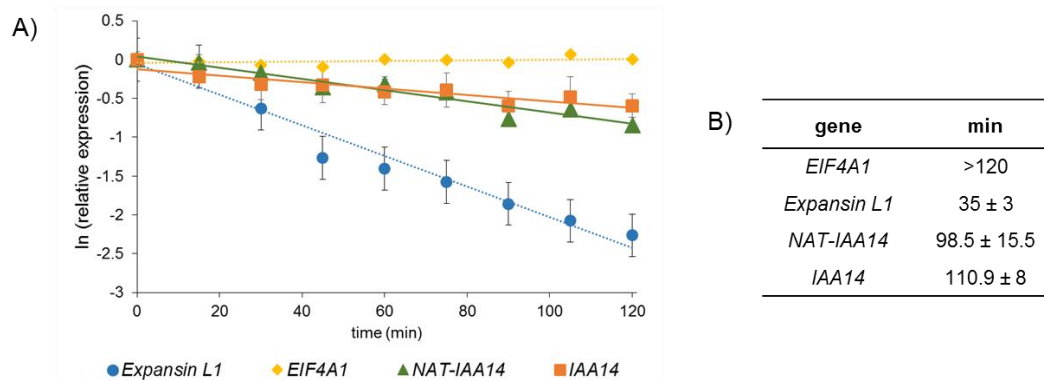


Figure 6.5: RNA half-life determination of *NAT-IAA14* transcripts performed in Col-0 seedlings. Half-life (B) was calculated based on degradation curves after cordycepin treatment (A) using stable (transcript of eukaryotic translation initiation factor 4A1, *EIF4A1*) and short-lived (*EXPANSIN-LIKE1*, *Expansin L1*) transcripts as controls. Values correspond to averages with SD from three independent experiments.

6.1.3 *NAT-IAA14* is localized in the cytosol

In order to confirm *NAT-IAA14* localization in the cytosol and to strengthen its *trans*-acting mode of action (section 6.1.2), nuclear and cytosolic transcripts were isolated by subcellular fractionation from Col-0 seedlings and analyzed by qRT-PCR. The purity of the fractions was evaluated by the detection of the internal controls *U6*, a nuclear small RNA involved in splicing (Dunn & Rader, 2010) present in the nucleus, and *GAPDH*, a protein-coding mRNA localized in the cytosol. C_t -values representing the levels of the individual transcripts in the extracts are shown in Figure 6.6. Low C_t -values or high C_t -values point to high or low transcript abundance, respectively.

The protein-coding RNAs *GAPDH* and *IAA14* were detected in high levels in the “cytosolic” fraction. The lncRNA *NAT-IAA14* was enriched in the “cytosolic” RNA extract and at the detection limit in the nuclear extract, suggesting the transport of the *NAT-IAA14* RNA to the cytosol. In nuclear extracts the mRNAs *GAPDH* and *IAA14* were not detected or only in small amounts, while *U6* was present in high levels in the nuclear fraction, which suggests a clean nuclear extract without cytosolic contamination. However, *U6* was also present in the “cytosolic” fraction, implying that some nuclei broke during the purification process.

Taken together, these results and the high stability of *NAT-IAA14* (section 6.1.2) indicate a transport to the cytosol and suggest a *trans*-acting mode of action.

A)	gene	nuclear extract ^Z	„cytosolic“ extract ^Z
	<i>GAPDH</i>	n.d. ^Y	22.6
	<i>U6</i>	17.9	13.8
	<i>NAT-IAA14</i>	39.2	25.7
	<i>IAA14</i>	37.9	25.2

B)	gene	nuclear extract ^Z	„cytosolic“ extract ^Z
	<i>GAPDH</i>	n.d. ^Y	22.7
	<i>U6</i>	17.1	14.5
	<i>NAT-IAA14</i>	n.d. ^Y	23.3
	<i>IAA14</i>	n.d. ^Y	23.8

C)	gene	nuclear extract ^Z	„cytosolic“ extract ^Z
	<i>GAPDH</i>	n.d. ^Y	23.4
	<i>U6</i>	15.6	15.4
	<i>NAT-IAA14</i>	32.0	26.8
	<i>IAA14</i>	36.0	26.8

Figure 6.6: *NAT-IAA14* localization in the cytosolic fraction of Col-0 seedlings.

The mRNA *GAPDH* and the nuclear small RNA *U6* were used as internal controls for cytosolic and nuclear fractions, respectively. The threshold cycle C_t values between the two extracts cannot be compared due to the different quantities of input RNA (5x more RNA in the cytosolic fraction than in the nuclear fraction). Additionally, a 1:2 dilution of cDNA from the nuclear fraction was used in the qRT-PCR. Shown are C_t -values of three biological replicates (A)-C) determined by qRT-PCR. n.d. = not detectable

6.1.4 *NAT-IAA14* expression is reduced by cycloheximide treatment

Nonsense-mediated decay (NMD) is known to determine the fate of incorrect RNAs carrying premature termination codons to prevent the synthesis of truncated proteins, but it also regulates levels of normal mRNAs (Rayson et al., 2012). Furthermore, it has been reported that several lncRNAs with features like mRNAs are degraded by NMD (Kurihara et al., 2009). Since the lncRNA *NAT-IAA14* has a poly(A)-tail (Figure 6.3) and no introns, is located in the cytosol and contains five potential open-reading frames (pORFs, Supplemental Figure 11.14) it is likely that the *NAT-IAA14* transcript is target of the NMD pathway in *A. thaliana*. It is reported that the *NAT-IAA14* transcript level is slightly increased in the NMD mutants *upstream frame shift protein 1-1* (*upf1-1*) and *upstream frame shift protein 3-1* (*upf3-1*, (Kurihara et al., 2009)).

NMD-sensitive transcripts accumulate in plants when protein synthesis is blocked (Rayson et al., 2012). To test whether the cytosolic lncRNA *NAT-IAA14* is degraded by NMD, Col-0 seedlings were treated with the translation elongation inhibitor cycloheximide for 45 min and 4 h (Figure 6.7). In response to the treatment, the levels of the *SUPPRESSOR OF MORPHOLOGICAL DEFECTS ON GENITALIA PROTEIN 7* (*SMG7*, Figure 6.7 A) mRNA, a known target of NMD that was analyzed as control, were significantly increased. Analysis of the *NAT-IAA14* transcript initially showed a slight but significant increase after 45 min of treatment with cycloheximide. This result, like that of the control transcript *SMG7*, indicates RNA stabilization after treatment and *NAT-IAA14* as target of NMD. Nevertheless, the *NAT-IAA14* transcript level was significantly decreased to 50% after 4 h treatment compared to the mock control (Figure 6.7 B), suggesting that protein synthesis is required for basal *NAT-IAA14* transcription. Hypothetically, a protein involved in the expression or stabilization of the *NAT-IAA14* RNA could be blocked by cycloheximide treatment itself, resulting in a reduction of the *NAT-IAA14* transcript level.

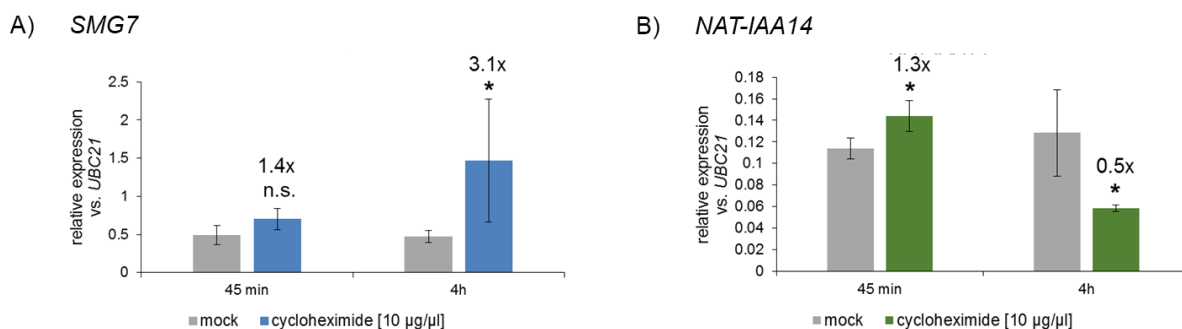


Figure 6.7: Analysis of *NAT-IAA14* transcript as NMD target.

10 d old Col-0 seedlings grown in long-day conditions were treated with cycloheximide (10 µg/µl in DMSO) or DMSO (mock) for 45 min and 4 h. qRT-PCR results of *SMG7* (A) and *NAT-IAA14* (B) transcript levels were normalized by *UBC21*. Values correspond to averages with SD from two independent experiments with two biological replicates each. (Mann-Whitney Rank Sum Test: * ≤ 0.05 (A), Student's t-test: * ≤ 0.05 (B), n.s. = not significant, Mann-Whitney Rank Sum Test was applied, because the data were not equally distributed.)

6.2 *NAT-IAA14* and *IAA14* transcript levels undergo changes during plant development

The expression of several genes is tightly regulated and altered by the development of *A. thaliana*. In addition to the analysis of the promoter activity at different developmental stages performed in a previous work (section 4, (Pogoda, 2015), the transcript levels of the lncRNA *NAT-IAA14* and the protein-coding RNA *IAA14* were analyzed by qRT-PCR (Figure 6.8). *NAT-IAA14* RNA levels increased up to 4.6-fold in rosettes during plant senescence. In contrast, *IAA14* transcript levels decreased to one-third along plant aging. The expression of sense and antisense RNA showed opposite levels during plant development. In young rosettes (14 d-25 d) *IAA14* levels are higher than those of the *NAT-IAA14* transcript, while in older rosettes *NAT-IAA14* levels are similar or even higher than *IAA14* mRNA levels. Both transcripts are expressed in flowers of 45 d old plants with relatively similar transcript abundance. The high error bars of the three replicates of *IAA14* can be explained by the sampling at different time points, because *IAA14* is reported to be regulated by light and the circadian clock (Covington & Harmer, 2007).

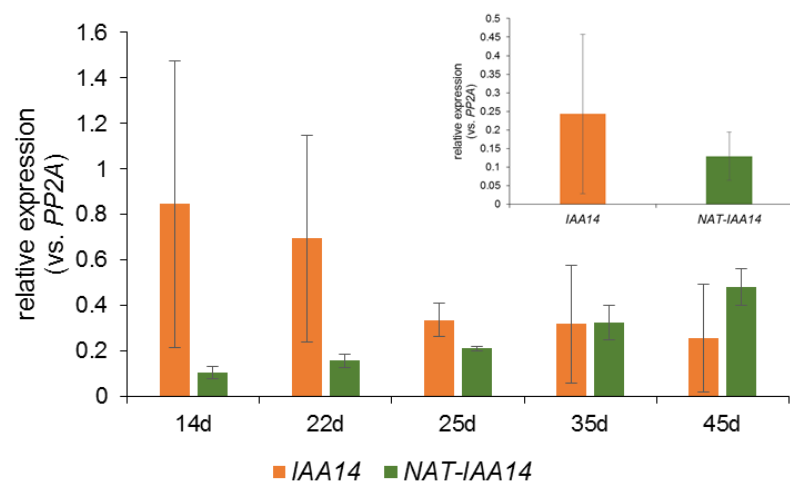


Figure 6.8: *NAT-IAA14* and *IAA14* transcript levels are altered during Arabidopsis life cycle.

Rosettes of Col-0 plants were harvested at different time points (each sample includes at least three rosettes without stems). Expression in flower tissue of 45 d old plants is shown as inset. *NAT-IAA14* (green) and *IAA14* (orange) qRT-PCR results were normalized by *PP2A* and values correspond to averages with SD from three independent experiments.

In addition, qRT-PCR analysis over cDNA using Oligo(dT) from total RNA extracts of 8 d and 10 d old Col-0 seedlings dissected in leaf, root and shoot apex showed a higher basal *IAA14* transcript level compared to *NAT-IAA14* RNA abundance (Figure 6.9). Interestingly, small changes in one transcript are reflected in a similar expression alteration of the other gene.

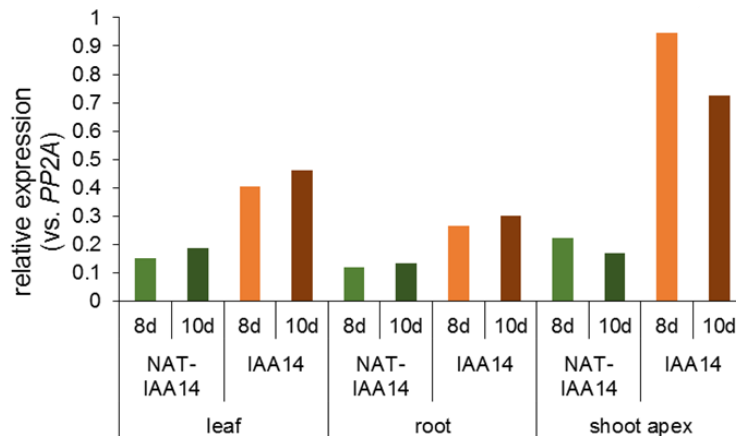


Figure 6.9: *NAT-IAA14* and *IAA14* transcript levels showed a correlated expression pattern in leaf, root and shoot apex in young seedlings.

Leaves, roots and shoot apices were collected from 8 d and 10 d old Col-0 seedlings grown in long-day conditions. qRT-PCR results of *NAT-IAA14* (green) and *IAA14* (orange) were normalized by *PP2A* and values correspond to one representative experiment of two independent experiments.

Collectively, these data demonstrate that *NAT-IAA14* is expressed in Col-0 rosettes during all stages of plant development and that the transcript level increases with plants senescence, while *IAA14* RNA levels decrease, suggesting a discordant regulation of *IAA14* and *NAT-IAA14* transcript abundance at these developmental stages.

6.3 *NAT-IAA14* expression shows a variable response to light

Light is a key factor in *A. thaliana* growth and development by modulating the expression of several genes. Furthermore, light has been reported to reduce free auxin and to increase LONG HYPOCOTYL 5 (HY5), which is involved in the regulation of transcription of light-induced genes (Ang et al., 1998, Chattopadhyay et al., 1998), resulting in elevated *IAA14* transcription (Cluis et al., 2004).

To test whether *NAT-IAA14* expression is also affected by light and thus involved in *IAA14* light expression regulation, a time-course experiment was performed with Col-0 seedlings (Figure 6.10). As reported, *IAA14* expression significantly increased between 40 min and 80 min up to 2-fold once the light switched on after 8 h of darkness (Figure 6.10 A). In contrast, *NAT-IAA14* expression in the three independent experiments did not show such a consistent pattern (Figure 6.10 C-D). In Figure 6.10 B) and C) an expression peak was detected at 30 min or 70 min, respectively. Nevertheless, this experimental design does not allow to establish a reliable correlation with the *IAA14* expression change in response to light and suggests a *NAT-IAA14* independent light induction of *IAA14* transcription.

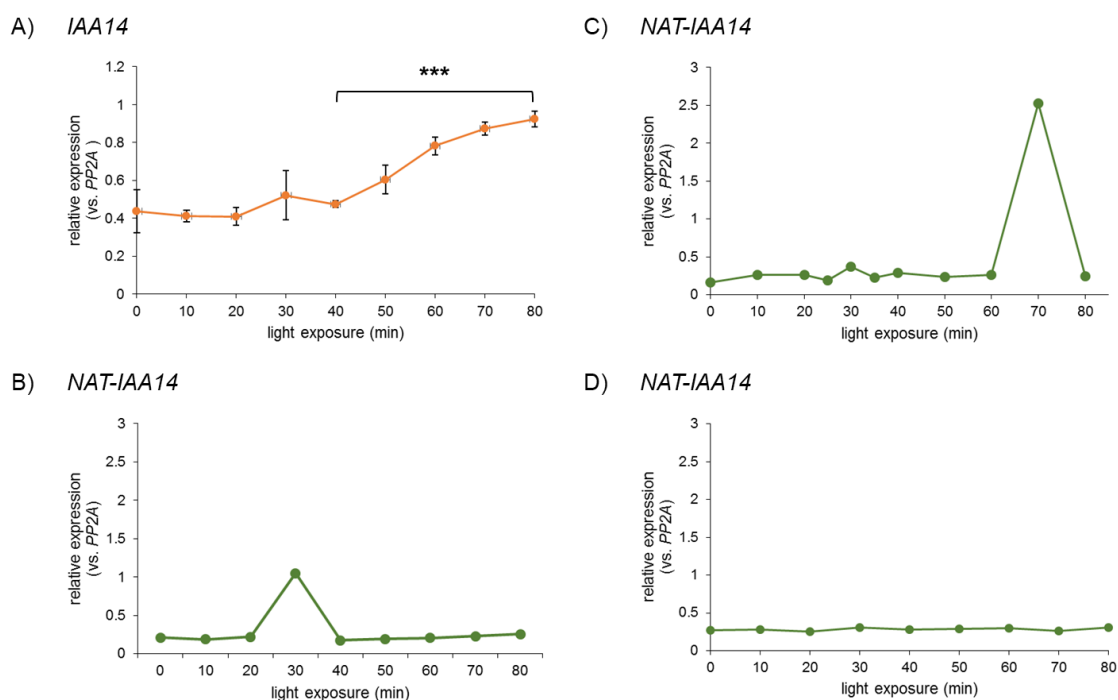


Figure 6.10: *NAT-IAA14* expression shows a variable response to light.

Transcript levels of *IAA14* (A) and *NAT-IAA14* (B-D) were determined by qRT-PCR in 11 d old Col-0 seedlings after light was switched on after 8 h of darkness. qRT-PCR results were normalized by *PP2A* and values correspond to averages with SD from three independent biological replicates (A). In (B-D) *PP2A* normalized values for individual experiment out of three independent biological replicates are shown. (Student's t-test: *** ≤ 0.005)

6.4 *NAT-IAA14* transcript levels remain unaffected in response to auxin

AUX/IAAs are reported to be auxin-responsive genes and treatment with exogenous auxin alters their expression levels. Previous studies demonstrated that treatment with 1 μM 1-naphthaleneacetic acid (NAA), a synthetic auxin, results in a three-fold increase of the basal expression level of *IAA14* (Gao et al., 2015).

To test the auxin responsiveness of *NAT-IAA14*, Col-0 plants were treated with 1 μM IAA for 30 min and 3 h (Figure 6.11). No significant change in *NAT-IAA14* expression level was detected in the used conditions (Figure 6.11 A). As control the auxin response of *IAA14* was analyzed and according to previous reports, the *IAA14* level showed a 1.8-fold and a 2.3-fold significant increase after 30 min and 3 h treatment, respectively (Figure 6.11 B). This result suggests that the *IAA14* promoter can be activated by auxin independently of the simultaneous *NAT-IAA14* transcription. However, a possible auxin response of *NAT-IAA14* cannot be completely ruled out, as earlier or later time points might show different results than the obtained ones.

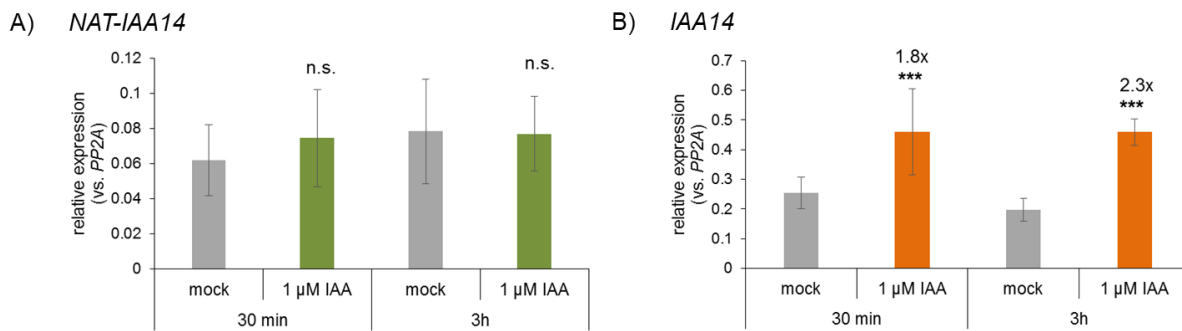


Figure 6.11: NAT-IAA14 and IAA14 response upon IAA treatment.

7 d old Col-0 seedlings, grown in long day conditions, were mock (0.001% ethanol) or 1 μM IAA (in ethanol) treated for 30 min and 3 h. qRT-PCR results of *NAT-IAA14* (A) and *IAA14* (B) transcript levels were normalized by *PP2A* and values correspond to averages with SD from one representative experiment with three biological replicates. In total three independent experiments with three biological replicates each were performed and showed consistent results. (Student's t-test: *** ≤ 0.005; n.s. = not significant)

6.5 *NAT-IAA14* and *IAA14* can be transiently co-expressed in the same *N. benthamiana* cell

Transient assay in *N. benthamiana* was used to analyze the effect of the lncRNA *NAT-IAA14* on *IAA14* expression upon simultaneous co-infiltration in the same cell. Two plasmids containing either *IAA14* tagged with GFP (GREEN FLUORESCENT PROTEIN, construct generated by Seidel, 2014, Supplemental Figure 11.8) or *NAT-IAA14*, including the gene encoding for *mCherry* on the vector (Supplemental Figure 11.7), were co-infiltrated in *N. benthamiana* leaves. For this experiment, the 124 nt-longer *IAA14* variant with an 67 nt overlap with the *NAT-IAA14* transcript was used (section 4). Fluorescence signals were investigated three days post-infiltration (dpi) with confocal laser scanning microscopy (Zeiss). GFP signal was detected in the nucleus as expected from the localization of *IAA14* (Fukaki et al., 2002) that acts as a transcriptional repressor (Figure 6.12 A). *NAT-IAA14* expression was indirectly estimated by the *mCherry* signal localized in the cytoplasm and directly confirmed by RT-PCR (Figure 6.12 B). By merging both fluorescence signals, cells, in which *NAT-IAA14* and *IAA14* are present, were detected in *N. benthamiana*, suggesting no negative transcriptional or post-transcriptional effect between both transcripts in *trans*.

Taken together, *NAT-IAA14* and *IAA14* transcripts can be expressed at the same time in the same cell in *N. benthamiana*. Further quantifications of *IAA14* protein levels are necessary to determine whether *NAT-IAA14* affects *IAA14* translation.

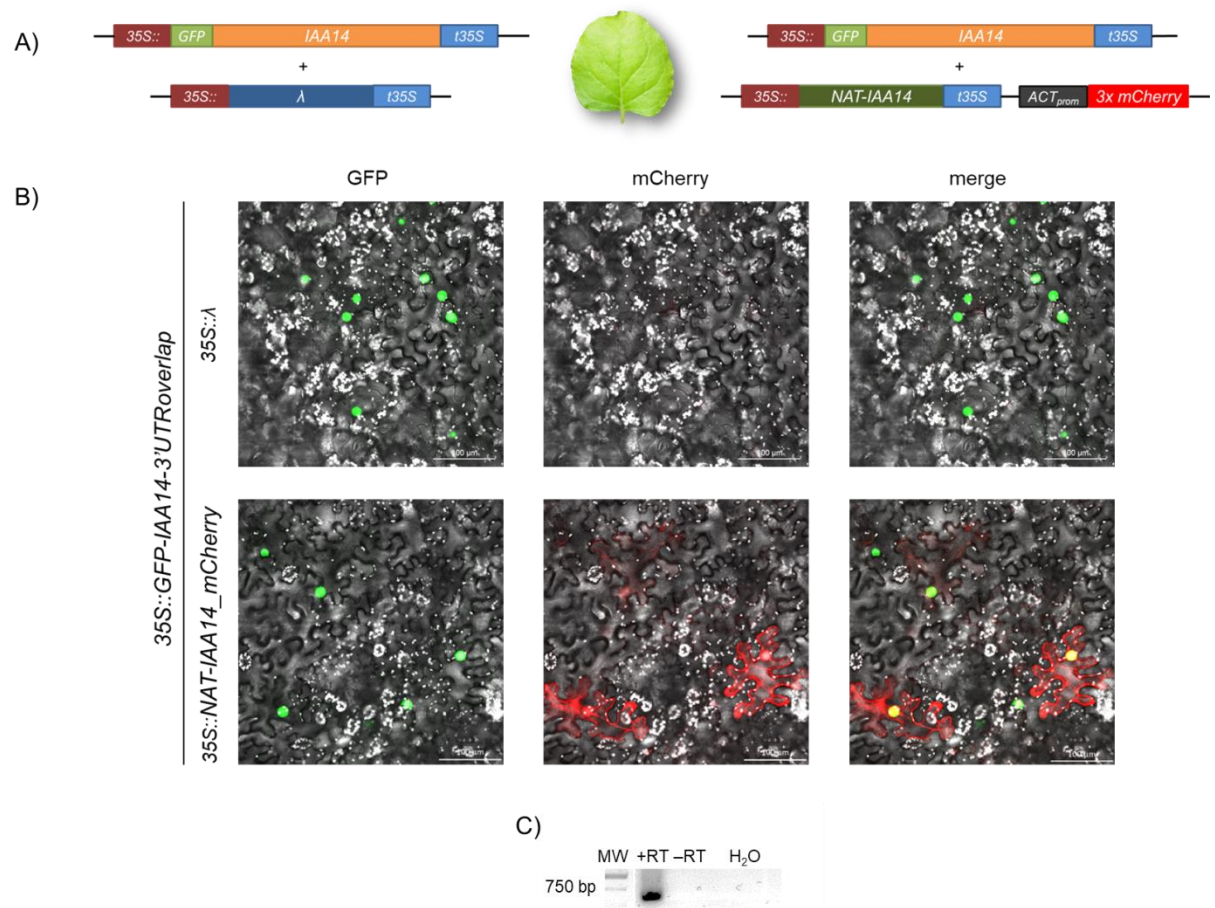


Figure 6.12: NAT-IAA14 and IAA14 co-expression upon co-infiltration in *N. benthamiana*.

Co-infiltration of the GFP-tagged *IAA14* 124 nt-longer transcript variant (with a 67 nt overlap with *NAT-IAA14*) and *NAT-IAA14* expressed from a vector including *mCherry* (A) in *N. benthamiana* leaves was analyzed 3 dpi by confocal laser scanning microscopy (B). RT-PCR confirmation of *NAT-IAA14* expression in *mCherry*-positive leaf material (C). Co-infiltration with a plasmid expressing an unrelated sequence (35S::λ, Supplemental Figure 11.9) was included as control. Pictures and RT-PCR results corresponds to one representative out of three independent experiments. (scale bar = 100 μm)

6.6 Induction of *NAT-IAA14* transcription has no influence on *IAA14* expression in *N. benthamiana*

The transient assay was used to analyze a potential impact of the *NAT-IAA14* expression on the *IAA14* transcript level. A construct containing the *NAT-IAA14*- and *IAA14*-encoding genes keeping the locus organization was generated using golden gate cloning (Supplemental Figure 11.3). In this construct, the endogenous promoter of *NAT-IAA14* was replaced by an ethanol-inducible promoter. By using the system to induce a controlled *NAT-IAA14* expression, a potential *cis*, by altering *IAA14* transcription, or *trans*, by modulating *IAA14* RNA stability, mode of action of the lncRNA on *IAA14* transcript levels can be investigated.

N. benthamiana leaves were infiltrated with the construct containing *NAT-IAA14*, including a *mS1*-tag, driven by the ethanol inducible promoter *AlcA* (Werner et al., 2011) and

IAA14 tagged with *c-Myc* under its endogenous promoter (Figure 6.13 A). Co-infiltration with another plasmid coding for *AlcR*, a transcription factor, is necessary for the ethanol induction (Supplemental Figure 11.6).

At first, the effect of ethanol on the *IAA14* expression was tested in Col-0 plants to determine whether *IAA14* levels are generally affected in response to ethanol. The *IAA14* transcript level was significantly reduced by 70% after a 4% EtOH vapor treatment for 24 h (Figure 6.13 B).

To investigate whether induction of *NAT-IAA14* expression affects *IAA14* expression or transcript level, the construct shown in Figure 6.13 A) was infiltrated in *N. benthamiana* leaves (Supplemental Figure 11.3). In three independent experiments a 9.2 to 44.6-fold induction of *NAT-IAA14* was observed by 4% EtOH vapor for 24 h in leaves that were infiltrated two days before (Figure 6.13 D-F). Accordingly, the *IAA14* transcript levels increased 2.7 to 5.4-fold, suggesting that the *IAA14* transcription could be modulated by *NAT-IAA14*.

To further confirm this data, a *prom_{IAA14}::IAA14* construct (Supplemental Figure 11.4) was included to test whether the *IAA14* promoter in *N. benthamiana* can be induced by ethanol on its own. A significant 5-fold increase in *IAA14* transcript levels was shown in *N. benthamiana* transiently expressing *prom_{IAA14}::IAA14* (Figure 6.13 C) that is similar to the obtained *IAA14* levels after *NAT-IAA14* ethanol-induced transcription (Figure 6.13 D-F). These results suggest that the increase in *IAA14* levels is not a consequence of the *NAT-IAA14* ethanol induction, but rather of the ethanol inducibility of the *IAA14* promoter in *N. benthamiana*.

Another construct was created removing the *AlcA* promoter (Supplemental Figure 11.5), abolishing the expression of *NAT-IAA14*. Nevertheless, the *NAT-IAA14* expression was still induced up to 18.3-fold (Figure 6.13 G), so that no new conclusion about the *IAA14* level could be drawn. One reason for the *NAT-IAA14* expression increase might be that the removal of the *AlcA* promoter sequence in the vector brought the gene in front of *NAT-IAA14* into close proximity and incomplete termination of this gene by the used conditions induced *NAT-IAA14* expression. On the other hand, it might be that *IAA14* is involved in the expression regulation of *NAT-IAA14* and the vector still encoded for regulatory elements that are important for *NAT-IAA14* expression.

Taken together, it has been shown that the *IAA14* transcription level increases by ethanol treatment independently of *NAT-IAA14* expression in the conditions tested. Moreover, *NAT-IAA14* expression regulation by *IAA14* cannot be excluded.

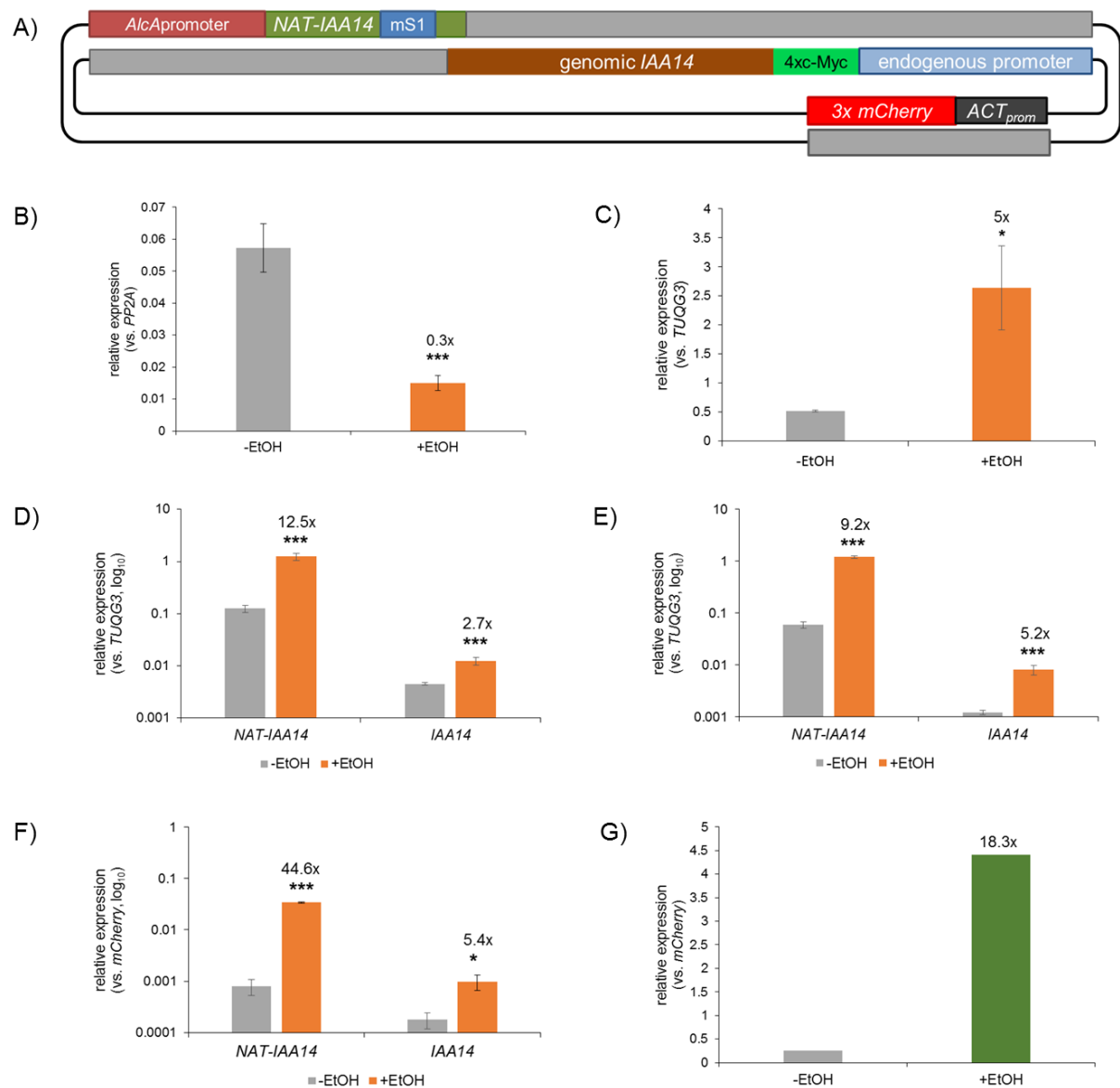


Figure 6.13: *NAT-IAA14* transcription does not influence *IAA14* expression upon ethanol induction in *N. benthamiana*.

Schematic representation of the ethanol inducible construct (A). Shown are *NAT-IAA14* (green) tagged with *mS1*-sequence (blue), which is driven by the ethanol inducible *AlcA* promoter (red) and *IAA14* (brown), tagged with *c-Myc* (light green) under its endogenous promoter (light blue, A). The ethanol inducibility of the endogenous *IAA14* promoter in *A. thaliana* was analyzed in total RNA extracts of 25 d old Col-0 rosettes (B) and by using the *prom_{IAA14}::IAA14* construct in *N. benthamiana* (C). Transcript levels were normalized by *PP2A* (B) or *TUQG3* (C) and values correspond to averages with SD from three (B) or four (C) biological replicates. In D-F) the three independent experiments with three biological replicates each the *NAT-IAA14* and *IAA14* induction by ethanol using the represented construct (A) are shown. Ethanol inducibility of *NAT-IAA14* is still present after removing the *AlcA* promoter from the construct (G). Transcript levels were normalized by *TUQG3* (D-E) and *mCherry* (F-G) and values correspond to averages with SD. All experiments (B-G) were performed in a closed system, either mock (no ethanol, -EtOH) or 4% EtOH vapor (+EtOH) treated for 24 h in leaves infiltrated two days before with the constructs. (Student's t-test (B, D, E, F): *** ≤ 0.005 , * ≤ 0.05 ; Mann-Whitney Rank Sum Test (C): * ≤ 0.05 , Mann-Whitney Rank Sum Test was applied, because the data were not equally distributed.)

6.7 *NAT-IAA14* and *IAA14* response to different abiotic and biotic stresses

As sessile organisms, plants need to respond to changing environmental conditions by regulating their gene expression. RNA sequencing (Di et al., 2014) and tiling array (Matsui et al., 2008) data already indicated that *NAT-IAA14* expression is altered in response to various abiotic stresses like cold, heat, high light, abscisic acid, salt and drought. To test the responsiveness of *NAT-IAA14* and *IAA14* transcripts to abiotic and biotic stresses, salinity, high light stress and mycotoxin Deoxynivalenol (DON) treatment were used.

To evaluate the relationship between *NAT-IAA14* and *IAA14* transcript levels in response to salt stress, Col-0 seedlings were treated with 150 mM NaCl for 6 h. *NAT-IAA14* as well as *IAA14* transcript levels were significantly decreased to 0.7-fold and 0.5-fold, respectively (Figure 6.14 A). These results confirmed the *promoter::GUS*-reporter line data from a previous study in the lab (unpublished data from Maria Pogoda) showing reduced promoter activity for *NAT-IAA14_{prom}::GUS* and *IAA14_{prom}::GUS* in response to high salinity.

Light is one of the most crucial environmental factors for plants growth and development. By changing the light intensity from 130 $\mu\text{mol m}^{-2} \text{s}^{-1}$ (mock) to 1300 $\mu\text{mol m}^{-2} \text{s}^{-1}$ (high light), the plant needs to adapt to the stress. *NAT-IAA14* and *IAA14* transcript levels increased to 2.2-fold and 2.8-fold, respectively, in plants subjected to light stress (Figure 6.14 B).

DON treatment was used to test *NAT-IAA14* and *IAA14* sensitivity to a biotic stress factor. The lncRNA transcript level was significantly reduced to 50% upon 16.9 μM DON treatment for 4 h (Figure 6.14 C left). Consistently, the *IAA14* expression level was also decreased to 80% upon treatment (Figure 6.14 D right).

Collectively, these data demonstrate that *NAT-IAA14* and *IAA14* transcripts showed concordant expression patterns in response to the different stresses tested. On the one hand, this correlation could be explained by a general modulation of gene expression caused by stress. On the other hand, it could be that *NAT-IAA14* is directly involved in the expression regulation of *IAA14* levels by stress, or inversely, *IAA14* regulates the *NAT-IAA14* expression in response to stress.

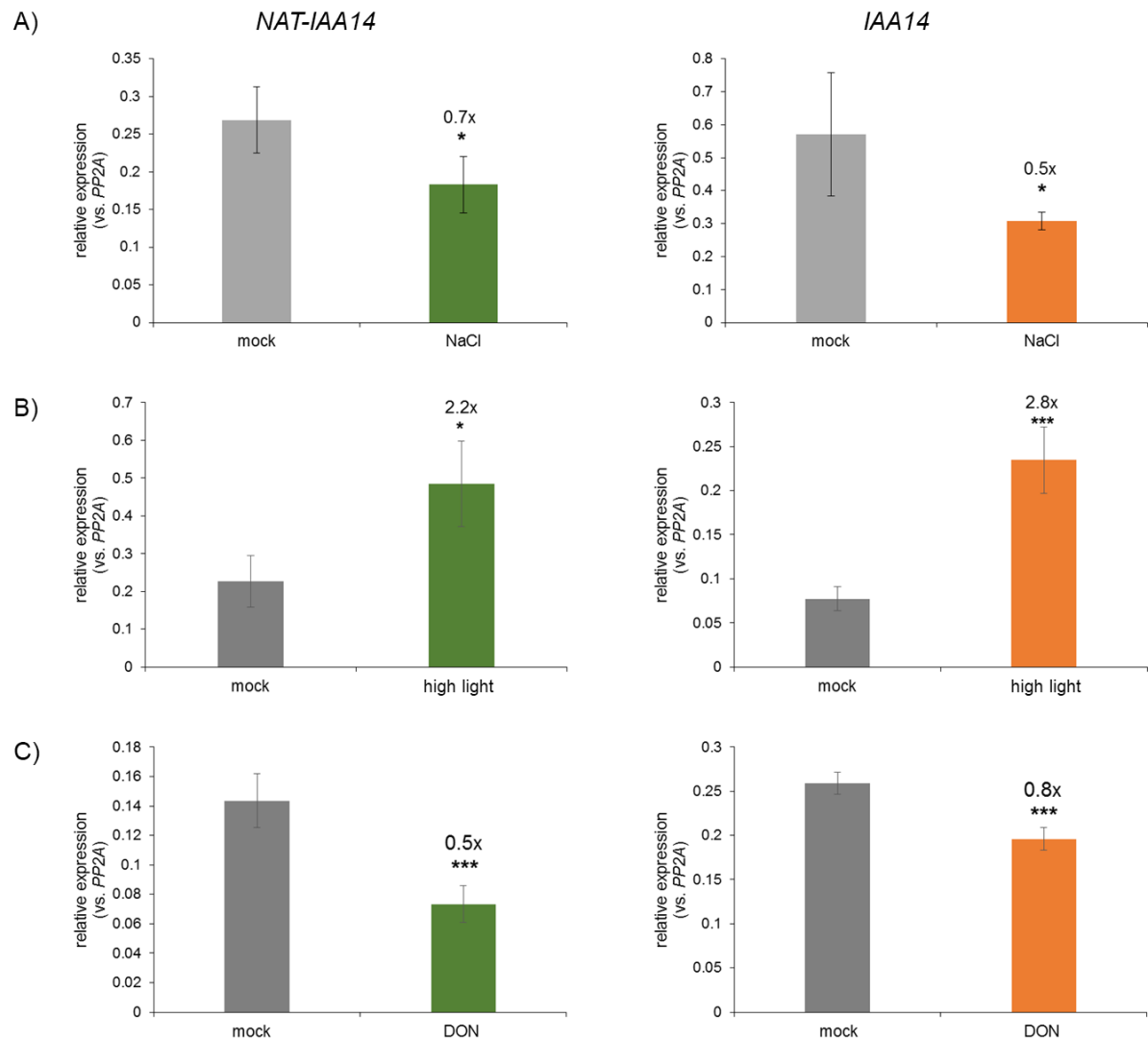


Figure 6.14: *NAT-IAA14* and *IAA14* expression is affected by different stresses.

Col-0 plants were treated with either 150 mM NaCl for 6 h (A), grown in high light ($1300 \mu\text{mol m}^{-2} \text{s}^{-1}$) (B) or incubated with deoxynivalenol ($16.9 \mu\text{M}$ DON in ethanol) for 4 h (C), or with the corresponding controls (mock). *NAT-IAA14* (left panel) and *IAA14* (right panel) transcript levels determined using qRT-PCR were normalized by *PP2A* and values correspond to averages with SD from four independent biological replicates. Samples for the light experiment were kindly provided by Dr. Balcke. (Student's t-test: * ≤ 0.05 ; *** ≤ 0.005 , Mann-Whitney Rank Sum Test: * ≤ 0.05 ((A) right panel))

6.8 Effects of *NAT-IAA14* expression alteration in Col-0 plants

A well-established method to evaluate possible transcriptional and phenotypic effects of a gene with unknown function *in planta* is the analysis of transgenic lines that overexpress or downregulate the gene of interest.

6.8.1 *NAT-IAA14* overexpression slightly alters *IAA14* transcript levels

Stable transformed, homozygous T₃-overexpression (ox)-lines of *NAT-IAA14* in *A. thaliana* were previously generated in the laboratory (Seidel, 2014). The *NAT-IAA14* construct covers the complete annotated gene region of 755 bp and is driven by the strong

35S-promoter of Cauliflower mosaic virus (CaMV). Prior to this work, a first analysis of these lines showed an opposite effect on root length and fresh weight depending on the level of *NAT-IAA14* overexpression in 7 d old seedlings (Pogoda, 2015). In the previous work it was described that a high *NAT-IAA14* overexpression resulted in lower fresh weight and shorter roots compared to 7 d old Col-0 seedlings. In contrast, a slight overexpression of *NAT-IAA14* caused a higher fresh weight and longer roots. These previously reported results could not be confirmed in this study using 14 d old seedlings.

First, *NAT-IAA14* expression level in ox-lines was determined by qRT-PCR (Figure 6.15 A). The four used stable transformed *NAT-IAA14ox* lines showed a significant *NAT-IAA14* upregulation between 13.7- and 296-fold compared to Col-0 seedlings. In these plants, the *IAA14* transcript levels are slightly, but significantly increased between 1.4- to 1.9-fold in three out of four *NAT-IAA14ox* lines (Figure 6.15 B). Nevertheless, the *IAA14* increase is not correlated with the level of *NAT-IAA14* overexpression.

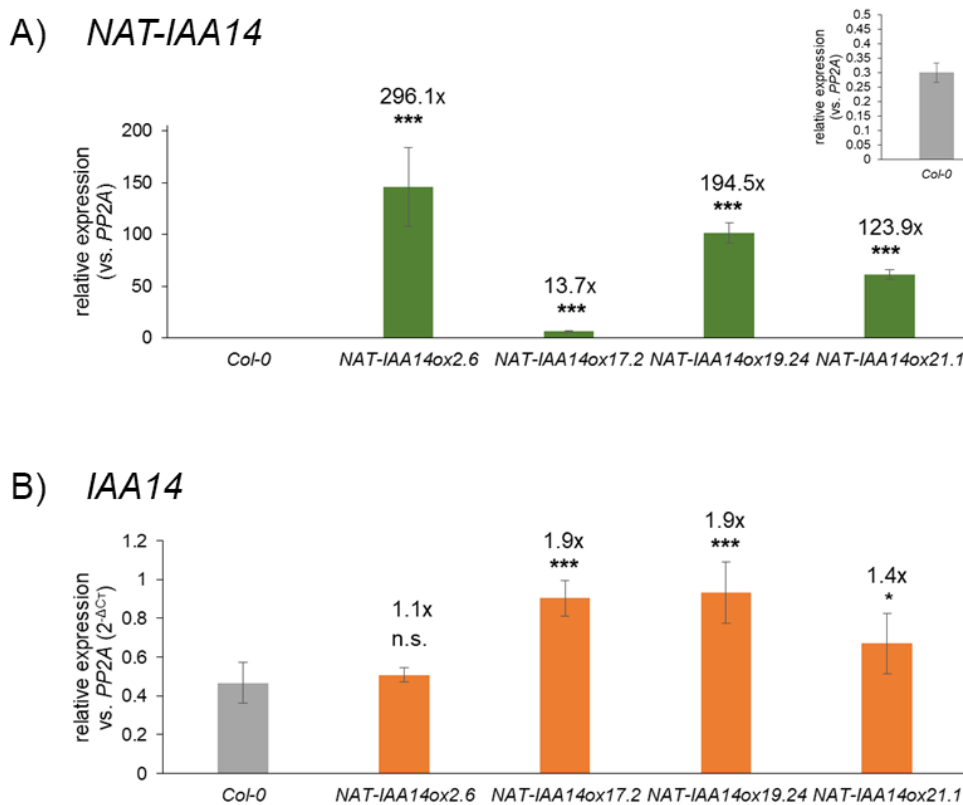


Figure 6.15: *IAA14* transcript levels are increased in three out of four *NAT-IAA14* overexpression lines.

Transcript levels of *NAT-IAA14* (A) and *IAA14* (B) were determined by qRT-PCR in 14 d old Col-0 and *NAT-IAA14ox* seedlings. The overexpressed *NAT-IAA14* construct encodes the annotated genomic region of 755 bp and is controlled by the 35S-promoter. qRT-PCR results were normalized by PP2A and values correspond to averages with SD from three independent experiments. (Student's t-test: * \leq 0.05; *** \leq 0.005; n.s. = not significant)

In the next step, the phenotype of 14 d old *NAT-IAA14ox* seedlings was analyzed. All lines showed a slightly decreased fresh weight compared to the Col-0 seedlings, and in consistency a reduced primary root length and lateral root number (Figure 6.16). Only in the lines *NAT-IAA14ox2.6* and *NAT-IAA14ox17.2*, the *NAT-IAA14* overexpression resulted in a significant decrease of plant growth. No correlation between the level of overexpression and the obtained phenotype could be determined.

Taken together, the results suggest that the overexpression of *NAT-IAA14* might reduce plants growth by decreasing its fresh weight and accordingly also primary root length and lateral root number.

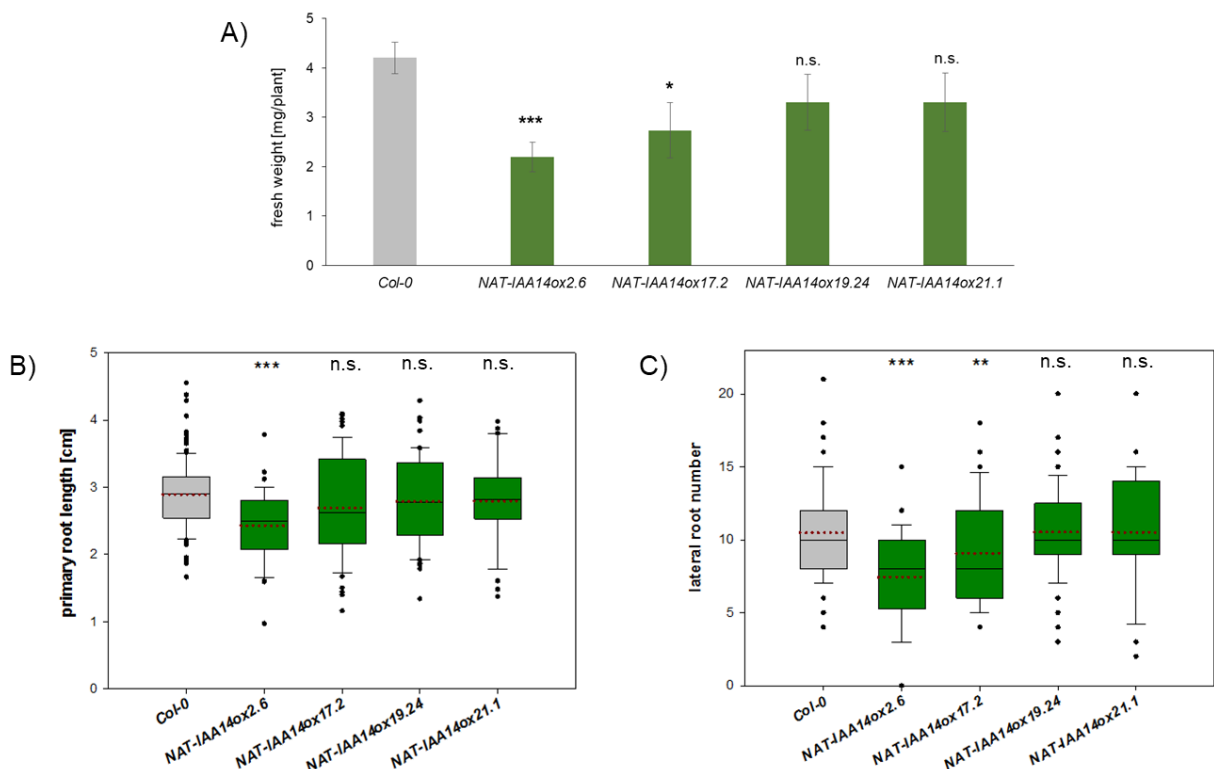


Figure 6.16: Phenotypic analysis of transgenic lines overexpressing the annotated *NAT-IAA14* transcript.

The average fresh weight of 14 d old seedlings was determined by micro scale measurements and is represented in mg/number of seedlings (A). Values correspond to averages with SD from three biological independent experiments. Boxplots of the primary root length (B) and lateral root number (C) of 14 d old light-grown seedlings (red dotted line: average). The primary root length was analyzed in cm using the ImageJ program. Shown data correspond to values with SD from three biological independent experiments with a total $N \geq 35$. Average and median are indicated with red dotted and black continuous lines, respectively. (Student's t-test: * ≤ 0.05 ; ** ≤ 0.01 ; *** ≤ 0.005 ; n.s. = not significant)

6.8.2 *NAT-IAA14* knockdown slightly reduces *IAA14* transcript levels

In addition to the analysis of *NAT-IAA14* overexpression lines, the investigation of loss of function mutants is important.

6.8.2.1 *NAT-IAA14* knockdown in DNA-insertion lines

A. tumefaciens transfer-DNA (T-DNA) insertion lines are derived from the random insertion of about 4-5 kb of foreign DNA in the *A. thaliana* genome. Insertion into genes often disrupts their function allowing the identification of relevant genes (Krysan et al., 1999, Alonso et al., 2003).

Three T-DNA insertion lines for the *NAT-IAA14* genome region in Col-0 background were reported at the TAIR10 database and seeds were obtained at the Nottingham Arabidopsis Stock Centre (NASC). All available SALK-lines have a T-DNA insertion in the *NAT-IAA14* promoter. The position of the insertion was determined by sequencing of PCR products obtained during the genotyping (Supplemental Figure 11.15). The T-DNA insertions are located at 122, 288 and 349 bp upstream of the *NAT-IAA14* annotated 5' end in the *SALK_113294* (referred to *nat-iaa14_1*), *SALK_012231* (referred to *nat-iaa14_2*) and *SALK_118398* (referred to *nat-iaa14_3*) lines, respectively (Figure 6.17 A). *NAT-IAA14* transcript levels were not affected in the line *nat-iaa14_1*, which was therefore not further analyzed. In homozygous plants from *nat-iaa14_2* and *nat-iaa14_3* lines the *NAT-IAA14* expression level was significantly reduced between 0.3- to 0.6-fold compared to Col-0 (Figure 6.17 B). Accordingly, the *IAA14* transcript level in the tested SALK-lines was slightly decreased compared to the control (Figure 6.17 C).

Phenotypic analysis including the measurement of fresh weight, primary root length and number of lateral roots that was performed in a previous work in the laboratory showed no significant effect of the T-DNA insertion in the *NAT-IAA14* promoter region on plants development at 14 days (Hüfner, 2017).

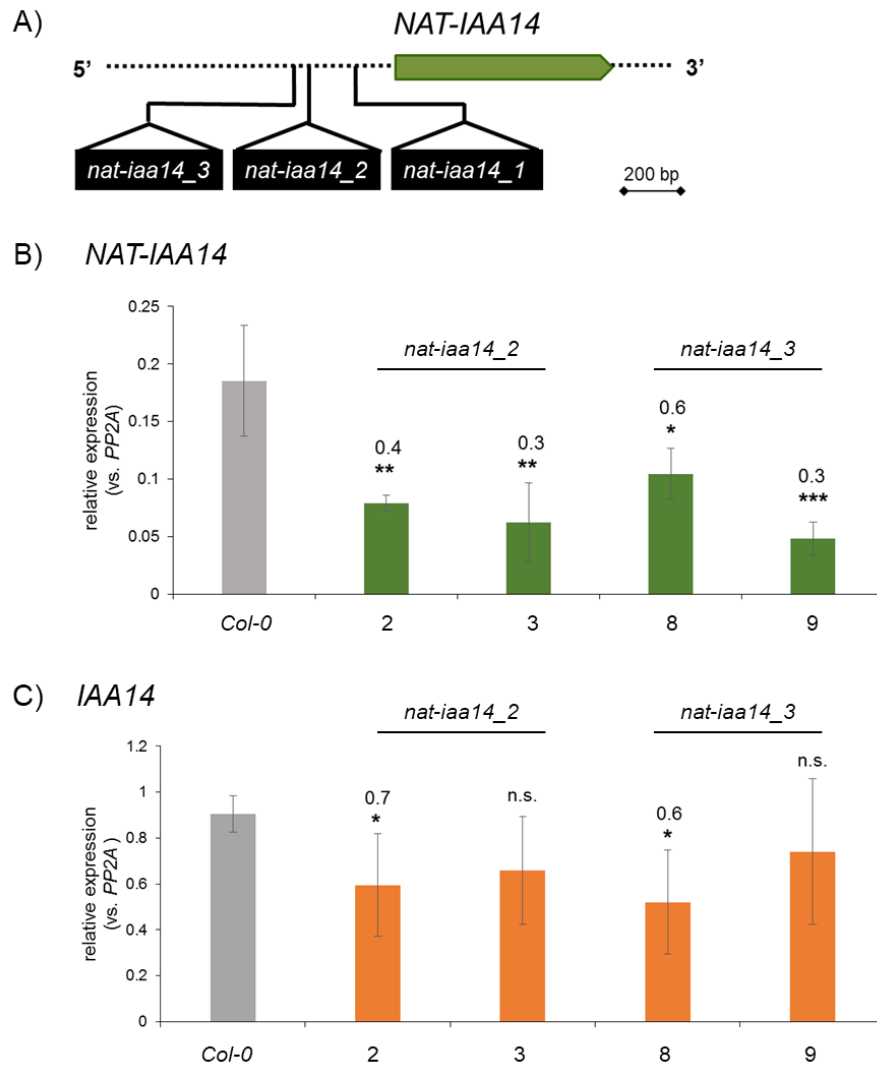


Figure 6.17: T-DNA insertions in the promoter region decreases *NAT-IAA14* expression.

Schematic representation of the in TAIR10 annotated genomic region of *NAT-IAA14* (green) with black arrows indicating the position of the T-DNA insertions in the promoter region (A). Transcript levels of *NAT-IAA14* (B) and *IAA14* (C) were determined by qRT-PCR in 12 d old Col-0 seedlings grown in long-day conditions. Seeds from two individual plants from each T-DNA line were used. qRT-PCR results were normalized by *PP2A* and values correspond to averages with SD from three biological independent experiments. (Student's t-test: * ≤ 0.05 ; ** ≤ 0.01 ; *** ≤ 0.005 ; n.s. = not significant)

6.8.2.2 *NAT-IAA14* knockdown by artificial mircoRNAs

In addition to commonly used T-DNA-insertion lines, RNAi-based approaches can be applied to knockdown or knockout a gene of interest post-transcriptionally. Artificial microRNAs (amiRNAs) act in *trans* and after transcription to reduce the transcript level in the cytosol. Therefore, stable transformed homozygous T₃ lines from *A. thaliana* for downregulation of *NAT-IAA14* transcript levels by artificial amiRNAs were previously generated in the laboratory (Pogoda, 2015). In contrast to the T-DNA lines, the amiRNA approach allows to discriminate *NAT-IAA14* function in *cis* or *trans*.

The use of amiRNAs directed against the desired target has been described by Carbonell and collaborators (Carbonell et al., 2014). miRNA390 was used as backbone for the amiRNA construct and 21 bp of the original sequence were replaced by the selected *NAT-IAA14* sequence. The amiRNA strand complementary to the *NAT-IAA14* transcript served as guide strand and is incorporated in the RNA-induced silencing complex (RISC). Figure 6.18 A) shows a scheme of the *NAT-IAA14* transcript, in which the positions of the target site of the three amiRNAs are indicated. First, the correct processing and expression level of the amiRNAs in *A. thaliana* was determined by northern blot using complementary oligoprobes, showing that the amiRNAs-encoding constructs are expressed and mature amiRNAs of the expected size are produced in *planta* (Supplemental Figure 11.16).

Moreover, the level of *NAT-IAA14* downregulation in the amiRNA lines was analyzed by qRT-PCR (Figure 6.18 B). *NAT-IAA14* levels were significantly decreased between 0.4- and 0.6-fold compared to plants transformed with the empty vector (EV) used as control. Based on the amiRNA cleavage position and a similar decrease in *NAT-IAA14* levels, the amiRNA1 and amiRNA2 lines were used for further analysis. In addition, we determined that the *IAA14* transcript level in these lines (Figure 6.18 C) was only slightly reduced in the *amiRNA1.8.2* and *amiRNA2.13.10* lines compared to the control.

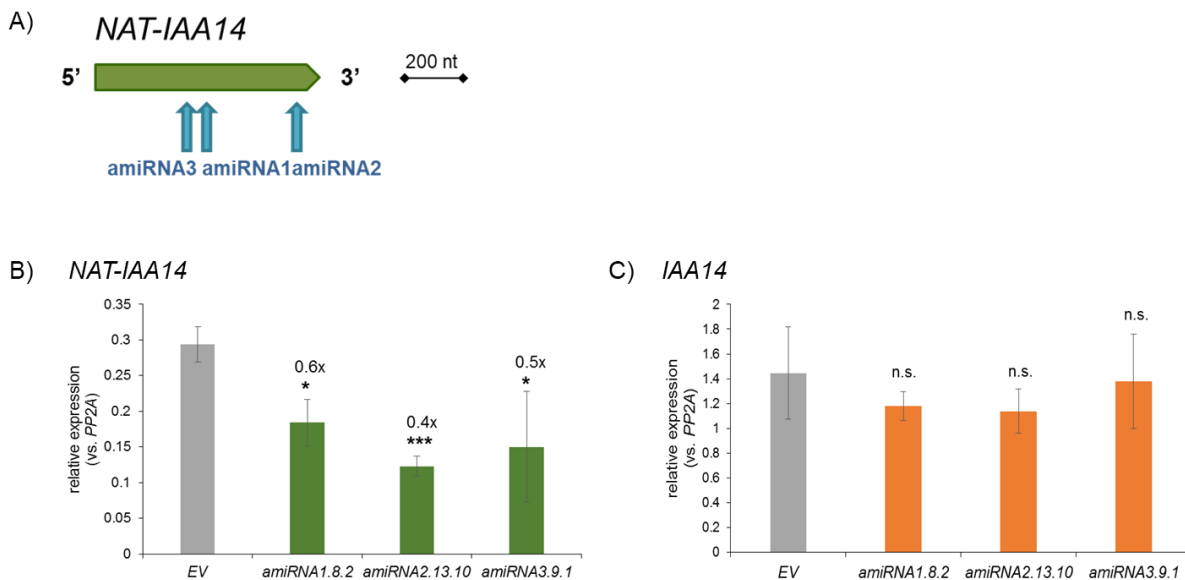


Figure 6.18: *NAT-IAA14* downregulation by amiRNAs.

Schematic representation of *NAT-IAA14* transcript (green) with blue arrows indicating the position of the three amiRNAs (A). Transcript levels of *NAT-IAA14* (B) and *IAA14* (C) were determined by qRT-PCR in 14 d old seedlings. qRT-PCR results were normalized by *PP2A* and values correspond to averages with SD from three biological independent experiments. (Student's t-test: * ≤ 0.05 ; *** ≤ 0.005 ; n.s. = not significant). The first number of each transgenic line represents the corresponding amiRNA construct.

In the next step, the phenotypic effect of *NAT-IAA14* knockdown was analyzed by using transgenic lines expressing the amiRNAs 1 and 2. *A. thaliana* plants transformed with a construct expressing an amiRNA targeting the β -glucuronidase (*amiRNAGUS3.4.1*) transcript, that is absent in wildtype plants, were used as control. The fresh weight and primary root growth were significantly increased in *amiRNA1.3.1*, *amiRNA2.4.2* and *amiRNA2.13.10* compared to the control (Figure 6.19) without correlating to the reduced *NAT-IAA14* levels (Supplemental Figure 11.17). Plant growth was impaired in only 50% of the tested lines, suggesting that the phenotypic alteration is caused by intrinsic variation in the experiment.

To sum up, no significant change in *IAA14* transcript level or phenotypic effect on the plant was detected in the lines with reduced *NAT-IAA14* levels due to the expression of amiRNAs. The downregulation of *NAT-IAA14* level in *A. thaliana* was in a similar range to the T-DNA lines (section 6.8.2.1) and potentially too low to affect the *IAA14* transcript level or the plant phenotype.

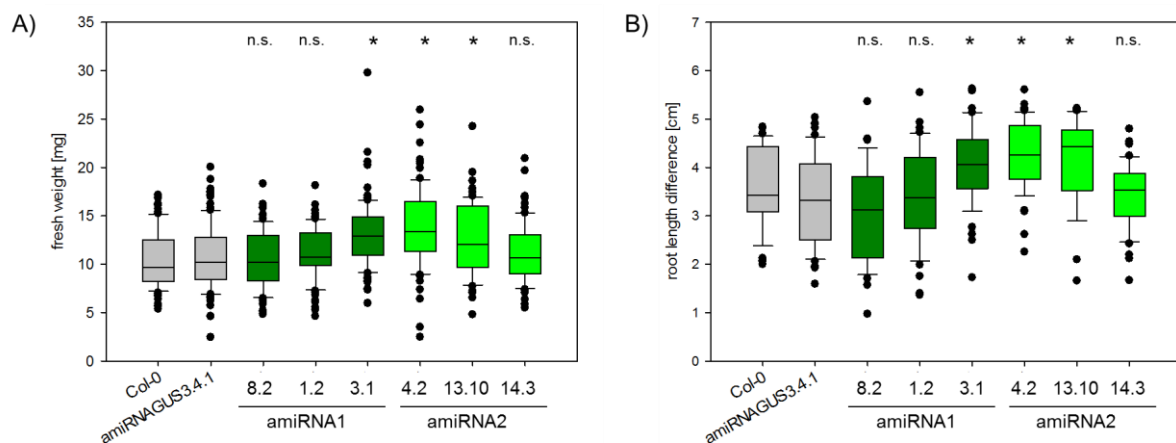


Figure 6.19: Phenotypic analysis of transgenic lines with reduced *NAT-IAA14* levels.

Boxplots of the fresh weight (A) and primary root length difference (B) of 14 d old seedlings. The fresh weight was determined by micro scale measurements (A) and the primary root length difference between day 3 and day 14 was analyzed in cm through the program ImageJ. Shown data correspond to values with SD from three (A) or two (B) biological independent experiments with a total $N \geq 25$. Median values are indicated with black continuous lines. (Kruskal-Wallis One Way Analysis of Variance on Ranks: * ≤ 0.05 ; n.s. = not significant)

6.8.3 *IAA14* levels are not affected by *NAT-IAA14* knockout

To achieve a complete *NAT-IAA14* knockout, clustered regularly interspaced short palindromic repeats (CRISPR)/CRISPR-associated Protein9 (Cas9)-based technology was used in *A. thaliana*. Five specific guide RNAs (gRNAs) were used to target the *NAT-IAA14* promoter and gene region, resulting in various DNA deletions by different gRNA combinations (Figure 6.20 A).

The first established, stably transformed, homozygous T₃ CRISPR/Cas line *cr_nat-iaa14_12.1* had a deletion of 277 bp (gRNA2 and 3); 208 bp were deleted at the 3' end of the *NAT-IAA14* promoter and 69 bp of the transcript at the 5' end (Supplemental Figure 11.18 A). The *NAT-IAA14* transcript level was significantly reduced to 0.4-fold (Figure 6.20 B), which is in a similar range as in the T-DNA (section 6.8.2.1) and amiRNA lines (section 6.8.2.2). Accordingly, *IAA14* levels were also significantly decreased to 0.8-fold (Figure 6.20 B).

Since the deletion of 277 bp in the *NAT-IAA14* gene could not achieve a complete *NAT-IAA14* knockout, other lines were generated by using gRNA1 and 3, in which 1261 bp of the *NAT-IAA14* promoter are additionally removed (in total removing 1538 bp, Supplemental Figure 11.19). However, the truncated *NAT-IAA14* transcript was still expressed in the T₂ generation of these lines, as determined by RT-PCR (Figure 6.20 C).

Therefore, additional lines were generated, in which the complete promoter and close to the complete *NAT-IAA14*-encoding gene were deleted without modifying the sequence of the 124 nt-longer *IAA14* variant. Combination of gRNA1 and 4 resulted in a 1884 bp (*cr_nat-iaa14_40.3*) and 1910 bp (*cr_nat-iaa14_14.5*) deletion, and gRNA1 and 5 led to a 2104 bp (*cr_nat-iaa14_3.1*) and 2109 bp (*cr_nat-iaa14_8.8*) deletion (Figure 6.20 A, Supplemental Figure 11.20). In the lines *cr_nat-iaa14_40.3* and *cr_nat-iaa14_14.5*, 315 bp and 312 bp of the *NAT-IAA14* 3' end were still present, respectively, while in the lines *cr_nat-iaa14_3.1* and *cr_nat-iaa14_8.8*, only 94 bp and 89 bp were retained, respectively (Figure 6.20 C). These lines were assumed to be *NAT-IAA14* knockout lines because the complete promoter and more than 50% of the *NAT-IAA14* gene were deleted. Nevertheless, the *IAA14* transcript levels in 14 days old seedlings were not significantly affected in comparison to the Col-0 control (Figure 6.20 D). As previous results showed that *NAT-IAA14* expression increases at later developmental stages of the plant (section 6.2), it was interesting to see whether the *IAA14* expression is modulated in older *NAT-IAA14* knockout plants. However, no effect on *IAA14* levels could be determined in 29 days old *NAT-IAA14* knockout plants (Supplemental Figure 11.21).

In conclusion, the knockout of *NAT-IAA14* showed no significant effect on *IAA14* expression levels. Nevertheless, it cannot be excluded that expression of the short 3' end of *NAT-IAA14* is completely abolished in the lines *cr_nat-iaa14_40.3*, *cr_nat-iaa14_14.5*, *cr_nat-iaa14_3.1* and *cr_nat-iaa14_8.8*, since the lines *cr_nat-iaa14_7.14*, *7.46* and *7.54* also still express *NAT-IAA14*.

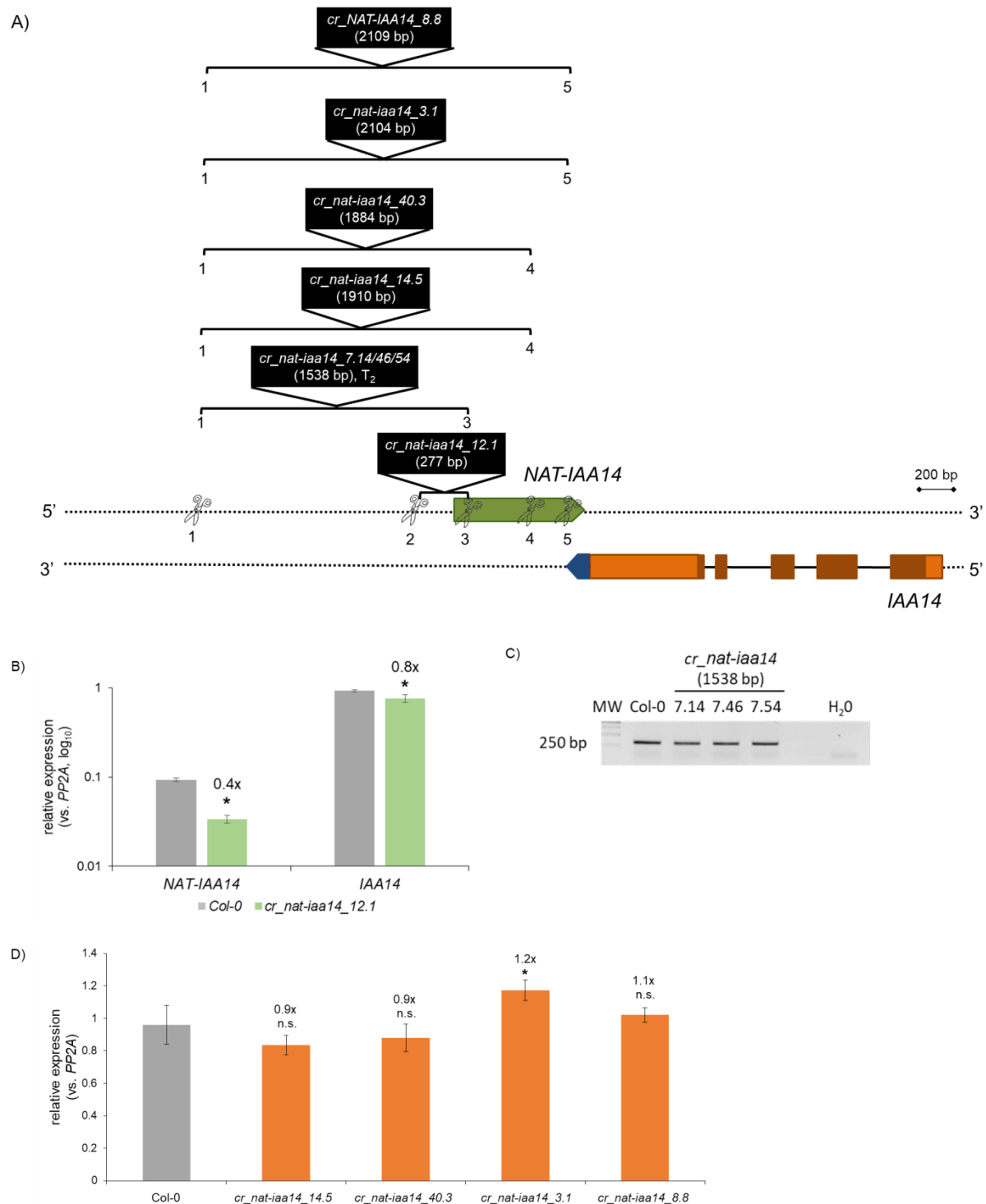


Figure 6.20: *NAT-IAA14* knockout has no effect on *IAA14* transcript levels.

The CRISPR/Cas9 cleavage sites (1 to 5) generated by five gRNAs were indicated with a scissors symbol in the schematic representation of *NAT-IAA14* (green) and *IAA14* (brown: exon; orange: UTR), and the resulting deletion size in the genome of the each *cr_nat-iaa14* line is shown (A). The 124 nt-longer *IAA14* 3'UTR region is indicated in dark-blue. By qRT-PCR (B, D) or PCR (C) the transcript levels of *NAT-IAA14* and *IAA14* were determined in 14 day old seedlings of Col-0 and the *cr_nat-iaa14* lines. In the case of *cr_nat-iaa14_7.14*, *cr_nat-iaa14_7.46* and *cr_nat-iaa14_7.54*, the T₂ generation was analyzed, while for the other *cr_nat-iaa14* lines the homozygous T₃ generation was used. qRT-PCR results were normalized by *PP2A* and values correspond to averages with SD from three experiments. (Student's t-test: * ≤ 0.05; n.s. = not significant)

6.9 Alteration of *IAA14* levels results in changes of the *NAT-IAA14* transcript abundance

6.9.1 Overexpression of *IAA14* slightly reduces *NAT-IAA14* levels and increases root growth

To determine a potential influence of the protein-coding gene *IAA14* on the *NAT-IAA14* transcript level, *IAA14* overexpression was used. Prior to this work, stable transformed homozygous T₃ *IAA14* overexpression (ox)-lines of *A. thaliana* were generated in the laboratory (Seidel, 2014). The *IAA14* construct driven by the 35S-promoter corresponds to the cDNA sequence covering the annotated coding region of the gene (1482 bp) and including the 5' and 3'UTR.

First, the level of *IAA14* overexpression was determined by qRT-PCR (Figure 6.21 A). In transgenic lines, the *IAA14* transcript level was significantly increased between 8- and 23-fold compared to wild-type Col-0 plants used as control. In contrast, the *NAT-IAA14* level was decreased between 0.7- and 0.8-fold in the *IAA14ox* lines. These results were statistically significant in two of the three lines (Figure 6.21 B), suggesting a detrimental effect in *trans* of the *IAA14* RNA or protein on *NAT-IAA14* expression.

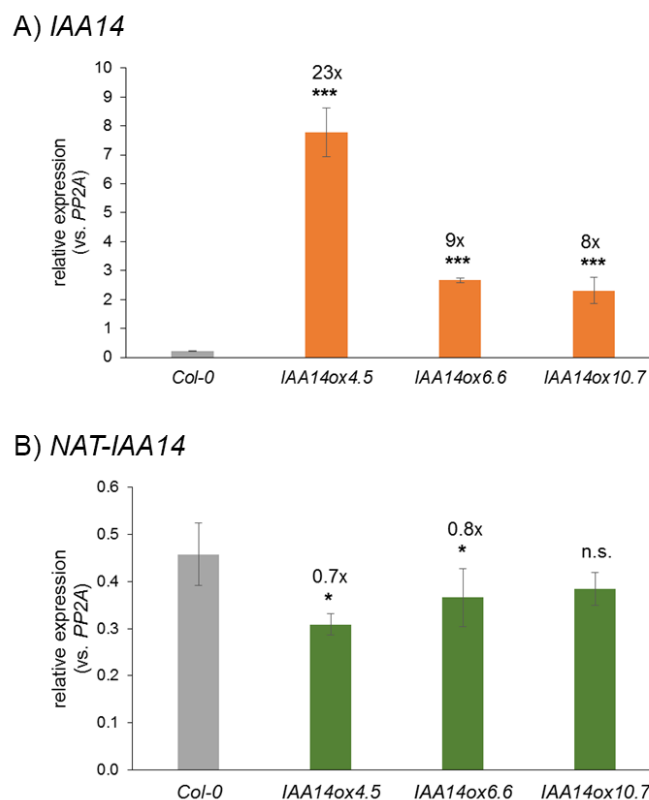


Figure 6.21: *IAA14* overexpression results in a reduction of *NAT-IAA14* transcript levels. Transcript levels of *IAA14* (A) and *NAT-IAA14* (B) were determined by qRT-PCR over cDNA of total RNA preparations from 14 d old seedlings. The *IAA14* construct under the control of the 35S-promoter covers the complete annotated coding region of the gene and includes the 3' and 5'UTRs. qRT-PCR results were normalized by *PP2A* and values correspond to averages with SD from three independent experiments. (Student's t-test: * ≤ 0.05 ; *** ≤ 0.005 ; n.s. = not significant)

In addition, the phenotype of the *IAA14ox* lines was analyzed. In principle, overexpression of *IAA14* should lead to an increase in IAA14 protein. Therefore, a *slr-1* like phenotype, characterized by a lack of lateral roots and root hairs, and an abnormal gravitropic response (section 3.8, (Fukaki et al., 2002)), was expected in the *IAA14ox* lines. In contrast, lines overexpressing *IAA14* showed significantly longer primary roots and increased number of lateral roots (Figure 6.22), suggesting that the IAA14 protein level was not increased in the *IAA14ox* lines. Since both endogenous and overexpression levels were measured by qRT-PCR, a masked effect on the endogenous *IAA14* level cannot be excluded. These results suggest that ectopic overexpression of *IAA14* might result in downregulation of the endogenous gene that might also explain the reduction of *NAT-IAA14* levels in these lines (Figure 6.21).

In future analysis, it is necessary to determine the endogenous *IAA14* transcript level in the *IAA14ox* lines and to include *IAA14* overexpression lines with the 124 nt-longer *IAA14* 3'UTR overlapping *NAT-IAA14* (section 4). In addition, IAA14 protein levels in the overexpression lines could be determined to obtain a clearer insight into the observed phenotype.

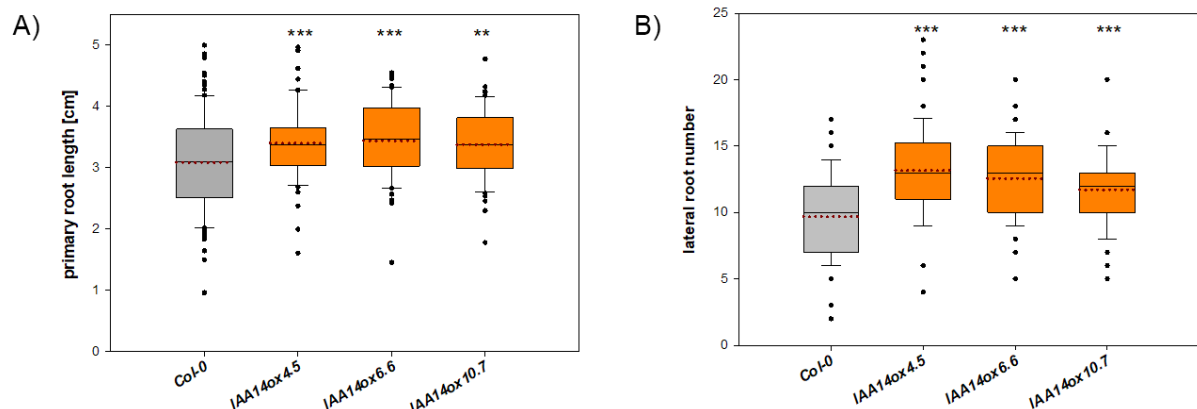


Figure 6.22: *IAA14* overexpression results in increased primary root length and lateral root number.

Boxplots of the primary root length (A) and lateral root number (B) of 14 d old seedlings grown in long-day conditions (red dotted line: average). The primary root length was analyzed in cm with the ImageJ program. Data correspond to values with SD from three independent experiments with a total $N \geq 55$. Average and median are indicated with red dotted and black continuous lines, respectively. (Student's t-test: *** ≤ 0.005)

6.9.2 NAT-*IAA14* expression alteration in CRISPR/Cas9-edited *IAA14* lines

In addition to the analysis of *IAA14* overexpression lines, CRISPR/Cas9-edited plants were generated to eliminate the mature *IAA14* transcript and protein in *A. thaliana*. Specific gRNAs for targeting the *IAA14* gene region were generated (Figure 6.23 A) and various deletions in the *IAA14* gene were obtained (Supplemental Figure 11.22, Supplemental Figure 11.23). Two gRNAs were designed using the webpage CHOPCHOP to target the first and the second exon of *IAA14*. gRNA1 and gRNA2 cleave 109 bp and 582 bp downstream of the transcriptional start site, respectively. *In silico* translation of the CRISPR/Cas9-edited *IAA14* sequences indicated no functional *IAA14* protein (Supplemental Figure 11.24). Deletion of 473 bp in the *cr_iaa14_8.5* (Supplemental Figure 11.23) resulted in a truncated *IAA14* protein, starting with the first six native *IAA14* amino acids (aa), followed by a 92 aa deletion that did not change the open reading frame of the remaining *IAA14* protein sequence (Supplemental Figure 11.24). The open reading frame of the truncated *IAA14* in the line *cr_iaa14_46.7* with a 19 bp deletion (Supplemental Figure 11.22) initiated 89 aa downstream of the native N-terminus (Supplemental Figure 11.24). In both lines, domain II, which is essential for the degradation of *IAA14* by the SCF^{TIR1/AFB} E3 ubiquitin ligase complex (Figure 3.3), is removed. In lines *cr_iaa14_46.6*, *cr_iaa14_46.8*, and *cr_iaa14_46.9*, gRNA1 cleavage resulted in a 30 bp deletion (Supplemental Figure 11.22) that caused a shift in the open reading frame encoding a completely *IAA14*-unrelated peptide (Supplemental Figure 11.24). An additional line, *cr_iaa14_29.6*, had a deletion of 488 bp (Supplemental Figure 11.23) that resulted in a 17 aa truncated *IAA14* peptide (Supplemental Figure 11.24). The first five amino acids belong to native *IAA14*, while the other 12 aa are *IAA14*-unrelated, caused by a frameshift due to the deletion.

In all tested CRISPR/Cas9-edited and stably transformed homozygous T₃ lines, the *IAA14* transcript level showed a 30-50% significant reduction (Figure 6.23 B). The obtained deletions did not affect the promoter region of *IAA14*, suggesting that transcription initiation is not affected and that the fast turnover of the resulting *IAA14* mRNA is responsible for the observed reduction in the transcript level. Furthermore, *NAT-IAA4* transcript levels in these lines were determined by qRT-PCR (Figure 6.23 C). In the *cr_iaa14_46.6/8/9* lines, which share the same gRNA1-mediated deletion, a significant reduction of the lncRNA levels in two out of three lines was determined. Also in the *cr_iaa14_46.7* line that encodes for a truncated *IAA14* protein lacking 89 aa at the N-terminus, *NAT-IAA14* abundance is statistically significant decreased to 80%. In contrast, the line *cr_iaa14_8.5*, which has an intrinsic deletion of 92 aa in the truncated *IAA14* protein, showed unaltered *NAT-IAA14* levels compared to Col-0. If translated, the truncated *IAA14* proteins from line *cr_iaa14_46.7* and

cr_iaa14_8.5 could potentially interact with ARF7 and ARF19 through domains III and IV, but cannot be degraded due to the deletion of domain II (Supplemental Figure 11.24), and therefore might show similar results to the *slr-1* mutant, in which the IAA14 protein is stabilized as a result of a point mutation in domain II (Fukaki et al., 2002). However, in *slr-1*, a 2.5-fold significant increase in *NAT-IAA14* transcript levels was determined (Figure 6.23 C). In addition, seedlings of the lines *cr_iaa14_46.7* and *cr_iaa14_8.5* showed no *slr-1*-like phenotype, suggesting that the truncated IAA14 proteins are not translated or not functional. On the other hand, the *NAT-IAA14* levels were also significantly increased to 1.5-fold in the *cr_iaa14_29.6* line that encodes for a 17 aa truncated IAA14 peptide.

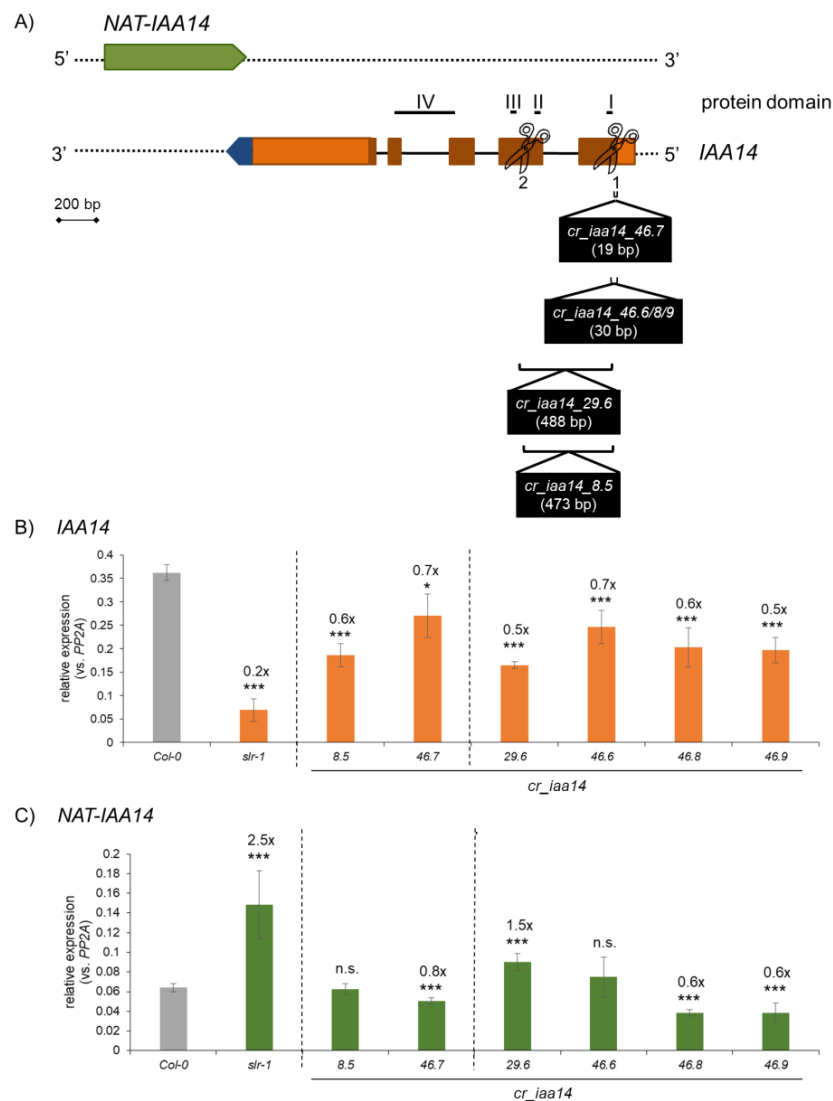


Figure 6.23: Alteration in *NAT-IAA14* transcript levels in *slr-1* and the *cr_iaa14* lines.

The two CRISPR/Cas9 cleavage sites mediated by gRNAs (1 and 2) are indicated with a scissor symbol in the schematic representation of *NAT-IAA14* (green) and *IAA14* (brown: exon; orange: UTR) (A). The 124 nt-longer *IAA14* 3'UTR region is indicated in dark-blue. The IAA14 protein domains are shown and the length of the deletions are indicated between brackets. Transcript levels of *IAA14* (B) and *NAT-IAA14* (C) were determined by qRT-PCR using 14 d old seedlings of *Col-0*, *slr-1* and *cr_IAA14* lines. qRT-PCR results were normalized by *PP2A* and values correspond to averages with SD from one representative experiments with three biological replicates. (Student's t-test: *** ≤ 0.005 ; * ≤ 0.05 ; n.s. = not significant)

To sum up, these results suggest that alteration of chromatin structure by deletion of parts of the *IAA14* genomic region, resulting in truncated IAA14 proteins if translated differentially affects *NAT-IAA14* transcript levels. The *NAT-IAA14* upregulation in *slr-1* might be explained by decreased *IAA14* transcription or a positive effect on *NAT-IAA14* transcription by the stabilized IAA14 protein. Further analysis including the phenotype of the *IAA14* CRISPR/Cas lines and a complementation of these lines needs to be performed.

6.10 *NAT-IAA14* decreases the *in vitro* translation of the annotated *IAA14* transcript

It was shown in this study that the lncRNA *NAT-IAA14* is localized to the cytoplasm (sections 6.1.2; 6.1.3) and therefore could achieve its function in the cytosol. To test a potential *NAT-IAA14*-dependent translation regulation of *IAA14*, an *in vitro* translation assay with evacuated tobacco Bright Yellow-2 (BY-2) cell lysate (Buntru et al., 2014) was performed (Dr. T. Gursinsky, MLU Halle (Saale)). A schematic representation of the transcript variants used in the assay is shown in the Figure 6.24 A). The *in vitro* transcripts used in this assay were capped and polyadenylated (section 5.6.6). With this assay an efficient ³⁵S-IAA14 protein synthesis can be achieved using *IAA14* transcripts carrying the TAIR10 annotated 3'end or a 124 nt-longer variant detected *in vivo* (section 4). The inclusion of the variant containing the 124 nt-longer 3'UTR allows to study the translational impact of the 67 nt overlap with the full-length *NAT-IAA14*. In addition to the full-length *NAT-IAA14*, a shorter variant (truncated) with a length of 665 nt, in which 90 nt of the *NAT-IAA14* 3'end were missing, was incorporated in the assay.

In a first experiment, 0.02 pmol of *IAA14* transcripts and 5-fold excess (0.1 pmol) of each type of *NAT-IAA14* transcripts were used (Figure 6.24 B). ³⁵S-IAA14 (25 kDa) band intensity decreased to a similar extent compared to the controls (lane 1 or 4), regardless of which *NAT-IAA14* variant was incorporated. Nevertheless, the protein synthesis of the annotated *IAA14* transcript was more affected by the *NAT-IAA14* RNA (lane 2 and 3) than the 124 nt-longer *IAA14* transcript (lane 5 and 6). Increasing the *IAA14* concentration to 0.1 pmol with a 5-fold excess (0.5 pmol) of *NAT-IAA14* transcripts showed similar results (Figure 6.24 C).

Independent from the *NAT-IAA14* RNA length the protein synthesis from the annotated *IAA14* transcript was reduced to 17-19% whereas the translation from the 124 nt-longer *IAA14* transcript variant was less affected and reduced only up to 40-43% (Figure 6.24 C). When the ³⁵S-IAA14 translation efficiency of the 124 nt-longer transcripts variant (lane 4) was compared with the annotated *IAA14* mRNA (lane 1) equal efficiency was determined (96 (B)-

98% (C)), demonstrating similar RNA stability in the *in vitro* assay. These results indicate that the translation of the annotated *IAA14* transcript by *NAT-IAA14* was more reduced than the 124 nt-longer *IAA14* RNA, suggesting that regulatory elements important for *IAA14* translation regulation by *NAT-IAA14* are missing in the annotated *IAA14* transcript. Nevertheless, the overlap between the *IAA14* and *NAT-IAA14* transcripts seems not to be necessary for the *IAA14* translation regulation, as both the truncated and full-length *NAT-IAA14* transcripts showed similar results.

In general, the addition of *NAT-IAA14* transcript decreased the overall *IAA14* translation. To test whether this is a common effect, an *in vitro* translation assay with an unrelated sequence (*LUC-RNA*) was performed (Figure 6.24 D), lane 1-3). The full-length *NAT-IAA14* transcript used in a 2-fold (lane 2) or 5-fold (lane 3) excess was leading to a 15% or 68% reduction in ³⁵S-LUC (60.6 kDa) translation, respectively. These results were comparable with the effect of each type of *NAT-IAA14* on the 124 nt-longer *IAA14* transcript in the same assay (lane 7-9). In contrast, the translation of the annotated *IAA14* transcript was up to 91% less efficient (lane 4-6).

Taken together, the *in vitro* translation assay showed that the addition of *NAT-IAA14* transcript reduces translation. This effect could be caused by an increased number of RNA molecules in the assay, which leads to a reduction of free ribosomes and thus to fewer translation products. To test this, further experiments including a *NAT-IAA14*-unrelated RNA have to be performed. In all experiments the annotated *IAA14* transcript was less translated in the presence of *NAT-IAA14* compared to the *LUC-RNA* and the 124 nt-longer *IAA14* transcript, suggesting a specific effect of the lncRNA on its translation or stability.

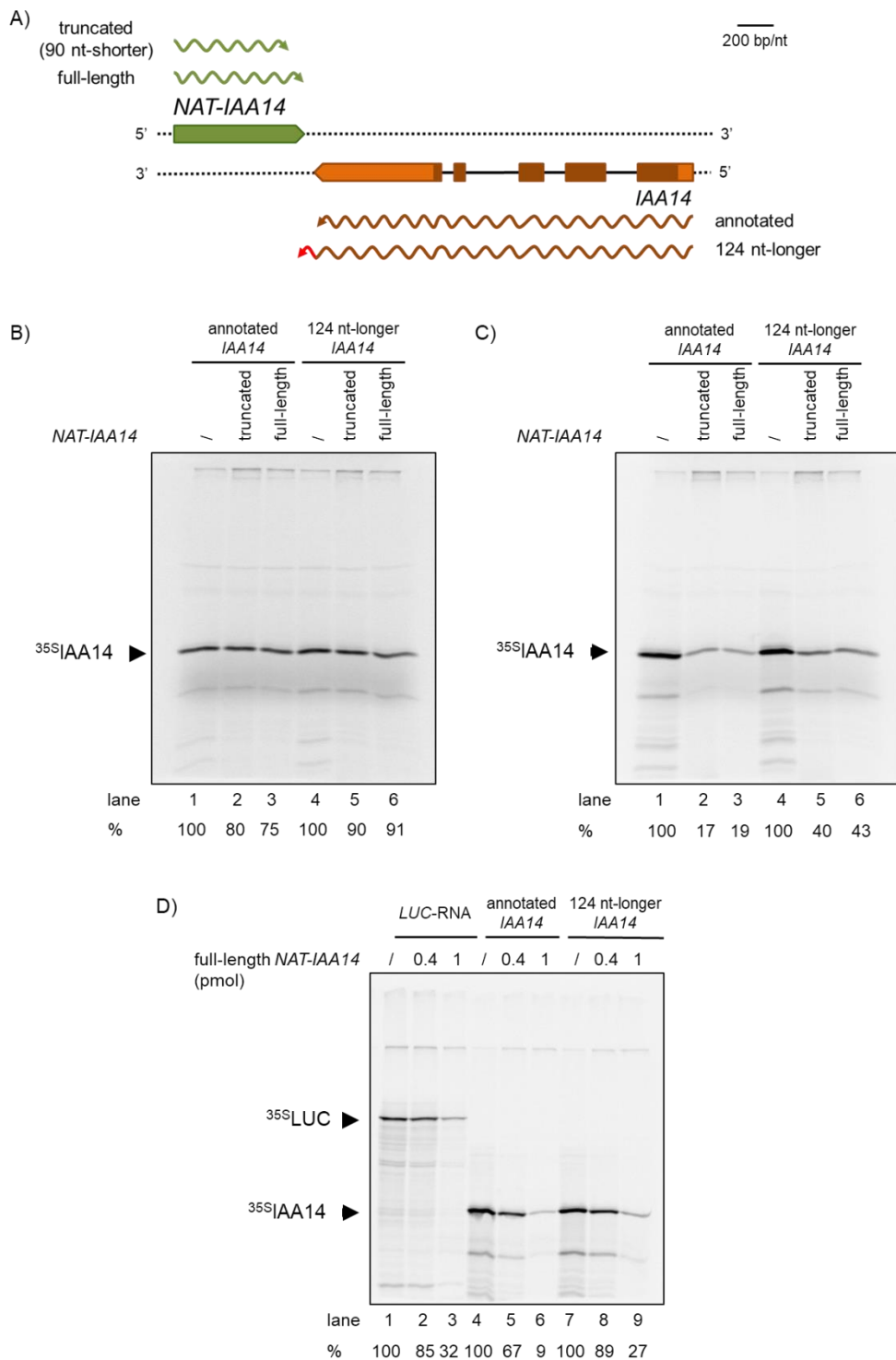


Figure 6.24: The presence of *NAT-IAA14* in the *in vitro* translation assay has a stronger effect on translation of the annotated *IAA14* transcript.

Schematic representation of the *NAT-IAA14* (green) and *IAA14* (brown: exon; orange: UTR) transcripts used in the *in vitro* translation assay (A). Evacuolated BY-2 lysate was incubated with 0.02 pmol (B) or 0.1 pmol (C) of the *IAA14* transcript (annotated or 124 nt-longer variant) and with a 5-fold excess of the full-length or a 90 nt-shorter, truncated *NAT-IAA14*. In D) 0.2 pmol of *luciferase* (*LUC*-RNA) or of *IAA14* transcript (annotated or 124 nt-longer variant) were each incubated with a 2 or 5-fold excess of *NAT-IAA14* (full-length or truncated). The quantification of the band intensity (%) was performed with Image Lab Software (Bio-Rad). The expected bands of ^{35}S IAA14 (25 kDa) and ^{35}S LUC (60.6 kDa) are indicated with an arrowhead.

7 Discussion

7.1 *NAT-IAA14* is autonomously expressed in *A. thaliana*

70% of the Arabidopsis mRNAs are associated with an antisense transcript (Wang et al., 2014a). A non-protein coding RNA referred to as *NAT-IAA14* is reported in TAIR10 database and is originated from the *At4g14548* gene, which is located on the opposite DNA strand and in close proximity to the *IAA14* locus. The autonomous, tissue-specific expression of *NAT-IAA14* in *A. thaliana* (Seidel, 2014, Pogoda, 2015) suggests that the lncNAT is not generated by random transcriptional noise and strengthens the assumption that *NAT-IAA14* might have a relevant biological function. *NAT-IAA14* expression increases during *A. thaliana* lifespan, suggesting a potential role in senescence (Figure 6.8). The high variation of *IAA14* transcript levels during the time course experiment (Figure 6.8) could result from the different layers of *IAA14* transcriptional regulation, e.g. disregarding of the circadian clock regulation (section 3.9) while sampling in this particular case. Both genes are controlled by promoters that are active in the shoot (cotyledons, true leaves and hypocotyls), root crown and base of the lateral roots (Pogoda, 2015).

The next step to try to get a first insight into its function was the molecular analysis of the lncRNA. One of the most expected modes of action of lncNATs is based on the generation of natural antisense siRNAs (nat-siRNAs, (Borsani et al., 2005, Held et al., 2008)) by the formation of double-stranded RNA (dsRNA) between the lncNAT and its complementary sense transcript. This regulatory mechanism requires an overlap between the *NAT-IAA14* and *IAA14* RNAs that was not reported in the annotated transcripts. By 5'RACE it was determined that the transcriptional start site (TSS) of *NAT-IAA14* is located 15 nt downstream of the TSS reported in TAIR10 (Figure 6.2). Reference-guided transcriptome assembly of genome-wide approaches could lead to the discrepancy in the obtained transcript 5'end compared to the databases. For example, RNA sequencing relies on alignment of short fragments of a cDNA sequence with a pre-existing reference genome to reconstruct full-length transcripts (Kovaka et al., 2019). Therefore, the resolution of RNA-seq is limited and can be biased, e. g. by the cDNA synthesis and by the number, abundance and length of the reads (Tripathi et al., 2017, Ozsolak & Milos, 2011). Furthermore, 3'end sequencing after 3'RACE revealed a segment with several adenosines at the annotated 3'end (Figure 6.3), indicating that *NAT-IAA14* is polyadenylated and therefore most likely transcribed by DNA-dependent RNA polymerase II (RNA pol II, (Zhang et al., 2019)).

In addition, results from walking RT-PCR using primer combinations at different points downstream of the reported *NAT-IAA14* 3'end showed in two independent experiments a PCR product that covers the complete *IAA14* transcript (Supplemental Figure 11.10). Leaky transcript termination might be the reason for the 3'end variation of *NAT-IAA14* transcripts between the two different methods. Transcriptional read-through of *NAT-IAA14* at the fully expanded cotyledons stage might happen in response to a specific, yet unknown, condition, such as reported for the cryptic antisense *CBF1* lncRNA (*asCBF1*) that is expressed as transcriptional read-through product of the lncRNA *SVALKA* in response to cold (Kindgren et al., 2018). *asCBF1* transcription limits *CBF1* expression by collision of RNA pol II at the 3'end of *CBF1*. The observation from Kindgren et al. that multiple lncRNAs originating from one locus can act together is consistent with findings in yeast (Moretto et al., 2018, Fauquenoy et al., 2018) and might increase the accuracy of target regulation. Moreover, it was shown that the selective transcriptional termination of the lncRNA *COOLAIR* also determines the chromatin state of the *FLC* locus and thus *FLC* expression (Liu et al., 2010). Nevertheless, the read-through transcript of *NAT-IAA14* seems to be expressed in low levels in *A. thaliana* as the majority of the transcripts possess the reported 3'end. However, approximately 60% of the *IAA14* transcripts are 124 nt-longer than reported (Figure 6.4) and overlap the *NAT-IAA14* 3'end by 67 nt (Seidel, 2014).

Expression analysis of *NAT-IAA14* and *IAA14* using *promoter::GUS*-reporter lines and transient expression assays revealed that the promoters of both genes are active in the same tissue in *A. thaliana* (Pogoda, 2015) and that *NAT-IAA14* and *IAA14* genes can be expressed at the same time in the same cell in *N. benthamiana* (Figure 6.12 B). It remains undetermined if sense and antisense RNAs are transcribed from the same locus simultaneously or mutually exclusively, as it is reported for the lncRNA *COOLAIR* and the sense gene *FLC* (Rosa et al., 2016). Rosa and collaborators detected individual sense and antisense transcripts in the same cell by using single-molecule fluorescence *in situ* hybridization (smFISH) and showed accumulation of *COOLAIR* transcripts at the *FLC* locus leading to transcriptional shutdown of *FLC* expression in the early phase of vernalization. Therefore, smFISH could be used to detect *NAT-IAA14* and *IAA14* at the single molecule level to further investigate their interplay.

Nonsense-mediated decay (NMD) has been reported to be responsible for degradation of lncRNAs that contain mRNA-like features (Kurihara et al., 2009). Although the *NAT-IAA14* transcript is intronless, polyadenylated and encodes potential open-reading frames (pORFs, Supplemental Figure 11.14), the studies showed that it is relatively stable and localizes to the cytoplasm as demonstrated by cordycepin-based assay (Figure 6.5) and nuclear isolation (Figure 6.6), respectively. Blocking translation for 45 minutes by cycloheximide, and thus

temporarily suppressing the NMD system, increased *NAT-IAA14* levels (Figure 6.7) to a similar extent as reported in whole-genome tiling array data from the NMD mutants *upstream frame shift protein 1-1 (upf1-1)* and *upstream frame shift protein 3-1 (upf3-1)*, in which the *NAT-IAA14* RNA was upregulated 1.53- and 1.21-fold, respectively (Kurihara et al., 2009). In contrast, prolonged cycloheximide treatment for 4 h decreased *NAT-IAA14* transcript levels to the half. As cycloheximide is a general translational inhibitor, other RNA degradation pathways or cellular processes might also be affected by this treatment (Kalyna et al., 2012) and influence *NAT-IAA14* transcript levels. Potentially, the synthesis of a protein involved in *NAT-IAA14* expression or transcript stabilization could be blocked by the prolonged cycloheximide treatment, resulting in a reduction of the *NAT-IAA14* RNA.

7.2 *NAT-IAA14* expression is modulated by external stimuli

In nature, plants are exposed to numerous stress factors, such as drought, high salinity, extreme temperatures, and infections caused by diverse pathogens that limit plant development and reproduction. To adapt and to survive these adverse conditions, plants alter multiple gene regulatory mechanisms to maintain cellular homeostasis (McClung, 2006). The knowledge of the role of lncRNAs in stress tolerance is still in its early infancy.

Altered *NAT-IAA14* expression in response to various abiotic stresses has been previously shown by RNA sequencing (Di et al., 2014) and tiling array data (Matsui et al., 2008). To confirm these data and to investigate a potential correlation with *IAA14* expression, various stress experiments were performed in the present study. In response to salt and to the mycotoxin deoxynivalenol (DON), *NAT-IAA14* expression was decreased, while being increased in response to high light stress. *IAA14* expression was affected to a similar extent, suggesting concordant regulation of *IAA14* and *NAT-IAA14* transcription in response to the stresses tested. Comparable results were reported for *MADS AFFECTING FLOWERING 4 (MAF4)* regulation by lncNAT *MAS* in response to cold acclimation (Zhao et al., 2018). Zhao and coworkers showed in a genome wide study that the expression of many lncNATs often positively correlates with the expression of their sense genes. Nevertheless, co-upregulation of a lncNAT and its cognate sense gene is puzzling as it is unclear how two converging RNA pol II molecules transcribing the same DNA strand can pass each other (Kindgren et al., 2018). Perhaps gene repression by RNA pol II is relatively rare, as the expression states of sense and antisense transcription might be divergent (Rosa et al., 2016). Further analysis, e.g. by using overexpressing or knockdown lines, are required to determine whether *NAT-IAA14* affects plants sensitivity in response to the stress, involving or not the regulation of *IAA14* expression; or if changes on *NAT-IAA14* expression levels are part of the general regulatory effect caused by the stress.

Besides the coincident regulation of *NAT-IAA14* and *IAA14* expression in response to high salinity, high light stress, and deoxynivalenol, *NAT-IAA14* transcription was not affected by the day-night cycle or by auxin treatment, while *IAA14* expression was elevated in response to both stimuli. *IAA14* has been previously reported to be regulated by the circadian clock (Voß et al., 2015). In the present study, *IAA14* transcript abundance doubled after 80 minutes in the light, while *NAT-IAA14* levels showed inconsistent expression peaks at unspecified time points that are not reflected in the *IAA14* levels (Figure 6.10). After the rapid transcriptional switch within 10 minutes, basal *NAT-IAA14* levels were recovered. Crisp and coworkers reported a similar phenomenon, termed rapid recovery gene downregulation (RRGD), by analyzing mRNAs upregulated by repeated excess of light stress in *Arabidopsis* (Crisp et al., 2017). Hallmark of RRGD is transcriptome resetting after a rapid induction, followed by an equally rapid decline in mRNA abundance. The decreased RNA level can be a consequence of modulated RNA stability that has been hypothesized to be dynamically regulated during stress and recovery, e.g. by changing the half-life of *ASCORBATE PEROXIDASE 2 (APX2)* to 12.1 min, while the measured half-life in the absence of stress is >17 h (Crisp et al., 2017, Park et al., 2012). An altered *NAT-IAA14* stability might also explain the discrepancy between the fast turnover within 10 min and the half-life of more than 1.5 h determined by cordycepin treatment (Figure 6.5), although the reason for the rapid induction and decay of the *NAT-IAA14* level remains to be investigated.

As *IAA14* is involved in auxin-mediated signaling and auxin alters *IAA14* expression, the effect of auxin treatment on *NAT-IAA14* expression was analyzed (Figure 6.11). Notably, *NAT-IAA14* abundance remained unaffected in response to auxin, suggesting an autonomous *NAT-IAA14*-independent regulatory mechanism of *IAA14* transcriptional activation by auxin and the circadian clock that is distinct compared with the concordant *NAT-IAA14* and *IAA14* responses to abiotic and biotic stresses.

7.3 *NAT-IAA14* and *IAA14* regulatory network

Antisense genes in plants have been reported to act either through their transcription or through the generated lncRNA molecule and has been shown to affect transcription, mRNA degradation or protein translation (Pelechano & Steinmetz, 2013). The stability of a lncRNA can provide an indication of its cellular localization and consequent function (Quinn & Chang, 2016). The *NAT-IAA14* transcript is relatively stable compared to a short-lived mRNA and displayed similar stability to its protein-coding partner *IAA14* (Figure 6.5). The similar half-life of the *NAT-IAA14* and *IAA14* transcripts might imply an effect of *NAT-IAA14* on *IAA14* transcript stability. In general, the long half-life of *NAT-IAA14* RNA points to a *trans* mode of action that requires an RNA molecule to diffuse in the nucleus (Quinn & Chang, 2016,

Fedak et al., 2016) or even be transported into the cytoplasm to achieve its function. In contrast, short-lived lncNATs usually act at the transcriptional level (Fedak et al., 2016, Tani et al., 2012).

The downregulation of *NAT-IAA14* transcripts by T-DNA insertions (Figure 6.17) or artificial miRNAs (amiRNAs, Figure 6.18) resulted in a slight decrease in *IAA14* transcript levels, however the *IAA14* expression alteration was inconsistent among the lines and not correlated to the level of changes in *NAT-IAA14* expression. A complete knockout of *NAT-IAA14* was achieved by CRISPR/Cas9 genome editing. However, the transcript level of *IAA14* was not affected in the *NAT-IAA14* knockout lines (Figure 6.20), suggesting that *NAT-IAA14* does not influence *IAA14* expression in *cis*. It is important to mention that another lncRNA (encoded by *At4g06195*) previously reported in TAIR10 to be upstream of *NAT-IAA14* was also deleted in the *cr_nat-iaa14* lines and should be taken into account in further analysis of these lines. Nevertheless, the other lncRNA showed a different expression pattern compared to *NAT-IAA14* (Supplemental Figure 11.25), suggesting an independent transcriptional regulation.

In addition, *IAA14* levels remained unaffected or were slightly elevated in lines overexpressing the reported *NAT-IAA14* transcript (Figure 6.15), however, no correlation with the *NAT-IAA14* overexpression level was obtained. An effect on endogenous *NAT-IAA14* transcription by the overexpression has not yet been elucidated. The tendency for *NAT-IAA14* overexpression to negatively affect plants fresh weight (Figure 6.16 A) might have been a result of delayed seed germination or plant growth. In addition, the *NAT-IAA14* construct used for overexpression potentially could lack some of the regulatory elements that are required for its function. To exclude this possibility, a transient assay in *N. benthamiana* was performed using a construct that includes the reported *NAT-IAA14* genomic sequence under the control of the ethanol-inducible promoter *AlcA*, and the annotated *IAA14* sequence, driven by its endogenous promoter, in the genomic context. This experimental setup allows the induction of the transcription of the gene encoding *NAT-IAA14* by ethanol and subsequently monitoring *IAA14* expression and translation. In fact, *NAT-IAA14* and *IAA14* levels increased after incubation with ethanol (Figure 6.13). However, by infiltrating a construct into *N. benthamiana* encoding only *IAA14* driven by its endogenous promoter, *IAA14* transcription itself was activated by ethanol (Figure 6.13 C), while *IAA14* expression in *A. thaliana* was decreased in response to ethanol stress (Figure 6.13 B). This discrepancy could be a consequence of different regulatory factors involved in *IAA14* transcription in *A. thaliana* and *N. benthamiana*, and thus differential adaptation of the two plant species to ethanol stress. Moreover, after removal of the *AlcA* promoter upstream of the lncNAT-encoding gene, *NAT-IAA14* expression still increased upon ethanol induction

(Figure 6.13 G). This effect could simply be a result of an incomplete transcriptional termination of the upstream gene of *NAT-IAA14* in the vector. However, it could also suggest that, despite the absence of the *NAT-IAA14* promoter region, the *IAA14* transcription itself or the action of the *IAA14* protein could induce *NAT-IAA14* transcription in *N. benthamiana*. This assumption is supported by the results obtained in the *cr_nat-iaa14_7.14/46/54* lines, where a *NAT-IAA14* transcript missing the first 69 nt is expressed independently of a deletion of 1469 bp of the promoter region located upstream of the TSS (Figure 6.20 C).

To determine a regulatory effect of the sense gene on *NAT-IAA14* expression, lines in which *IAA14* was overexpressed or downregulated were generated. Overexpression of the reported *IAA14* transcript resulted in a reduction of *NAT-IAA14* transcript levels (Figure 6.21), while *NAT-IAA14* levels are increased in the *IAA14* gain-of-function mutant *slr-1* (Figure 6.23 C) that has a reduced *IAA14* transcription and expresses a protein that is insensitive to ubiquitination. The *slr-1* seedlings do not develop lateral roots. Notably, *IAA14* overexpression lines showed an opposite phenotype, exhibiting increased primary root length and lateral root number compared to Col-0 (Figure 6.22), suggesting that although the transcript is expressed in high levels, *IAA14* protein levels might not be elevated or even decreased in these lines, potentially as a result of the naturally fast turnover rate of *IAA14* (Guseman et al., 2015). This phenotypic observation was unexpected since it has been reported that overexpression of the *IAA14* wildtype gene resulted in a *slr-1*-like phenotype (Fukaki et al., 2002). However, Fukaki and coworkers analyzed transgenic T₁ seedlings expressing the *IAA14* cDNA, while in the present study transgenic T₃ lines expressing the *IAA14* cDNA including the 5' and 3'UTRs, which may alter transcript stability or affect translation (Srivastava et al., 2018), were used. The altered protein level might be also responsible for the differential *NAT-IAA14* expression in these lines, suggesting a feedback regulation of *NAT-IAA14* transcription by *IAA14* translation. However, to confirm this, the *IAA14* protein level needs to be analyzed in the *IAA14* overexpression lines. On the other hand, transgenic overexpression of *IAA14* might lead to a decrease in endogenous *IAA14* transcription, resulting in a corresponding reduction in *NAT-IAA14* transcript levels.

This is the first study in which *IAA14* knockout lines were generated by frameshift mutations using CRISPR/Cas9 genome editing, resulting in truncated proteins (Supplemental Figure 11.22, 11.23 & 11.24). The two used guide RNAs target regions in the coding sequence of *IAA14*, therefore it can be considered that the transcription initiation is unaffected. Nevertheless, the *IAA14* transcript level is reduced in the lines (Figure 6.23 B), suggesting an increased RNA degradation. However, it cannot be excluded that the truncated *IAA14* proteins are translated in the plant. The lines *cr_iaa14_8.5* and

cr_iaa14_46.7 could potentially express a protein lacking domain I and II, whereas in the lines *cr_iaa14_29.6* and *cr_iaa14_46.6/8/9* the translation might generate only small peptides with unrelated amino acid sequence (Supplemental Figure 11.24). *NAT-IAA14* expression in the lines potentially expressing a truncated IAA14 protein is slightly decreased (*cr_iaa14_46.7*) or unaffected (*cr_iaa14_8.5*), while in the lines lacking the IAA14 protein, *NAT-IAA14* levels are slightly reduced (*cr_iaa14_46.7/8/9*) or elevated (*cr_iaa14_29.6*) (Figure 6.23 C). No correlation could be determined between *IAA14* levels and *NAT-IAA14* transcript abundance. In contrast to the mutant lines *cr_iaa14_8.5* and *cr_iaa14_46.7*, the *NAT-IAA14* transcript level is increased significantly in the gain-of-function mutant *slr-1* (Figure 6.23 C), in which the IAA14 protein is stabilized due to a mutation in domain II (Fukaki et al., 2002). However, the presence of domain III and IV of IAA14 in the *cr_iaa14_8.5* and *cr_iaa14_46.7* lines suggests that these truncated proteins can still repress ARF7 and ARF19 and thus carry out their biological function in the plant. The discrepancy compared to *slr-1* could be explained by altered auxin sensitivity of the truncated proteins in the CRISPR/Cas9-edited lines caused by the absence of the repression and degradation domains (Dreher et al., 2006). Complementation of *IAA14* in the CRISPR/Cas9-edited lines to restore basal transcript and protein levels is required in the future to determine *NAT-IAA14* transcriptional response.

7.4 Potential regulatory mechanism of *NAT-IAA14* on *IAA14* translation

Besides the regulatory transcriptional or post-transcriptional potential of *NAT-IAA14*, a regulation on *IAA14* translation cannot be ruled out. The relatively high stability of the *NAT-IAA14* transcript (Figure 6.5) combined with its absence in nuclear fraction (Figure 6.6) suggests a function in the cytoplasm. Some lncNATs are known to regulate translation of cognate sense mRNAs, e.g. by interfering with the interaction of RNA-binding proteins with the mRNA (Deforges et al., 2019). To test the hypothesis of an effect of *NAT-IAA14* on translation, *IAA14* translation efficiency was determined in the presence of *NAT-IAA14* using an *in vitro* translation assay system in evacuated tobacco Bright Yellow-2 (BY2) cell lysate. In general, the addition of the *NAT-IAA14* transcript seems to repress translation in the BY-2 cell lysate (Figure 6.24), potentially by titrating the translational machinery away from mRNA targets due to the presence of potential sORFs encoded by the *NAT-IAA14* transcript (Supplemental Figure 11.14). Nevertheless, translation of the annotated *IAA14* mRNA variant was reduced even more by *NAT-IAA14* than that of the 124 nt-longer *IAA14* variant and an unrelated *Luciferase* mRNA. Similar results were obtained with the variant of *NAT-IAA14* lacking the overlapping region, suggesting that an overlap between the lncRNA and *IAA14* mRNA is not required for *NAT-IAA14* translational regulation. Interestingly, only

approximately 40% of *IAA14* transcripts possess the reported 3'end (Figure 6.4), suggesting that the expression of the alternative polyadenylated, 124 nt-longer *IAA14* variant might be a mechanism to escape *NAT-IAA14* regulation. Recently, a subset of dehydration stress related genes were shown to undergo 3'end extension to regulate the expression of neighboring genes by acting as long non-coding RNAs (Sun et al., 2017). On the other hand, the decrease in translation of the annotated *IAA14* transcript could be explained by reduced RNA stability in the presence of the lncNAT. Therefore, in all transgenic *NAT-IAA14* lines used in this study, the ratio between the reported and the 124 nt-longer *IAA14* transcript variants and the protein level should be determined. Furthermore, polysome association on the *IAA14* mRNA can be compared between wild-type plants and *NAT-IAA14* mutants. To further confirm the effect of *NAT-IAA14* on translation of cognate *IAA14*, a protoplast co-infiltration assay utilized by Deforges and collaborators (Deforges et al., 2019), in which the sense-encoding gene fused to NanoLuc luciferase (Nluc) is transformed into protoplasts in the presence or absence of cognate lncNAT, can be used. In this system, the firefly luciferase (Fluc) cassette contained in the sense vector serves as an internal control, allowing measurement of the Nluc:Fluc ratio to assess the effect of lncNAT on accumulation of the sense encoded protein.

Up to now, repression of mRNA translation by a lncNAT has only been reported in mouse (Ebralidze et al., 2008). In the mentioned work, Ebralidze and coworkers showed that the negative regulation of *PU.1* translation goes in hand with an anticorrelated expression of the mRNA and lncNAT. In contrast, *NAT-IAA14* and *IAA14* more often showed a concurrent expression, which might be explained by the reported negative feedback loop of *IAA14* translation on its expression in which repression of *IAA14* mRNA translation, leads to increased *IAA14* transcription (Salehin et al., 2015). This in turn apparently leads to increased *NAT-IAA14* expression, resulting in suppression of *IAA14* translation. The mechanism by which *NAT-IAA14* represses *IAA14* translation, e.g. by interaction with specific proteins or by direct interaction with the mRNA, remains unknown.

7.5 Concluding remarks

The huge amount of identified and postulated lncNATs (Ariel et al., 2015) and their presence in various multigene families support the assumption of an essential role in the regulatory network of *A. thaliana*. Results of the present study suggest a novel regulatory mode of action of an antisense lncRNA on its sense target by repressing its translation (Figure 6.24), potentially leading to a feedback loop on lncNAT expression. In addition, it constitutes the first report of an *Aux/IAA* gene regulated by a lncNAT. The results obtained in this study are summarized in the Figure 7.1 and described as follows:

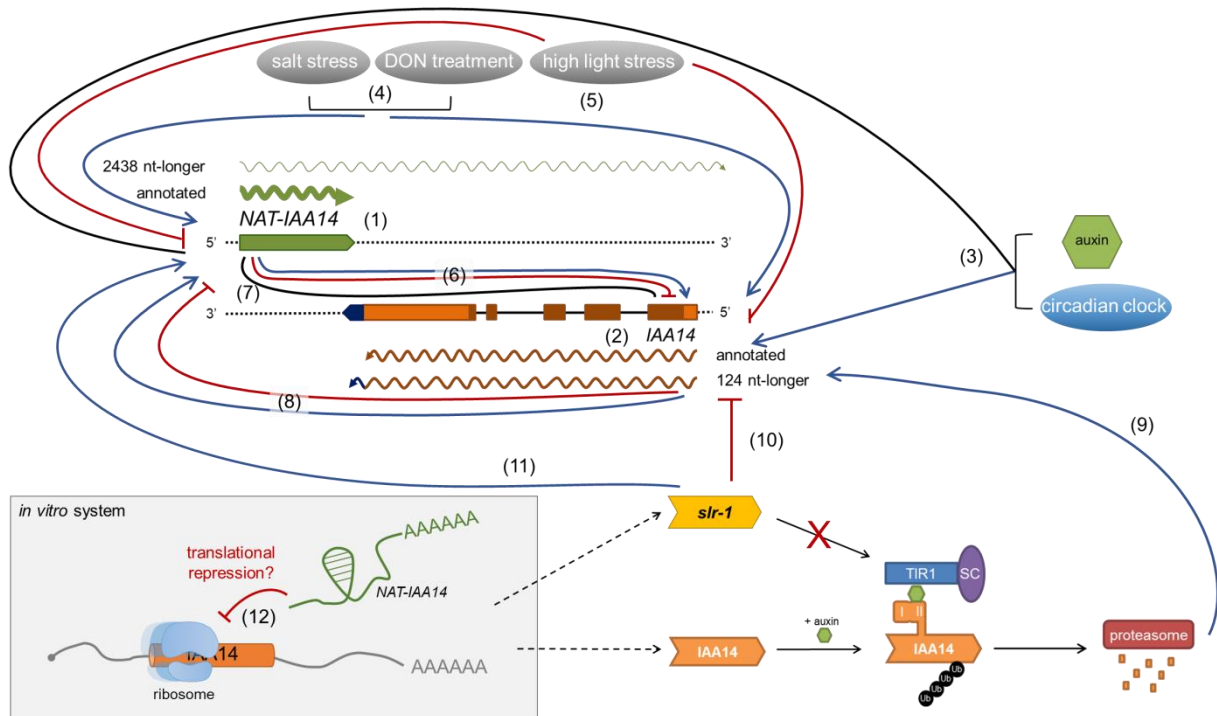


Figure 7.1: Proposed mechanism of *NAT-IAA14* mode of action and gene responses to various stresses.

Blue and red lines represent positive or negative regulation, respectively, while a black line corresponds to no regulation. The grey inset summarizes the results from *in vitro* assays that might provide evidence for translational regulation of *IAA14* by *NAT-IAA14* *in planta* (black dotted lines). TIR1 = TRANSPORT INHIBITOR RESPONSE 1, SC = ARABIDOPSIS SKP1 HOMOLOGUE (ASK1) and CULLIN 1, Ub =ubiquitylation

- (1) RACE results indicate that the *NAT-IAA14* transcript initiates 15 nt downstream of the TAIR10 reported transcription initiation site. *NAT-IAA14* transcripts possess the annotated 3'end, which is polyadenylated. Leaky transcription termination in response to a specific unknown condition(s) results in a transcriptional read-through product of *NAT-IAA14* (≥ 2438 nt-longer than the most abundant *NAT-IAA14* variant) that completely overlaps the *IAA14*-encoding gene.
- (2) 40% of the *IAA14* transcripts have the annotated 3'end, while the other 60% possess a 124 nt-longer 3'UTR.
- (3) *IAA14* expression is modulated in response to auxin and to the day-night cycle, while *NAT-IAA14* expression remained unaffected. The peaks of *NAT-IAA14* levels determined in the time course experiments suggest a rapid and dynamic regulation of gene expression.
- (4) Salt stress and mycotoxin (DON) treatment lead to increased transcript levels of *IAA14* and *NAT-IAA14*.
- (5) Sense and antisense gene expression is decreased in response to high light stress.

- (6) Changes of *NAT-IAA14* levels by overexpression or downregulation result in a concordant alteration of *IAA14* expression in most lines. However, the level of *IAA14* abundance is not consistently correlated with the level of *NAT-IAA14* overexpression or downregulation.
- (7) Knockout of the *NAT-IAA14*-encoding gene by CRISPR/Cas9 genome editing does not affect *IAA14* expression.
- (8) Overexpression of *IAA14* in *trans* results in a slight increase of *NAT-IAA14* levels. In most of the *cr_iaa14* lines, in which *IAA14* mRNA levels are reduced, the *NAT-IAA14* RNA abundance is not affected or slightly reduced.
- (9) Auxin-dependent release of ARFs by *IAA14* degradation activates the transcription of the *IAA14* gene by a negative feedback loop (Salehin et al., 2015).
- (10) In *slr-1*, the *IAA14* protein degradation is blocked, leading to a decrease in *IAA14* transcript levels, while *NAT-IAA14* abundance is elevated (11). This feedback loop on *NAT-IAA14* expression might be required to repress the translation of the mutated *IAA14* variant.
- (12) Based on *in vitro* translation assays, *NAT-IAA14*, which is localized in the cytoplasm of *A. thaliana* cells, represses translation of the annotated *IAA14* transcript to a higher extent compared to the 124 nt-longer *IAA14* variant and to the unrelated *Luciferase* mRNA.

Since the results advocate that *NAT-IAA14* most likely acts on the sense protein-coding gene *IAA14*, its activity could rely on different strategies. Besides the potential regulation of *IAA14* mRNA translation, e.g. by direct interaction with the translational machinery, an additional role of *NAT-IAA14* on *IAA14* transcription regulation, e.g. by chromatin modification or interaction with a yet unknown RNA-binding protein cannot be excluded. Notably, *NAT-IAA14* expression seems to be affected by *IAA14* expression or by a feedback loop mediated by *IAA14* translation. Future studies are clearly required to identify the details of the molecular mechanism underlying this bilateral regulation. Considering a function based on sequence homology, *NAT-IAA14* might also regulate other *Aux/IAAs*.

8 References

- Abas L, Benjamins R, Malenica N, *et al.*, 2006. Intracellular trafficking and proteolysis of the Arabidopsis auxin-efflux facilitator PIN2 are involved in root gravitropism. *Nat Cell Biol* **8**, 249-56.
- Abel S, Oeller PW, Theologis A, 1994. Early auxin-induced genes encode short-lived nuclear proteins. *Proc Natl Acad Sci U S A* **91**, 326-30.
- Alonso JM, Stepanova AN, Leisse TJ, *et al.*, 2003. Genome-wide insertional mutagenesis of Arabidopsis thaliana. *Science* **301**, 653-7.
- Andrade NM, Arismendi NL, 2013. DAPI staining and fluorescence microscopy techniques for phytoplasmas. *Methods Mol Biol* **938**, 115-21.
- Ang LH, Chattopadhyay S, Wei N, *et al.*, 1998. Molecular interaction between COP1 and HY5 defines a regulatory switch for light control of Arabidopsis development. *Mol Cell* **1**, 213-22.
- Ariel F, Jegu T, Latrasse D, *et al.*, 2014. Noncoding transcription by alternative RNA polymerases dynamically regulates an auxin-driven chromatin loop. *Mol Cell* **55**, 383-96.
- Ariel F, Romero-Barrios N, Jegu T, Benhamed M, Crespi M, 2015. Battles and hijacks: noncoding transcription in plants. *Trends Plant Sci* **20**, 362-71.
- Aslam M, Sugita K, Qin Y, Rahman A, 2020. Aux/IAA14 Regulates microRNA-Mediated Cold Stress Response in Arabidopsis Roots. *Int J Mol Sci* **21**.
- Bardou F, Ariel F, Simpson CG, *et al.*, 2014. Long noncoding RNA modulates alternative splicing regulators in Arabidopsis. *Dev Cell* **30**, 166-76.
- Bazin J, Baerenfaller K, Gosai SJ, Gregory BD, Crespi M, Bailey-Serres J, 2017. Global analysis of ribosome-associated noncoding RNAs unveils new modes of translational regulation. *Proc Natl Acad Sci U S A* **114**, E10018-e27.
- Ben Amor B, Wirth S, Merchan F, *et al.*, 2009. Novel long non-protein coding RNAs involved in Arabidopsis differentiation and stress responses. *Genome Res* **19**, 57-69.
- Bertani G, 1951. Studies on lysogeny. I. The mode of phage liberation by lysogenic Escherichia coli. *J Bacteriol* **62**, 293-300.
- Bonasio R, Shiekhhattar R, 2014. Regulation of transcription by long noncoding RNAs. *Annu Rev Genet* **48**, 433-55.
- Borsani O, Zhu J, Verslues PE, Sunkar R, Zhu JK, 2005. Endogenous siRNAs derived from a pair of natural cis-antisense transcripts regulate salt tolerance in Arabidopsis. *Cell* **123**, 1279-91.
- Buntru M, Vogel S, Spiegel H, Schillberg S, 2014. Tobacco BY-2 cell-free lysate: an alternative and highly-productive plant-based in vitro translation system. *BMC Biotechnol* **14**, 37.
- Calderón Villalobos LIA, Lee S, De Oliveira C, *et al.*, 2012. A combinatorial TIR1/AFB-Aux/IAA co-receptor system for differential sensing of auxin. *Nature chemical biology* **8**, 477-85.
- Campalans A, Kondorosi A, Crespi M, 2004. Enod40, a short open reading frame-containing mRNA, induces cytoplasmic localization of a nuclear RNA binding protein in Medicago truncatula. *Plant Cell* **16**, 1047-59.
- Carbonell A, Martinez De Alba AE, Flores R, Gago S, 2008. Double-stranded RNA interferes in a sequence-specific manner with the infection of representative members of the two viroid families. *Virology* **371**, 44-53.
- Carbonell A, Takeda A, Fahlgren N, Johnson SC, Cuperus JT, Carrington JC, 2014. New generation of artificial MicroRNA and synthetic trans-acting small interfering RNA vectors for efficient gene silencing in Arabidopsis. *Plant Physiol* **165**, 15-29.

- Carlevaro-Fita J, Johnson R, 2019. Global Positioning System: Understanding Long Noncoding RNAs through Subcellular Localization. *Mol Cell* **73**, 869-83.
- Chattopadhyay S, Ang LH, Puente P, Deng XW, Wei N, 1998. Arabidopsis bZIP protein HY5 directly interacts with light-responsive promoters in mediating light control of gene expression. *Plant Cell* **10**, 673-83.
- Chekanova JA, 2015. Long non-coding RNAs and their functions in plants. *Curr Opin Plant Biol* **27**, 207-16.
- Chen M, Wang C, Bao H, Chen H, Wang Y, 2016. Genome-wide identification and characterization of novel lncRNAs in Populus under nitrogen deficiency. *Mol Genet Genomics* **291**, 1663-80.
- Chomczynski P, Sacchi N, 2006. The single-step method of RNA isolation by acid guanidinium thiocyanate-phenol-chloroform extraction: twenty-something years on. *Nat Protoc* **1**, 581-5.
- Clark MB, Johnston RL, Inostroza-Ponta M, *et al.*, 2012. Genome-wide analysis of long noncoding RNA stability. *Genome Res* **22**, 885-98.
- Clough SJ, Bent AF, 1998. Floral dip: a simplified method for Agrobacterium-mediated transformation of Arabidopsis thaliana. *Plant J* **16**, 735-43.
- Cluis CP, Mouchel CF, Hardtke CS, 2004. The Arabidopsis transcription factor HY5 integrates light and hormone signaling pathways. *Plant J* **38**, 332-47.
- Covington MF, Harmer SL, 2007. The circadian clock regulates auxin signaling and responses in Arabidopsis. *PLoS Biol* **5**, e222.
- Crespi MD, Jurkevitch E, Poiret M, *et al.*, 1994. enod40, a gene expressed during nodule organogenesis, codes for a non-translatable RNA involved in plant growth. *Embo j* **13**, 5099-112.
- Crisp PA, Ganguly DR, Smith AB, *et al.*, 2017. Rapid Recovery Gene Downregulation during Excess-Light Stress and Recovery in Arabidopsis. *Plant Cell* **29**, 1836-63.
- Csorba T, Questa JI, Sun Q, Dean C, 2014. Antisense COOLAIR mediates the coordinated switching of chromatin states at FLC during vernalization. *Proc Natl Acad Sci U S A* **111**, 16160-5.
- Dallmeier K, Neyts J, 2013. Simple and inexpensive three-step rapid amplification of cDNA 5' ends using 5' phosphorylated primers. *Anal Biochem* **434**, 1-3.
- Deforges J, Reis RS, Jacquet P, *et al.*, 2019. Control of Cognate Sense mRNA Translation by cis-Natural Antisense RNAs. *Plant Physiol* **180**, 305-22.
- Di C, Yuan J, Wu Y, *et al.*, 2014. Characterization of stress-responsive lncRNAs in Arabidopsis thaliana by integrating expression, epigenetic and structural features. *Plant J* **80**, 848-61.
- Dreher KA, Brown J, Saw RE, Callis J, 2006. The Arabidopsis Aux/IAA protein family has diversified in degradation and auxin responsiveness. *Plant Cell* **18**, 699-714.
- Dunn EA, Rader SD, 2010. Secondary structure of U6 small nuclear RNA: implications for spliceosome assembly. *Biochemical Society Transactions* **38**, 1099-104.
- Ebralidze AK, Guibal FC, Steidl U, *et al.*, 2008. PU.1 expression is modulated by the balance of functional sense and antisense RNAs regulated by a shared cis-regulatory element. *Genes Dev* **22**, 2085-92.
- Engler C, Gruetzner R, Kandzia R, Marillonnet S, 2009. Golden gate shuffling: a one-pot DNA shuffling method based on type II restriction enzymes. *PLoS One* **4**, e5553.
- Fauquenoy S, Migeot V, Finet O, *et al.*, 2018. Repression of Cell Differentiation by a cis-Acting lincRNA in Fission Yeast. *Curr Biol* **28**, 383-91.e3.
- Fedak H, Palusinska M, Krzyczmonik K, *et al.*, 2016. Control of seed dormancy in Arabidopsis by a cis-acting noncoding antisense transcript. *Proc Natl Acad Sci U S A* **113**, E7846-E55.
- Franco-Zorrilla JM, Valli A, Todesco M, *et al.*, 2007. Target mimicry provides a new mechanism for regulation of microRNA activity. *Nat Genet* **39**, 1033-7.
- Friml J, Wiśniewska J, Benková E, Mendgen K, Palme K, 2002. Lateral relocation of auxin efflux regulator PIN3 mediates tropism in Arabidopsis. *Nature* **415**, 806-9.

- Fukaki H, Nakao Y, Okushima Y, Theologis A, Tasaka M, 2005. Tissue-specific expression of stabilized SOLITARY-ROOT/IAA14 alters lateral root development in Arabidopsis. *Plant J* **44**, 382-95.
- Fukaki H, Tameda S, Masuda H, Tasaka M, 2002. Lateral root formation is blocked by a gain-of-function mutation in the SOLITARY-ROOT/IAA14 gene of Arabidopsis. *Plant J* **29**, 153-68.
- Fukaki H, Taniguchi N, Tasaka M, 2006. PICKLE is required for SOLITARY-ROOT/IAA14-mediated repression of ARF7 and ARF19 activity during Arabidopsis lateral root initiation. *Plant J* **48**, 380-9.
- Gao Y, Zhang Y, Zhang D, Dai X, Estelle M, Zhao Y, 2015. Auxin binding protein 1 (ABP1) is not required for either auxin signaling or Arabidopsis development. *Proc Natl Acad Sci U S A* **112**, 2275-80.
- Gelvin SB, 2003. Agrobacterium-mediated plant transformation: the biology behind the "gene-jockeying" tool. *Microbiol Mol Biol Rev* **67**, 16-37, table of contents.
- Ghildiyal M, Zamore PD, 2009. Small silencing RNAs: an expanding universe. *Nat Rev Genet* **10**, 94-108.
- Goh T, Kasahara H, Mimura T, Kamiya Y, Fukaki H, 2012. Multiple AUX/IAA-ARF modules regulate lateral root formation: the role of Arabidopsis SHY2/IAA3-mediated auxin signalling. *Philos Trans R Soc Lond B Biol Sci* **367**, 1461-8.
- Gray WM, 2004. Hormonal regulation of plant growth and development. *PLoS Biol* **2**, E311.
- Gray WM, Kepinski S, Rouse D, Leyser O, Estelle M, 2001. Auxin regulates SCF(TIR1)-dependent degradation of AUX/IAA proteins. *Nature* **414**, 271-6.
- Guseman JM, Hellmuth A, Lanctot A, *et al.*, 2015. Auxin-induced degradation dynamics set the pace for lateral root development. *Development* **142**, 905-9.
- Hamann T, Benkova E, Bäurle I, Kientz M, Jürgens G, 2002. The Arabidopsis BODENLOS gene encodes an auxin response protein inhibiting MONOPTEROS-mediated embryo patterning. *Genes Dev* **16**, 1610-5.
- Hamann T, Mayer U, Jürgens G, 1999. The auxin-insensitive bodenlos mutation affects primary root formation and apical-basal patterning in the Arabidopsis embryo. *Development* **126**, 1387-95.
- Hanahan D, 1983. Studies on transformation of Escherichia coli with plasmids. *J Mol Biol* **166**, 557-80.
- Harmer SL, Hogenesch JB, Straume M, *et al.*, 2000. Orchestrated transcription of key pathways in Arabidopsis by the circadian clock. *Science* **290**, 2110-3.
- Held MA, Penning B, Brandt AS, *et al.*, 2008. Small-interfering RNAs from natural antisense transcripts derived from a cellulose synthase gene modulate cell wall biosynthesis in barley. *Proc Natl Acad Sci U S A* **105**, 20534-9.
- Henriques R, Wang H, Liu J, Boix M, Huang L-F, Chua N-H, 2017. The antiphasic regulatory module comprising CDF5 and its antisense RNA FLORE links the circadian clock to photoperiodic flowering. *New Phytologist* **216**, 854-67.
- Heo JB, Sung S, 2011. Vernalization-Mediated Epigenetic Silencing by a Long Intronic Noncoding RNA. *Science* **331**, 76-9.
- Hirsch J, Lefort V, Vankersschaver M, *et al.*, 2006. Characterization of 43 non-protein-coding mRNA genes in Arabidopsis, including the MIR162a-derived transcripts. *Plant Physiol* **140**, 1192-204.
- Hong L, Ye C, Lin J, Fu H, Wu X, Li QQ, 2018. Alternative polyadenylation is involved in auxin-based plant growth and development. *Plant J* **93**, 246-58.
- Hüfner D, 2017. Characterization of NAT-IAA14promoter and IAA14 3'UTR splicing variants. *Bachelor Thesis, Institute of Biochemistry and Biotechnology, Faculty I of Natural Science, Martin-Luther-University Halle-Wittenberg.*
- Hüttenhofer A, Schattner P, Polacek N, 2005. Non-coding RNAs: hope or hype? *Trends Genet* **21**, 289-97.
- Ito J, Fukaki H, Onoda M, *et al.*, 2016. Auxin-dependent compositional change in Mediator in ARF7- and ARF19-mediated transcription. *Proc Natl Acad Sci U S A* **113**, 6562-7.

- Jha UC, Nayyar H, Jha R, *et al.*, 2020. Long non-coding RNAs: emerging players regulating plant abiotic stress response and adaptation. *BMC Plant Biol* **20**, 466.
- Kalyna M, Simpson CG, Syed NH, *et al.*, 2012. Alternative splicing and nonsense-mediated decay modulate expression of important regulatory genes in Arabidopsis. *Nucleic Acids Res* **40**, 2454-69.
- Karimi M, De Meyer B, Hilson P, 2005. Modular cloning in plant cells. *Trends Plant Sci* **10**, 103-5.
- Karimi M, Inzé D, Depicker A, 2002. GATEWAY vectors for Agrobacterium-mediated plant transformation. *Trends Plant Sci* **7**, 193-5.
- Karlik E, Ari S, Gozukirmizi N, 2019. LncRNAs: genetic and epigenetic effects in plants. *Biotechnology & Biotechnological Equipment* **33**, 429-39.
- Kim BC, Soh MC, Kang BJ, Furuya M, Nam HG, 1996. Two dominant photomorphogenic mutations of Arabidopsis thaliana identified as suppressor mutations of hy2. *Plant J* **9**, 441-56.
- Kim DH, Sung S, 2017. Vernalization-Triggered Intragenic Chromatin Loop Formation by Long Noncoding RNAs. *Dev Cell* **40**, 302-12.e4.
- Kim J, Harter K, Theologis A, 1997. Protein-protein interactions among the Aux/IAA proteins. *Proc Natl Acad Sci U S A* **94**, 11786-91.
- Kim SH, Bahk S, An J, *et al.*, 2020. A Gain-of-Function Mutant of IAA15 Inhibits Lateral Root Development by Transcriptional Repression of LBD Genes in Arabidopsis. *Front Plant Sci* **11**, 1239.
- Kindgren P, Ard R, Ivanov M, Marquardt S, 2018. Transcriptional read-through of the long non-coding RNA SVALKA governs plant cold acclimation. *Nat Commun* **9**, 4561.
- Koncz C, Schell J, 1986. The promoter of TL-DNA gene 5 controls the tissue-specific expression of chimaeric genes carried by a novel type of Agrobacterium binary vector. *Molecular and General Genetics MGG* **204**, 383-96.
- Kovaka S, Zimin AV, Pertea GM, Razaghi R, Salzberg SL, Pertea M, 2019. Transcriptome assembly from long-read RNA-seq alignments with StringTie2. *Genome Biol* **20**, 278.
- Krysan PJ, Young JC, Sussman MR, 1999. T-DNA as an insertional mutagen in Arabidopsis. *Plant Cell* **11**, 2283-90.
- Kurihara Y, Makita Y, Shimohira H, Fujita T, Iwasaki S, Matsui M, 2020. Translational Landscape of Protein-Coding and Non-Protein-Coding RNAs upon Light Exposure in Arabidopsis. *Plant Cell Physiol* **61**, 536-45.
- Kurihara Y, Matsui A, Hanada K, *et al.*, 2009. Genome-wide suppression of aberrant mRNA-like noncoding RNAs by NMD in Arabidopsis. *Proc Natl Acad Sci U S A* **106**, 2453-8.
- Laneve P, Rea J, Caffarelli E, 2019. Long Noncoding RNAs: Emerging Players in Medulloblastoma. *Front Pediatr* **7**, 67.
- Leyser HM, Pickett FB, Dharmasiri S, Estelle M, 1996. Mutations in the AXR3 gene of Arabidopsis result in altered auxin response including ectopic expression from the SAUR-AC1 promoter. *Plant J* **10**, 403-13.
- Li QQ, Zhang Z, Wang YL, *et al.*, 2021. Phytochrome B inhibits darkness-induced hypocotyl adventitious root formation by stabilizing IAA14 and suppressing ARF7 and ARF19. *Plant J* **105**, 1689-702.
- Li S, Liberman LM, Mukherjee N, Benfey PN, Ohler U, 2013. Integrated detection of natural antisense transcripts using strand-specific RNA sequencing data. *Genome Res* **23**, 1730-9.
- Lindsey K, Casson S, Chilley P, 2002. Peptides: new signalling molecules in plants. *Trends Plant Sci* **7**, 78-83.
- Liu F, Marquardt S, Lister C, Swiezewski S, Dean C, 2010. Targeted 3' processing of antisense transcripts triggers Arabidopsis FLC chromatin silencing. *Science* **327**, 94-7.
- Liu J, Jung C, Xu J, *et al.*, 2012. Genome-wide analysis uncovers regulation of long intergenic noncoding RNAs in Arabidopsis. *Plant Cell* **24**, 4333-45.
- Luo J, Zhou JJ, Zhang JZ, 2018. Aux/IAA Gene Family in Plants: Molecular Structure, Regulation, and Function. *Int J Mol Sci* **19**.

- Maitra Majee S, Sharma E, Singh B, Khurana JP, 2020. Drought-induced protein (Di19-3) plays a role in auxin signaling by interacting with IAA14 in Arabidopsis. *Plant Direct* **4**, e00234.
- Matsui A, Ishida J, Morosawa T, *et al.*, 2008. Arabidopsis transcriptome analysis under drought, cold, high-salinity and ABA treatment conditions using a tiling array. *Plant Cell Physiol* **49**, 1135-49.
- Matsumoto A, Nakayama KI, 2018. Hidden Peptides Encoded by Putative Noncoding RNAs. *Cell Struct Funct* **43**, 75-83.
- Mcclung CR, 2006. Plant circadian rhythms. *Plant Cell* **18**, 792-803.
- Mcstee P, Leyser O, 2005. Shoot branching. *Annu Rev Plant Biol* **56**, 353-74.
- Mignone F, Gissi C, Liuni S, Pesole G, 2002. Untranslated regions of mRNAs. *Genome Biol* **3**, Reviews0004.
- Mohammadin S, Edger PP, Pires JC, Schranz ME, 2015. Positionally-conserved but sequence-diverged: identification of long non-coding RNAs in the Brassicaceae and Cleomaceae. *BMC Plant Biol* **15**, 217.
- Möller B, Weijers D, 2009. Auxin control of embryo patterning. *Cold Spring Harb Perspect Biol* **1**, a001545.
- Moretto F, Wood NE, Kelly G, Doncic A, Van Werven FJ, 2018. A regulatory circuit of two lncRNAs and a master regulator directs cell fate in yeast. *Nat Commun* **9**, 780.
- Murashige T, Skoog F, 1962. A Revised Medium for Rapid Growth and Bio Assays with Tobacco Tissue Cultures. *Physiologia Plantarum* **15**, 473-97.
- Nagpal P, Walker LM, Young JC, *et al.*, 2000. AXR2 encodes a member of the Aux/IAA protein family. *Plant Physiol* **123**, 563-74.
- Narise T, Kobayashi K, Baba S, *et al.*, 2010. Involvement of auxin signaling mediated by IAA14 and ARF7/19 in membrane lipid remodeling during phosphate starvation. *Plant Mol Biol* **72**, 533-44.
- Noh JH, Kim KM, McClusky WG, Abdelmohsen K, Gorospe M, 2018. Cytoplasmic functions of long noncoding RNAs. *Wiley Interdiscip Rev RNA* **9**, e1471.
- Obulareddy N, Panchal S, Melotto M, 2013. Guard cell purification and RNA isolation suitable for high-throughput transcriptional analysis of cell-type responses to biotic stresses. *Mol Plant Microbe Interact* **26**, 844-9.
- Okushima Y, Overvoorde PJ, Arima K, *et al.*, 2005. Functional genomic analysis of the AUXIN RESPONSE FACTOR gene family members in Arabidopsis thaliana: unique and overlapping functions of ARF7 and ARF19. *Plant Cell* **17**, 444-63.
- Ozsolak F, Milos PM, 2011. RNA sequencing: advances, challenges and opportunities. *Nat Rev Genet* **12**, 87-98.
- Park SH, Chung PJ, Juntawong P, *et al.*, 2012. Posttranscriptional control of photosynthetic mRNA decay under stress conditions requires 3' and 5' untranslated regions and correlates with differential polysome association in rice. *Plant Physiol* **159**, 1111-24.
- Pelechano V, Steinmetz LM, 2013. Gene regulation by antisense transcription. *Nat Rev Genet* **14**, 880-93.
- Perrot-Rechenmann C, 2010. Cellular responses to auxin: division versus expansion. *Cold Spring Harb Perspect Biol* **2**, a001446.
- Pogoda M, 2015. Analysis of the role of the natural antisense long non-coding RNA encoded by the At4g14548 gene from Arabidopsis thaliana. *Master Thesis, Institute of Biochemistry and Biotechnology, Faculty I of Natural Science, Martin-Luther-University Halle-Wittenberg.*
- Powers SK, Strader LC, 2020. Regulation of auxin transcriptional responses. *Dev Dyn* **249**, 483-95.
- Quinn JJ, Chang HY, 2016. Unique features of long non-coding RNA biogenesis and function. *Nat Rev Genet* **17**, 47-62.
- Ramos JA, Zenser N, Leyser O, Callis J, 2001. Rapid degradation of auxin/indoleacetic acid proteins requires conserved amino acids of domain II and is proteasome dependent. *Plant Cell* **13**, 2349-60.

- Rayson S, Arciga-Reyes L, Wootton L, *et al.*, 2012. A role for nonsense-mediated mRNA decay in plants: pathogen responses are induced in *Arabidopsis thaliana* NMD mutants. *PLoS One* **7**, e31917.
- Reed JW, 2001. Roles and activities of Aux/IAA proteins in *Arabidopsis*. *Trends Plant Sci* **6**, 420-5.
- Rinaldi MA, Liu J, Enders TA, Bartel B, Strader LC, 2012. A gain-of-function mutation in IAA16 confers reduced responses to auxin and abscisic acid and impedes plant growth and fertility. *Plant Mol Biol* **79**, 359-73.
- Rogg LE, Lasswell J, Bartel B, 2001. A gain-of-function mutation in IAA28 suppresses lateral root development. *Plant Cell* **13**, 465-80.
- Rohrig H, Schmidt J, Miklashevichs E, Schell J, John M, 2002. Soybean ENOD40 encodes two peptides that bind to sucrose synthase. *Proc Natl Acad Sci U S A* **99**, 1915-20.
- Rosa S, Duncan S, Dean C, 2016. Mutually exclusive sense-antisense transcription at FLC facilitates environmentally induced gene repression. *Nat Commun* **7**, 13031.
- Rouse D, Mackay P, Stirnberg P, Estelle M, Leyser O, 1998. Changes in auxin response from mutations in an AUX/IAA gene. *Science* **279**, 1371-3.
- Salehin M, Bagchi R, Estelle M, 2015. SCF^{TIR1/AFB}-Based Auxin Perception: Mechanism and Role in Plant Growth and Development. *Plant Cell* **27**, 9-19.
- Scarpella E, Barkoulas M, Tsiantis M, 2010. Control of leaf and vein development by auxin. *Cold Spring Harb Perspect Biol* **2**, a001511.
- Seidel K, 2014. Analysis of the role of the natural antisense long noncoding RNA encoded by At4g14548 in IAA14 regulation. *Master Thesis, Institute of Biochemistry and Biotechnology, Faculty I of Natural Science, Martin-Luther-University Halle-Wittenberg*.
- Seo JS, Sun H-X, Park BS, *et al.*, 2017. ELF18-INDUCED LONG-NONCODING RNA Associates with Mediator to Enhance Expression of Innate Immune Response Genes in *Arabidopsis*. *Plant Cell* **29**, 1024-38.
- Shani E, Salehin M, Zhang Y, *et al.*, 2017. Plant Stress Tolerance Requires Auxin-Sensitive Aux/IAA Transcriptional Repressors. *Curr Biol* **27**, 437-44.
- Shuai P, Liang D, Tang S, *et al.*, 2014. Genome-wide identification and functional prediction of novel and drought-responsive lincRNAs in *Populus trichocarpa*. *J Exp Bot* **65**, 4975-83.
- Song X, Liu G, Huang Z, *et al.*, 2016. Temperature expression patterns of genes and their coexpression with lncRNAs revealed by RNA-Seq in non-heading Chinese cabbage. *BMC Genomics* **17**, 297.
- Srivastava AK, Lu Y, Zinta G, Lang Z, Zhu JK, 2018. UTR-Dependent Control of Gene Expression in Plants. *Trends Plant Sci* **23**, 248-59.
- Sun HX, Li Y, Niu QW, Chua NH, 2017. Dehydration stress extends mRNA 3' untranslated regions with noncoding RNA functions in *Arabidopsis*. *Genome Res* **27**, 1427-36.
- Sun Q, Hao Q, Prasanth KV, 2018. Nuclear Long Noncoding RNAs: Key Regulators of Gene Expression. *Trends Genet* **34**, 142-57.
- Sun Z, Huang K, Han Z, Wang P, Fang Y, 2020. Genome-wide identification of *Arabidopsis* long noncoding RNAs in response to the blue light. *Scientific Reports* **10**, 6229.
- Swiezewski S, Liu F, Magusin A, Dean C, 2009. Cold-induced silencing by long antisense transcripts of an *Arabidopsis* Polycomb target. *Nature* **462**, 799-802.
- Tani H, Mizutani R, Salam KA, *et al.*, 2012. Genome-wide determination of RNA stability reveals hundreds of short-lived noncoding transcripts in mammals. *Genome Res* **22**, 947-56.
- Tanimoto M, Jowett J, Stirnberg P, Rouse D, Leyser O, 2007. pax1-1 partially suppresses gain-of-function mutations in *Arabidopsis* AXR3/IAA17. *BMC Plant Biol* **7**, 20.
- Tatematsu K, Kumagai S, Muto H, *et al.*, 2004. MASSUGU2 encodes Aux/IAA19, an auxin-regulated protein that functions together with the transcriptional activator NPH4/ARF7 to regulate differential growth responses of hypocotyl and formation of lateral roots in *Arabidopsis thaliana*. *Plant Cell* **16**, 379-93.

- Tian Q, Reed JW, 1999. Control of auxin-regulated root development by the Arabidopsis thaliana SHY2/IAA3 gene. *Development* **126**, 711-21.
- Tripathi R, Chakraborty P, Varadwaj PK, 2017. Unraveling long non-coding RNAs through analysis of high-throughput RNA-sequencing data. *Noncoding RNA Res* **2**, 111-8.
- Uehara T, Okushima Y, Mimura T, Tasaka M, Fukaki H, 2008. Domain II mutations in CRANE/IAA18 suppress lateral root formation and affect shoot development in Arabidopsis thaliana. *Plant Cell Physiol* **49**, 1025-38.
- Ulmasov T, Hagen G, Guilfoyle TJ, 1999. Activation and repression of transcription by auxin-response factors. *Proc Natl Acad Sci U S A* **96**, 5844-9.
- Voß U, Wilson MH, Kenobi K, *et al.*, 2015. The circadian clock rephases during lateral root organ initiation in Arabidopsis thaliana. *Nat Commun* **6**, 7641.
- Waititu JK, Zhang C, Liu J, Wang H, 2020. Plant Non-Coding RNAs: Origin, Biogenesis, Mode of Action and Their Roles in Abiotic Stress. *Int J Mol Sci* **21**.
- Wang H, Chung PJ, Liu J, *et al.*, 2014a. Genome-wide identification of long noncoding natural antisense transcripts and their responses to light in Arabidopsis. *Genome Res* **24**, 444-53.
- Wang HV, Chekanova JA, 2017. Long Noncoding RNAs in Plants. *Adv Exp Med Biol* **1008**, 133-54.
- Wang J, Meng X, Dobrovolskaya OB, Orlov YL, Chen M, 2017. Non-coding RNAs and Their Roles in Stress Response in Plants. *Genomics Proteomics Bioinformatics* **15**, 301-12.
- Wang J, Yan D-W, Yuan T-T, Gao X, Lu Y-T, 2013. A gain-of-function mutation in IAA8 alters Arabidopsis floral organ development by change of jasmonic acid level. *Plant Molecular Biology* **82**, 71-83.
- Wang J, Yu W, Yang Y, *et al.*, 2015. Genome-wide analysis of tomato long non-coding RNAs and identification as endogenous target mimic for microRNA in response to TYLCV infection. *Sci Rep* **5**, 16946.
- Wang J, Zhou L, Shi H, *et al.*, 2018a. A single transcription factor promotes both yield and immunity in rice. *Science* **361**, 1026-8.
- Wang R, Estelle M, 2014. Diversity and specificity: auxin perception and signaling through the TIR1/AFB pathway. *Curr Opin Plant Biol* **21**, 51-8.
- Wang Y, Fan X, Lin F, *et al.*, 2014b. Arabidopsis noncoding RNA mediates control of photomorphogenesis by red light. *Proceedings of the National Academy of Sciences* **111**, 10359-64.
- Wang Y, Luo X, Sun F, *et al.*, 2018b. Overexpressing lncRNA LAIR increases grain yield and regulates neighbouring gene cluster expression in rice. *Nature Communications* **9**, 3516.
- Weijers D, Schlereth A, Ehrismann JS, Schwank G, Kientz M, Jürgens G, 2006. Auxin triggers transient local signaling for cell specification in Arabidopsis embryogenesis. *Dev Cell* **10**, 265-70.
- Weijers D, Wagner D, 2016. Transcriptional Responses to the Auxin Hormone. *Annu Rev Plant Biol* **67**, 539-74.
- Werner S, Breus O, Symonenko Y, Marillonnet S, Gleba Y, 2011. High-level recombinant protein expression in transgenic plants by using a double-inducible viral vector. *Proc Natl Acad Sci U S A* **108**, 14061-6.
- Wilmoth JC, Wang S, Tiwari SB, *et al.*, 2005. NPH4/ARF7 and ARF19 promote leaf expansion and auxin-induced lateral root formation. *Plant J* **43**, 118-30.
- Wilson AK, Pickett FB, Turner JC, Estelle M, 1990. A dominant mutation in Arabidopsis confers resistance to auxin, ethylene and abscisic acid. *Mol Gen Genet* **222**, 377-83.
- Winkler M, Niemeyer M, Hellmuth A, *et al.*, 2017. Variation in auxin sensing guides AUX/IAA transcriptional repressor ubiquitylation and destruction. *Nat Commun* **8**, 15706.
- Wu L, Liu S, Qi H, Cai H, Xu M, 2020a. Research Progress on Plant Long Non-Coding RNA. *Plants (Basel)* **9**.

- Wu Z, Fang X, Zhu D, Dean C, 2020b. Autonomous Pathway: FLOWERING LOCUS C Repression through an Antisense-Mediated Chromatin-Silencing Mechanism. *Plant Physiol* **182**, 27-37.
- Wunderlich M, Gross-Hardt R, Schöffl F, 2014. Heat shock factor HSFB2a involved in gametophyte development of *Arabidopsis thaliana* and its expression is controlled by a heat-inducible long non-coding antisense RNA. *Plant Mol Biol* **85**, 541-50.
- Xin M, Wang Y, Yao Y, *et al.*, 2011. Identification and characterization of wheat long non-protein coding RNAs responsive to powdery mildew infection and heat stress by using microarray analysis and SBS sequencing. *BMC Plant Biol* **11**, 61.
- Xing Q, Zhang W, Liu M, Li L, Li X, Yan J, 2019. Genome-Wide Identification of Long Non-coding RNAs Responsive to *Lasioidiplodia theobromae* Infection in Grapevine. *Evol Bioinform Online* **15**, 1176934319841362.
- Xu XW, Zhou XH, Wang RR, Peng WL, An Y, Chen LL, 2016. Functional analysis of long intergenic non-coding RNAs in phosphate-starved rice using competing endogenous RNA network. *Sci Rep* **6**, 20715.
- Yang X, Lee S, So JH, *et al.*, 2004. The IAA1 protein is encoded by AXR5 and is a substrate of SCF(TIR1). *Plant J* **40**, 772-82.
- Yao Y, Ni Z, Peng H, *et al.*, 2010. Non-coding small RNAs responsive to abiotic stress in wheat (*Triticum aestivum* L.). *Funct Integr Genomics* **10**, 187-90.
- Yatusevich R, Fedak H, Ciesielski A, *et al.*, 2017. Antisense transcription represses *Arabidopsis* seed dormancy QTL DOG1 to regulate drought tolerance. *EMBO reports* **18**, 2186-96.
- Yin H, Zhang X, Zhang B, Luo H, He C, 2019. Revealing the dominant long noncoding RNAs responding to the infection with *Colletotrichum gloeosporioides* in *Hevea brasiliensis*. *Biol Direct* **14**, 7.
- Zajac P, Islam S, Hochgerner H, Lonnerberg P, Linnarsson S, 2013. Base preferences in non-templated nucleotide incorporation by MMLV-derived reverse transcriptases. *PLoS One* **8**, e85270.
- Zaynab M, Fatima M, Abbas S, Umair M, Sharif Y, Raza MA, 2018. Long non-coding RNAs as molecular players in plant defense against pathogens. *Microb Pathog* **121**, 277-82.
- Zhang H, Chen X, Wang C, *et al.*, 2013. Long non-coding genes implicated in response to stripe rust pathogen stress in wheat (*Triticum aestivum* L.). *Mol Biol Rep* **40**, 6245-53.
- Zhang W, Han Z, Guo Q, *et al.*, 2014a. Identification of maize long non-coding RNAs responsive to drought stress. *PLoS One* **9**, e98958.
- Zhang X, Wang W, Zhu W, *et al.*, 2019. Mechanisms and Functions of Long Non-Coding RNAs at Multiple Regulatory Levels. *Int J Mol Sci* **20**.
- Zhang Y-C, Liao J-Y, Li Z-Y, *et al.*, 2014b. Genome-wide screening and functional analysis identify a large number of long noncoding RNAs involved in the sexual reproduction of rice. *Genome Biology* **15**, 512.
- Zhao X, Li J, Lian B, Gu H, Li Y, Qi Y, 2018. Global identification of *Arabidopsis* lncRNAs reveals the regulation of MAF4 by a natural antisense RNA. *Nature Communications* **9**, 5056.
- Zhu QH, Stephen S, Taylor J, Helliwell CA, Wang MB, 2014. Long noncoding RNAs responsive to *Fusarium oxysporum* infection in *Arabidopsis thaliana*. *New Phytol* **201**, 574-84.

9 List of figures

Figure 3.1: Classification of lncRNA according to their relationship to nearby protein-coding genes. (modified after Wang & Chekanova, 2017)	4
Figure 3.2: Cartoon showing various mechanisms of lncRNA action. (modified after Laneve et al., 2019 and Noh et al., 2018)	5
Figure 3.3: General scheme of auxin signaling through the SCF ^{TIR1/AFB} pathway. (modified after Powers & Strader, 2020)	10
Figure 3.4: Schematic representation of the AUX/IAA and ARF domain structure. (modified after Powers & Strader, 2020)	11
Figure 3.5: Functions of the <i>AUX/IAA</i> genes in developmental processes of <i>A. thaliana</i> and phenotypes of the gain-of-function mutants. (modified after Luo et al., 2018)	12
Figure 3.6: Phenotypes of the <i>slr-1</i> mutant. (Fukaki et al., 2002)	13
Figure 3.7: <i>IAA14</i> gene expression oscillates like circadian clock genes <i>CCA1</i> and <i>TOC1</i> . (Voß et al., 2015)	15
Figure 3.8: Schematic representation of <i>IAA14</i> and <i>NAT-IAA14</i> location on the chromosome 4 of <i>A. thaliana</i>	16
Figure 4.1: Pattern of GUS-staining of <i>NAT-IAA14_{prom}::GUS</i> and <i>IAA14_{prom}::GUS</i> reporter lines during the <i>A. thaliana</i> life cycle. (modified after Pogoda, 2015)	17
Figure 4.2: <i>IAA14</i> transcript variant with a longer 3'end. (modified after Seidel, 2014)	18
Figure 6.1: RPA-mediated detection of the <i>NAT-IAA14</i> transcript in total RNA extracts of Col-0.	39
Figure 6.2: <i>NAT-IAA14</i> RNA starts 15 nt downstream of the annotated transcription start site.	40
Figure 6.3: Determination of <i>NAT-IAA14</i> 3'end by circular 3'RACE.	41
Figure 6.4: 60% of the <i>IAA14</i> transcripts have an overlap of 67 nt with <i>NAT-IAA14</i>	42
Figure 6.5: RNA half-life determination of <i>NAT-IAA14</i> transcripts performed in Col-0 seedlings.	43
Figure 6.6: <i>NAT-IAA14</i> localization in the cytosolic fraction of Col-0 seedlings.	44
Figure 6.7: Analysis of <i>NAT-IAA14</i> transcript as NMD target.	45
Figure 6.8: <i>NAT-IAA14</i> and <i>IAA14</i> transcript levels are altered during Arabidopsis life cycle.	46
Figure 6.9: <i>NAT-IAA14</i> and <i>IAA14</i> transcript levels showed a correlated expression pattern in leaf, root and shoot apex in young seedlings.	47

Figure 6.10: <i>NAT-IAA14</i> expression shows a variable response to light.....	48
Figure 6.11: <i>NAT-IAA14</i> and <i>IAA14</i> response upon IAA treatment.	49
Figure 6.12: <i>NAT-IAA14</i> and <i>IAA14</i> co-expression upon co-infiltration in <i>N. benthamiana</i> ...	50
Figure 6.13: <i>NAT-IAA14</i> transcription does not influence <i>IAA14</i> expression upon ethanol induction in <i>N. benthamiana</i>	52
Figure 6.14: <i>NAT-IAA14</i> and <i>IAA14</i> expression is affected by different stresses.....	54
Figure 6.15: <i>IAA14</i> transcript levels are increased in three out of four <i>NAT-IAA14</i> overexpression lines.....	55
Figure 6.16: Phenotypic analysis of transgenic lines overexpressing the annotated <i>NAT- IAA14</i> transcript.....	56
Figure 6.17: T-DNA insertions in the promoter region decreases <i>NAT-IAA14</i> expression. ...	58
Figure 6.18: <i>NAT-IAA14</i> downregulation by amiRNAs.	59
Figure 6.19: Phenotypic analysis of transgenic lines with reduced <i>NAT-IAA14</i> levels.	60
Figure 6.20: <i>NAT-IAA14</i> knockout has no effect on <i>IAA14</i> transcript levels.....	62
Figure 6.21: <i>IAA14</i> overexpression results in a reduction of <i>NAT-IAA14</i> transcript levels. ...	63
Figure 6.22: <i>IAA14</i> overexpression results in increased primary root length and lateral root number.....	64
Figure 6.23: Alteration in <i>NAT-IAA14</i> transcript levels in <i>slr-1</i> and the <i>cr_iaa14</i> lines.....	66
Figure 6.24: The presence of <i>NAT-IAA14</i> in the <i>in vitro</i> translation assay has a stronger effect on translation of the annotated <i>IAA14</i> transcript.....	69
Figure 7.1: Proposed mechanism of <i>NAT-IAA14</i> mode of action and gene responses to various stresses.....	78
Supplemental Figure 11.1: Map of the pENTR_L1/L2_Atu6gRNA vector used for CRISPR/Cas9 genome editing.	92
Supplemental Figure 11.2: Map of the pMR333_OLEp-OLE-GFP vector used for CRISPR/Cas9 genome editing.	93
Supplemental Figure 11.3: Map of the pAGG4 vector generated by golden gate cloning.	94
Supplemental Figure 11.4: Map of the <i>promIAA14::IAA14</i> vector.....	95
Supplemental Figure 11.5: Map of the pAGG17 vector generated by golden gate cloning...	96
Supplemental Figure 11.6: Map of the pAGG3 vector generated by golden gate cloning.	97
Supplemental Figure 11.7: Map of the pAGG8 vector used in the transient co-expression assay.	98
Supplemental Figure 11.8: Map of the pD_eGFP_IAA14_124 nt-longer 3'UTR vector used in the transient co-expression assay.....	99
Supplemental Figure 11.9: Map of the pD_35S_lambda1097 vector used in the transient co-expression assay.....	100

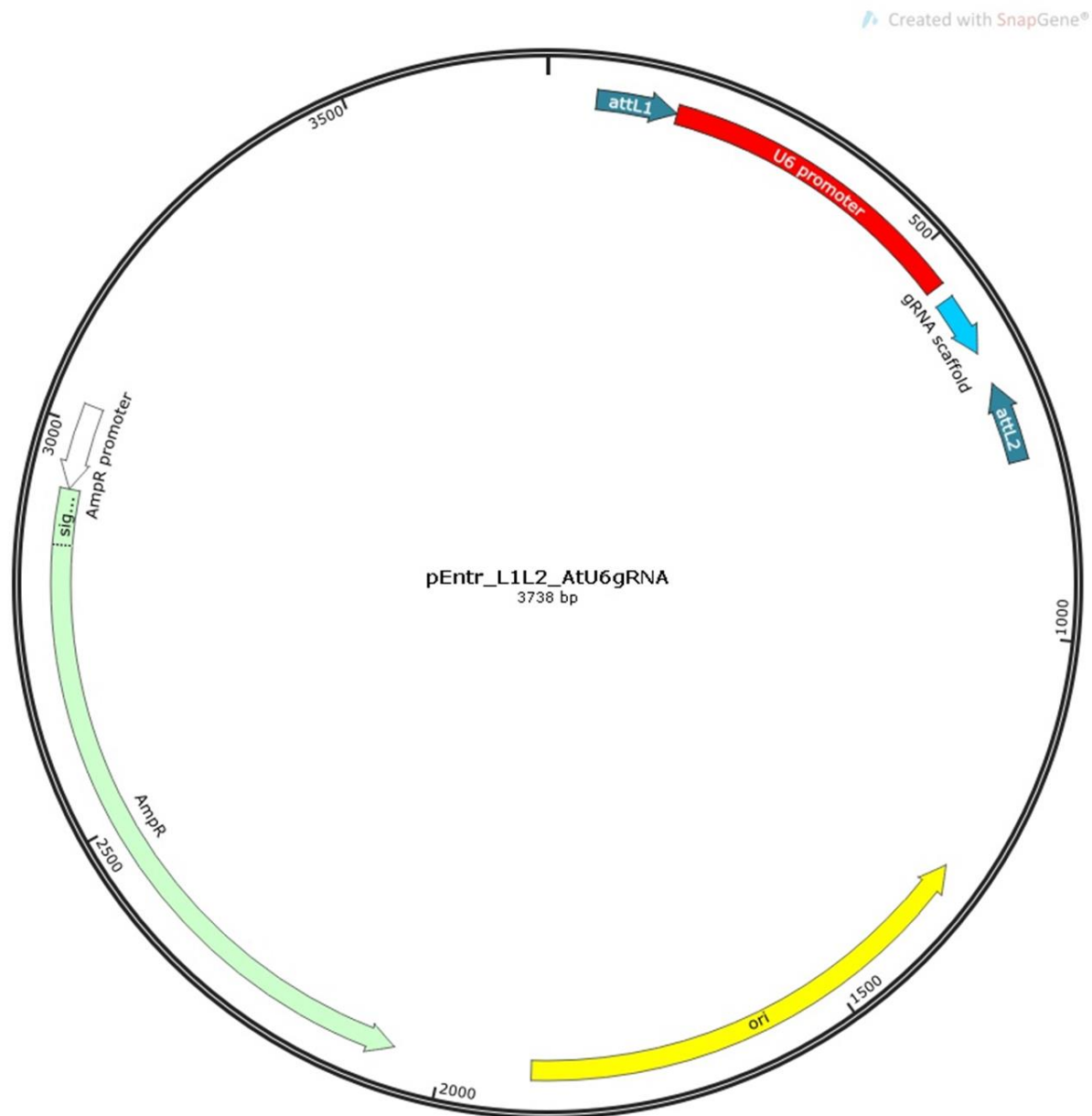
Supplemental Figure 11.10: <i>NAT-IAA14</i> amplicon covering the complete <i>IAA14</i> transcript.	101
Supplemental Figure 11.11: Experimental scheme of the circular 5' and 3'RACE.	102
Supplemental Figure 11.12: Sequence alignment of the 10 clones from circular 5'RACE. .	103
Supplemental Figure 11.13: Sequence alignment of the six clones from circular 3'RACE..	104
Supplemental Figure 11.14: potential open-reading frames (pORFs) encoded by <i>NAT-IAA14</i>	105
Supplemental Figure 11.15: Sequence alignment of the T-DNA insertion lines for <i>NAT-IAA14</i>	107
Supplemental Figure 11.16: Detection of amiRNAs targeting <i>NAT-IAA14</i> in homozygous <i>A. thaliana</i> transgenic lines.	108
Supplemental Figure 11.17: <i>NAT-IAA14</i> and <i>IAA14</i> expression in transgenic amiRNA lines.	109
Supplemental Figure 11.18: Sequence alignment of the line <i>cr_nat-iaa14_12.1</i>	109
Supplemental Figure 11.19: Sequence of the line <i>cr_nat-iaa14_7.14/46/54</i>	109
Supplemental Figure 11.20: Sequence alignment of the lines <i>cr_nat-iaa14_40.3</i> , <i>cr_nat-iaa14_3.1</i> , <i>cr_nat-iaa14_8.8</i> and <i>cr_nat-iaa14_14.5</i> compared to the Col-0 sequence.	110
Supplemental Figure 11.21: <i>NAT-IAA14</i> knockout has no effect on <i>IAA14</i> transcript levels in older plants.	111
Supplemental Figure 11.22: Sequence alignment of <i>cr_iaa14_46.7</i> and <i>cr_iaa14_46.6/8/9</i>	111
Supplemental Figure 11.23: Sequence alignment of <i>cr_iaa14_29.6</i> and <i>cr_iaa14_8.5</i>	112
Supplemental Figure 11.24: Protein sequence alignment of <i>cr_iaa14</i> transgenic lines.	113
Supplemental Figure 11.25: Expression pattern of the long non-coding RNA encoded by <i>At4g06195</i> compared to <i>NAT-IAA14</i> transcript levels in Col-0.	114

10 List of tables

Table 5.1: Plasmid vectors.....	20
Table 5.2: Culture media composition.....	21
Table 5.3: PCR components used for gene amplification with Phusion™ and DramTaq™ DNA Polymerase.....	27
Table 5.4: Thermal profiles of Phusion™ and DreamTaq™ PCR.....	28
Table 5.5: Components and volumes used for qRT-PCR.....	28
Table 5.6: qRT-PCR thermal profile.....	29
Table 5.7: Thermal profile for ligation-digestion reaction.....	31
Table 5.8: PCR primers for guide strand amplification used for CRISPR/Cas9 genome editing.....	32
Table 5.9: Components and volumes used for ³² P-labeling of <i>in vitro</i> synthesized transcripts.....	34
Table 5.10: Components and volumes used for <i>in vitro</i> synthesis of capped transcripts.....	37
Table 5.11: Components and volumes of the polyadenylation reaction of <i>in vitro</i> synthesized transcripts.....	37
Supplementary Table 11.1: List of used primers.....	115

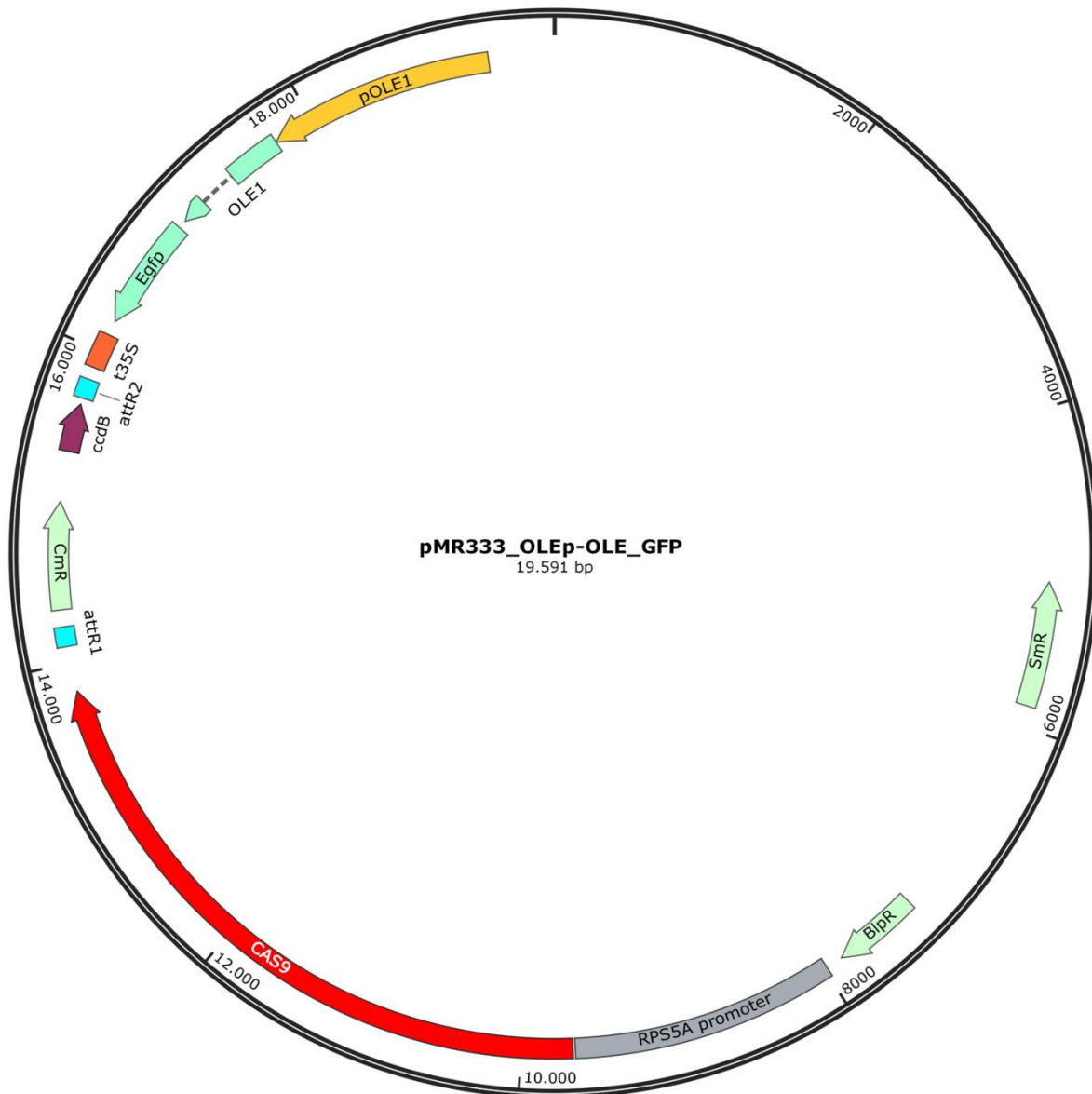
11 Appendix

11.1 Supplementary Figures

**Supplemental Figure 11.1: Map of the pENTR_L1/L2_AtU6gRNA vector used for CRISPR/Cas9 genome editing.**

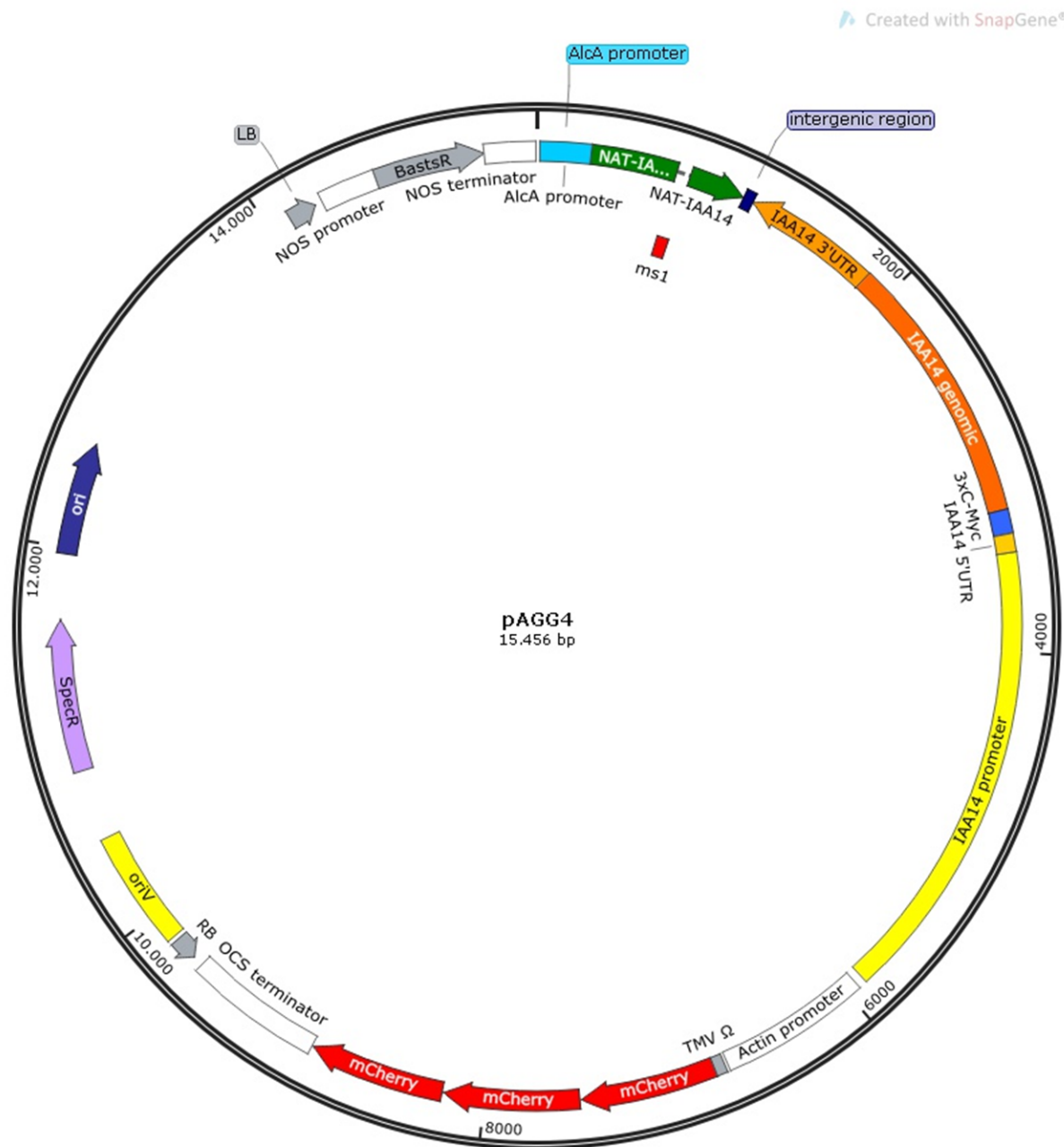
The specific gRNAs were cloned by digestion-ligation into the pENTR_L1/L2_AtU6gRNA vector downstream of the *A. thaliana* U6 promoter, which allows a nuclear expression of the gRNAs. AmpR = ampicillin resistance, ori = origin of replication, attL1/2 = attachment sites

Created with SnapGene®



Supplemental Figure 11.2: Map of the pMR333_OLEp-OLE-GFP vector used for CRISPR/Cas9 genome editing.

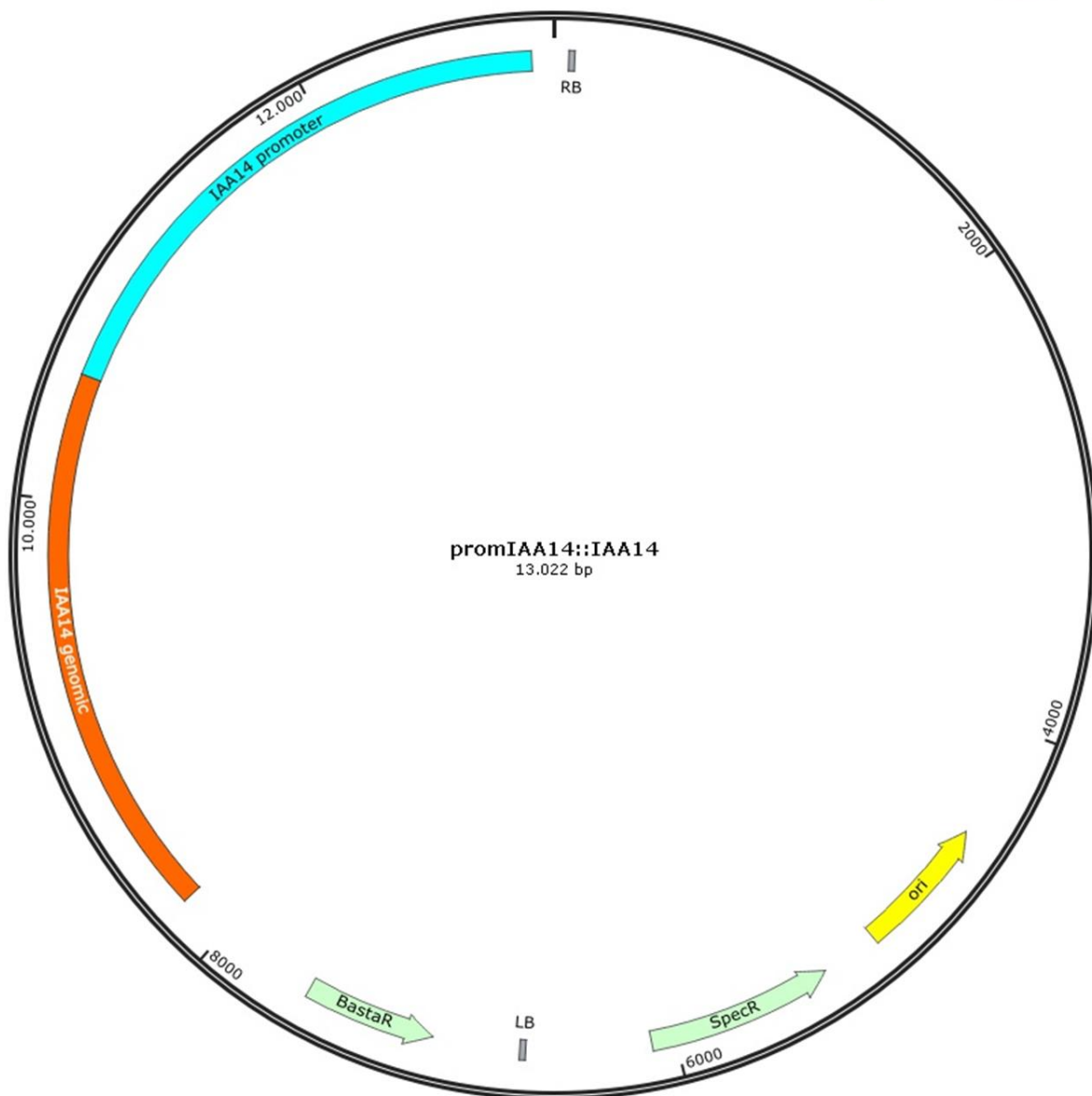
The specific gRNAs were cloned by digestion-ligation into the pMR333_OLEp-OLE-GFP vector that encodes also for the Cas9 protein necessary for gRNA-mediated DNA cleavage. SmR = spectinomycin resistance, attR1/2 = attachment sites, pOLE1 = *OLEOSIN 1* promoter, GFP = *GREEN FLOURESCENCE PROTEIN*, RPS5A = *RIBOSOMAL PROTEIN 5A*



Supplemental Figure 11.3: Map of the pAGG4 vector generated by golden gate cloning.

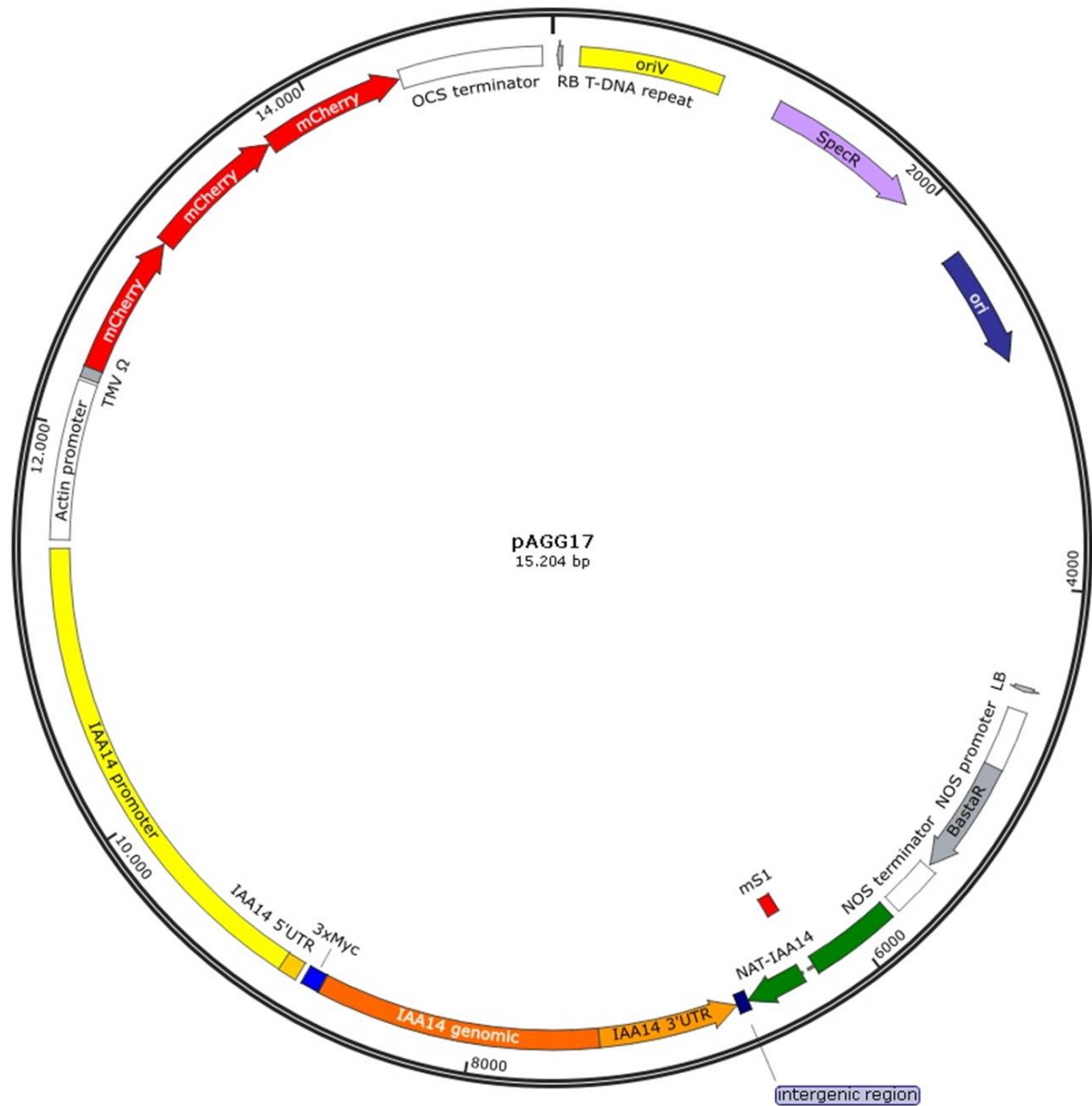
The cloned genomic *A. thaliana* region including *NAT-IAA14*, *IAA14* and *prom_{IAA14}* is displayed in the vector map. *NAT-IAA14* is driven by the *ALCA* promoter that is ethanol-inducible. An *ms1* sequence and a 3x3-MYC sequence were included to tag *NAT-IAA14* and *IAA14*, respectively. *prom_{Actin2}::3xmCherry* was used as fluorescence marker. SpecR = spectinomycin resistance, BastaR = Basta resistance, RB and LB = T-DNA right and left border sequences

Created with SnapGene®

**Supplemental Figure 11.4: Map of the *promIAA14::IAA14* vector.**

The cloned genomic *A. thaliana* region of *IAA14* driven by the endogenous promoter (*prom_{IAA14}*) is displayed in the vector map. SpecR = spectinomycin resistance, BastaR = Basta resistance, RB and LB = T-DNA right and left border sequences

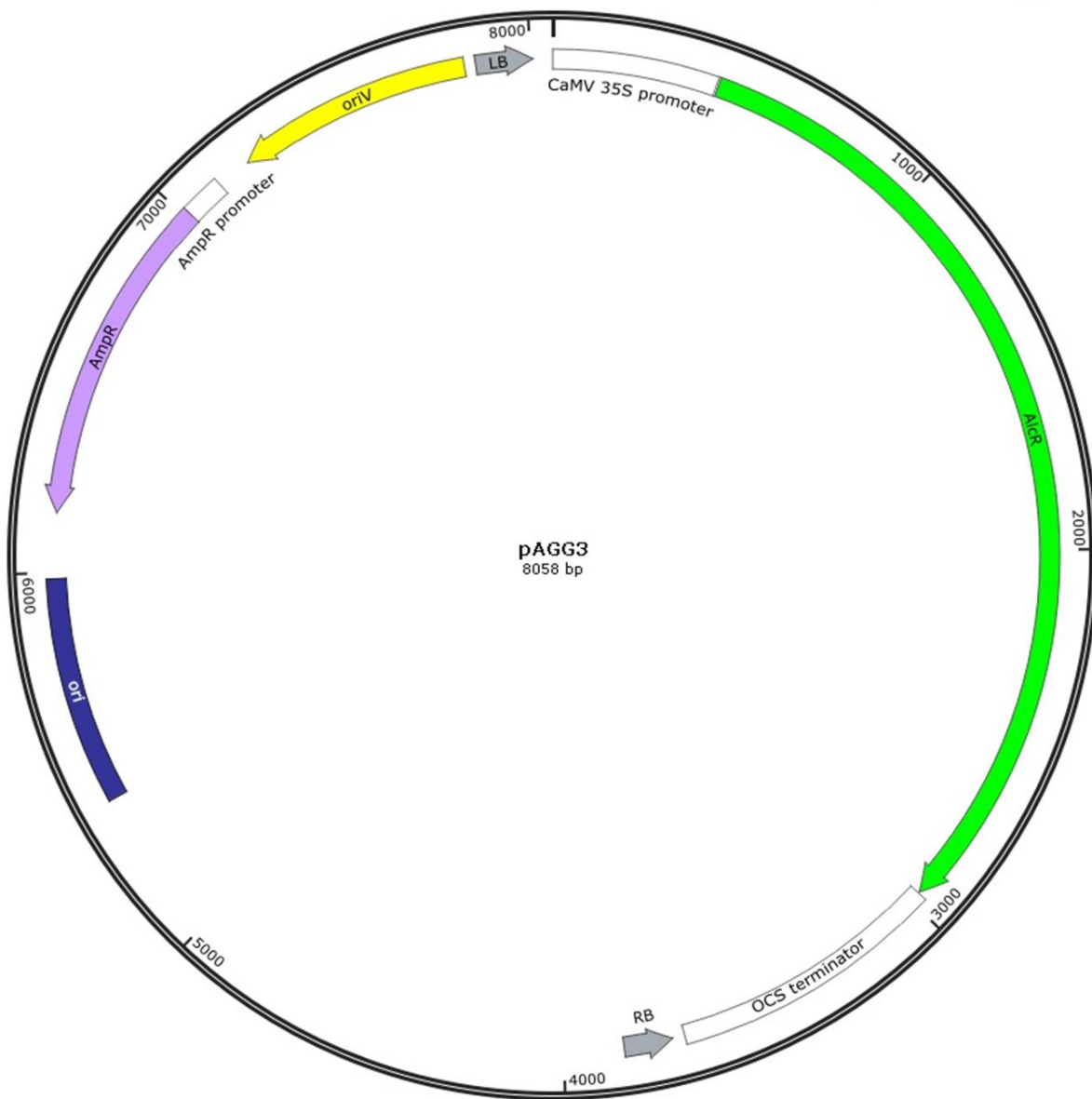
Created with SnapGene®



Supplemental Figure 11.5: Map of the pAGG17 vector generated by golden gate cloning.

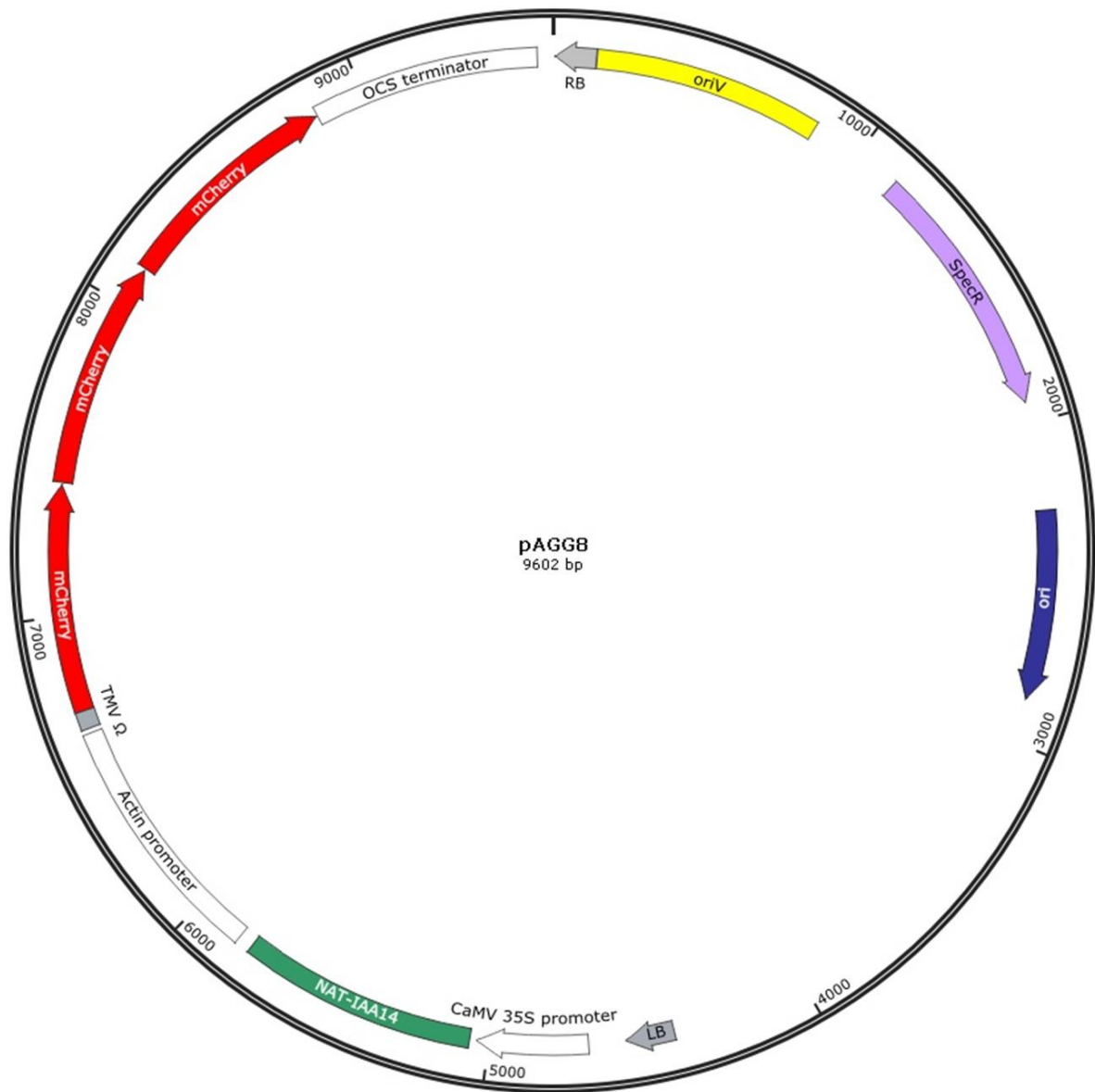
The vector map is like pAGG4, but the *AlcA* promoter located upstream of the *NAT-IAA14* sequence was deleted to abolish *NAT-IAA14* transcription. *prom_{Actin2}::3xmCherry* was used as fluorescence marker. SpecR = spectinomycin resistance, BastaR = Basta resistance, RB and LB = T-DNA right and left border sequences, ori = origin of replication

Created with SnapGene®

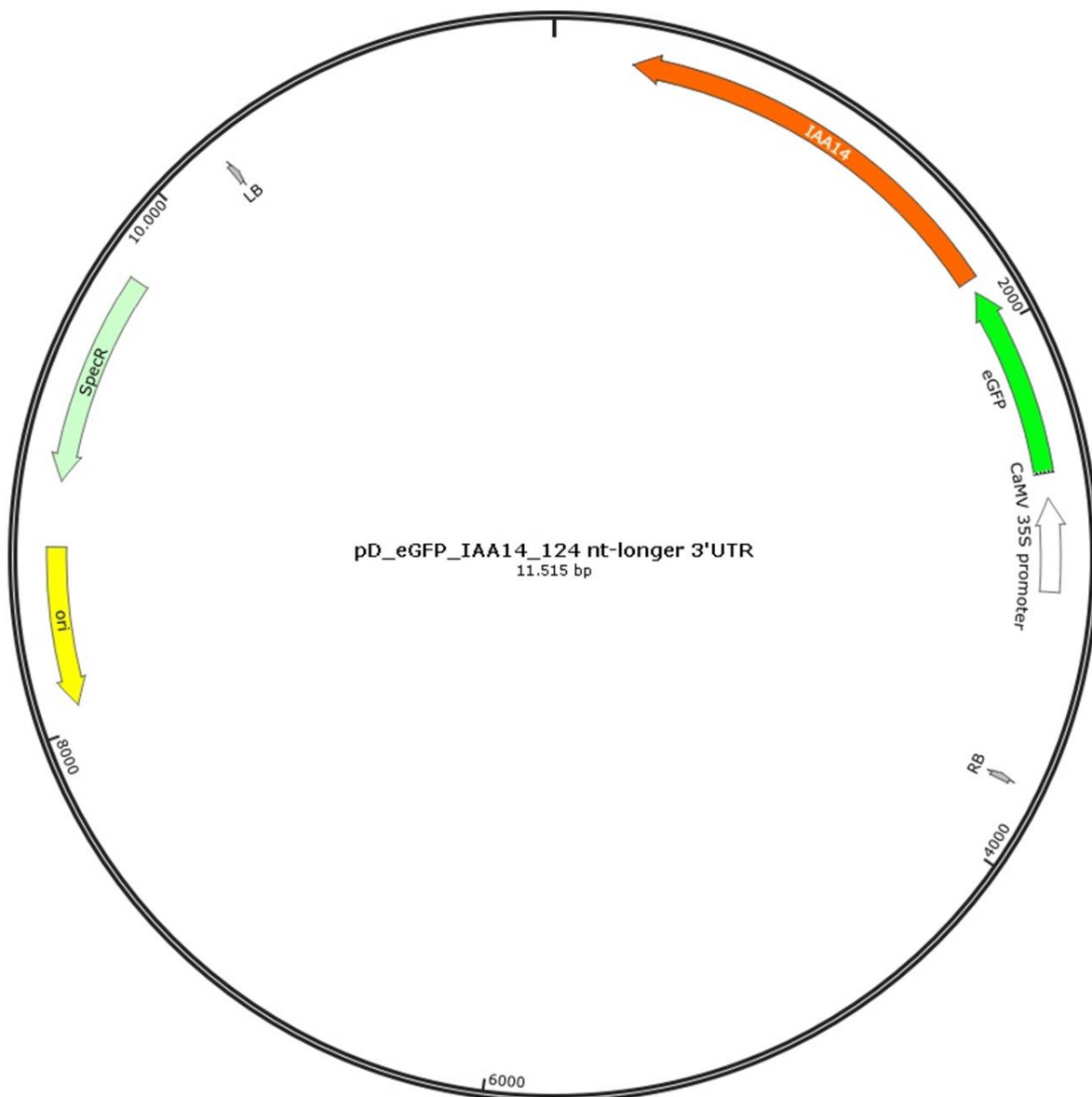
**Supplemental Figure 11.6: Map of the pAGG3 vector generated by golden gate cloning.**

In the vector map, the *AicR* gene, which is required for activation of the *AicA* promoter, is driven by the Cauliflower Mosaic Virus (CaMV) 35S promoter. AmpR = ampicillin resistance, RB and LB = T-DNA right and left border sequences, ori = origin of replication

Created with SnapGene®



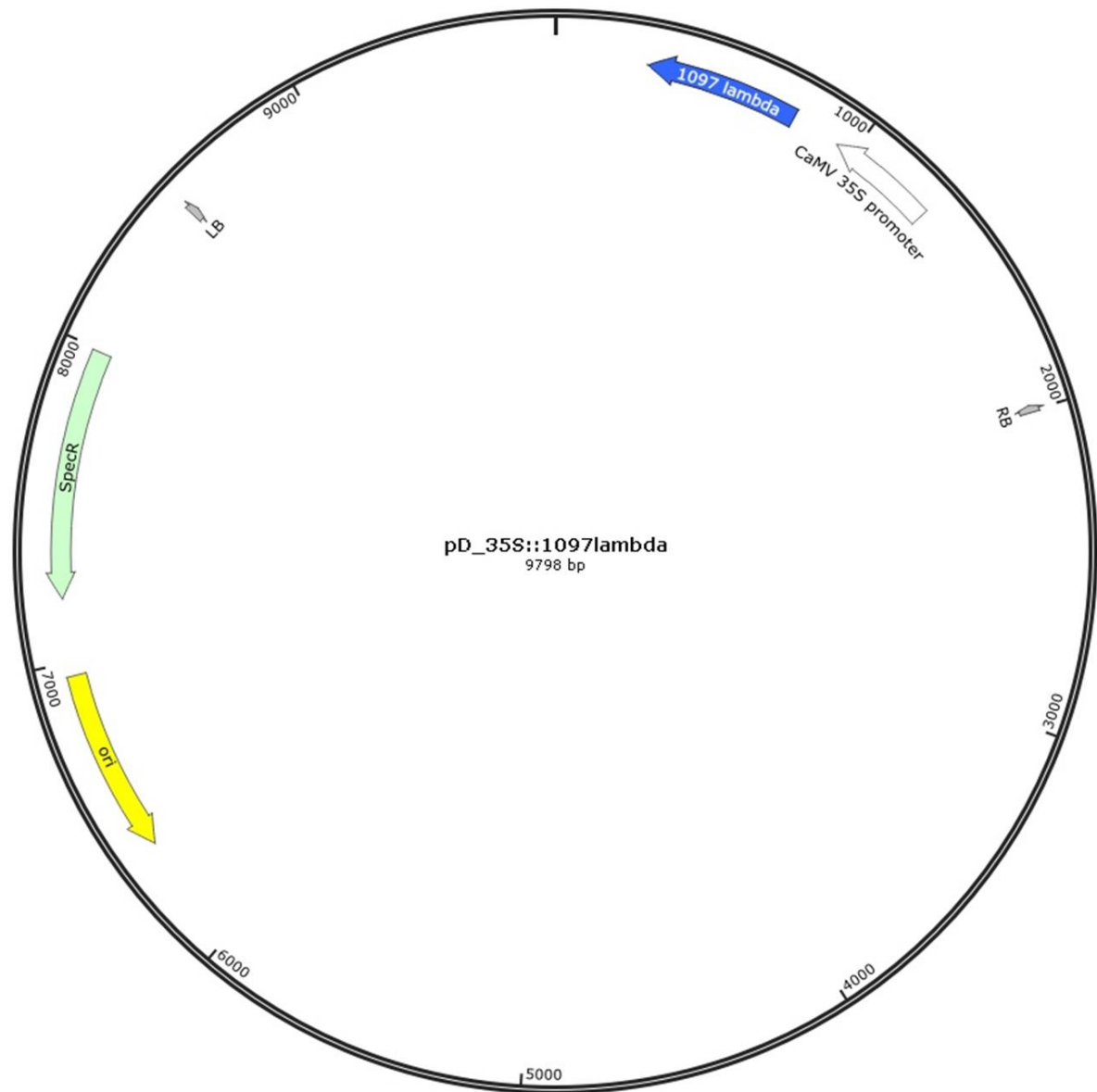
Supplemental Figure 11.7: Map of the pAGG8 vector used in the transient co-expression assay. In the vector map, the genomic *A. thaliana* region of *NAT-IAA14* driven by the Cauliflower Mosaic Virus (CaMV) 35S promoter is shown. $prom_{Actin2}::3xmCherry$ was used as fluorescence marker. SpecR = spectinomycin resistance, RB and LB = T-DNA right and left border sequences, ori = origin of replication



Supplemental Figure 11.8: Map of the pD_eGFP_IAA14_124 nt-longer 3'UTR vector used in the transient co-expression assay.

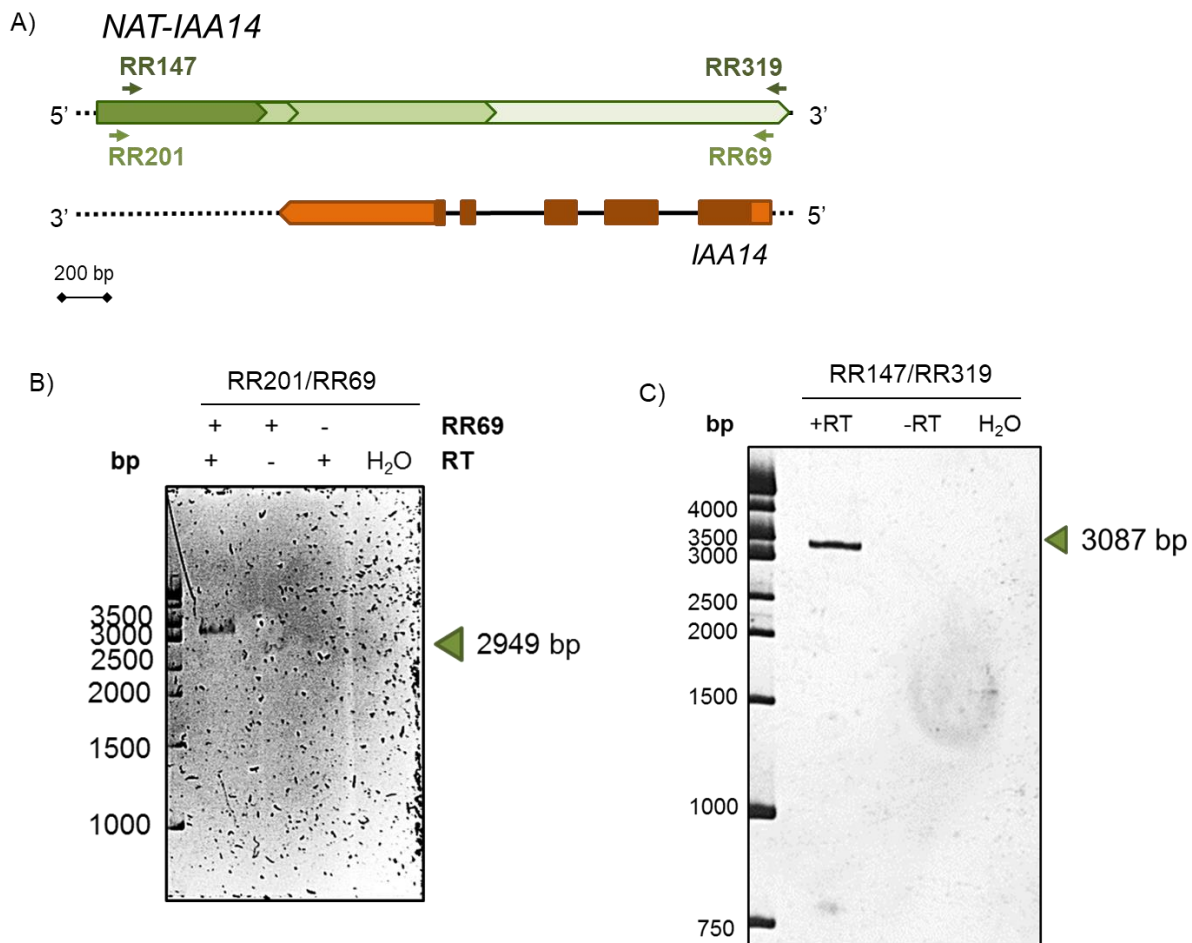
The cloned coding *IAA14* region including the 124 nt-longer 3'UTR and an N-terminal eGFP-tag driven by the Cauliflower Mosaic Virus (CaMV) 35S promoter is displayed in the vector map. eGFP = enhanced *GREEN FLOURESCENCE PROTEIN*, SpecR = spectinomycin resistance, RB and LB = T-DNA right and left border sequences, respectively, ori = origin of replication

Created with SnapGene®



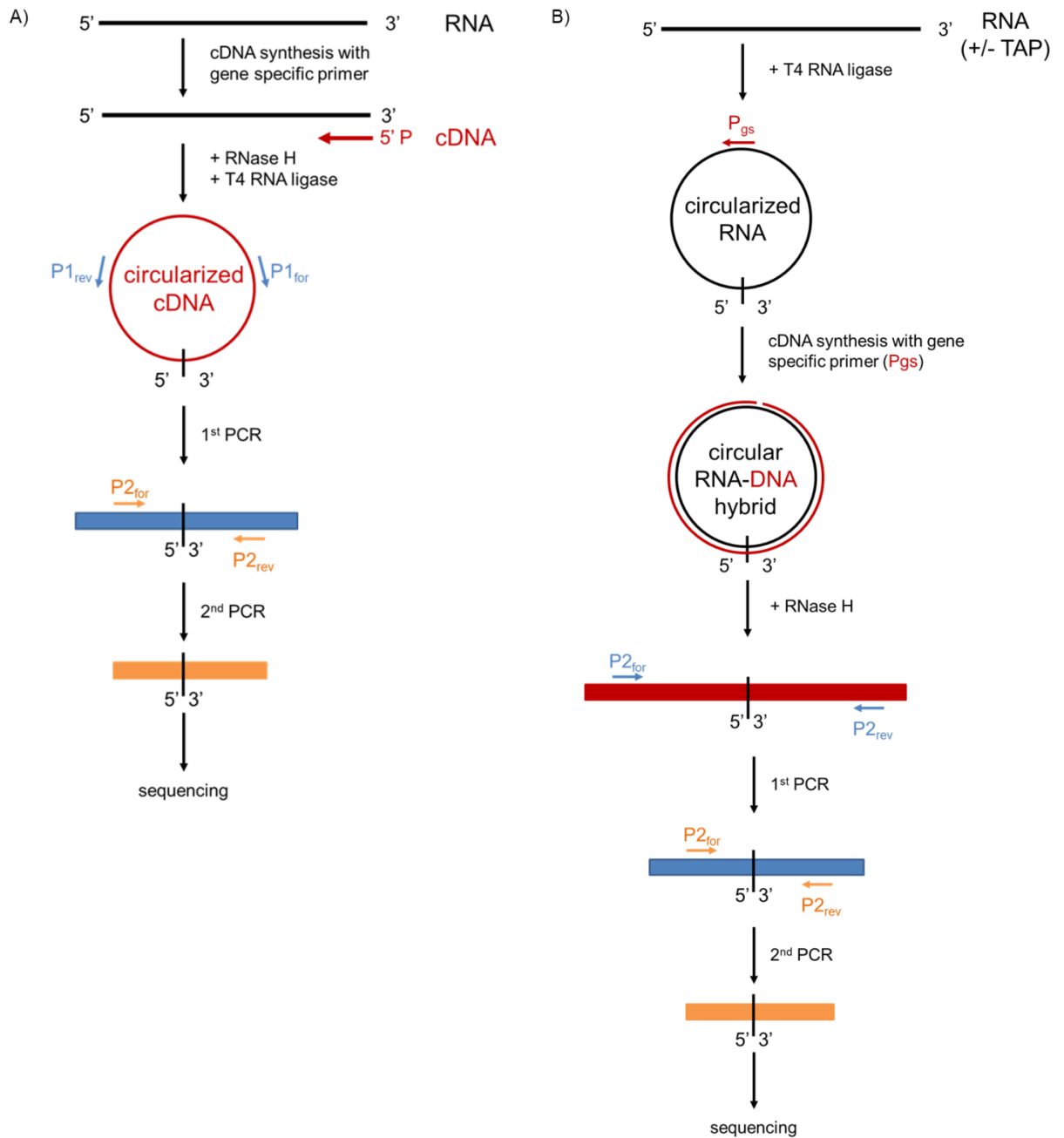
Supplemental Figure 11.9: Map of the pD_35S_lambda1097 vector used in the transient co-expression assay.

In the vector map, the 1097 λ gene driven by the Cauliflower Mosaic Virus (CaMV) 35S promoter is shown. SpecR = spectinomycin resistance, RB and LB = T-DNA right and left border sequences, respectively, ori = origin of replication



Supplemental Figure 11.10: *NAT-IAA14* amplicon covering the complete *IAA14* transcript.

The schematic representation of *NAT-IAA14* (green: annotated, light-green: potential 3'end) and *IAA14* (brown: exon; orange: UTR) including primers used for amplification reaction by RT-PCR is shown in (A). Alternative 3'end amplification product from the *NAT-IAA14* transcript is presented in a 5% non-denaturing PAGE (B) and in a 5% non-denaturing PAGE after silver staining (C). The PCR product obtained (green triangle) could be amplified only once for each primer combination in Col-0 seedlings at full-expanded cotyledons stage.



Supplemental Figure 11.11: Experimental scheme of the circular 5' and 3'RACE.

Schematic strategy of the circular 5' (A) and 3'RACE (B) is depicted. P_{gs} = gene-specific primer, TAP = tobacco acid pyrophosphatase

```

#1 ATCATACCAAAACAAAAAGAAATCAAACCTAAAGAAAGAAAGTAAAGAAACCTCGCTTCC
#2 ATCATACCAAAACAAAAAGAAATCAAACCTAAAGAAAGAAAGTAAAGAAACCTCGCTTCC
#3 ATCATACCAAAACAAAAAGAAATCAAACCTAAAGAAAGAAAGTAAAGAAACCTCGCTTCC
#4 ATCATACCAAAACAAAAAGAAATCAAACCTAAAGAAAGAAAGTAAAGAAACCTCGCTTCC
#5 ATCATACCAAAACAAAAAGAAATCAAACCTAAAGAAAGAAAGTAAAGAAACCTCGCTTCC
#6 ATCATACCAAAACAAAAAGAAATCAAACCTAAAGAAAGAAAGTAAAGAAACCTCGCTTCC
#7 ATCATACCAAAACAAAAAGAAATCAAACCTAAAGAAAGAAAGTAAAGAAACCTCGCTTCC
#8 ATCATACCAAAACAAAAAGAAATCAAACCTAAAGAAAGAAAGTAAAGAAACCTCGCTTCC
#9 ATCATACCAAAACAAAAAGAAATCAAACCTAAAGAAAGAAAGTAAAGAAACCTCGCTTCC
#10 ATCATACCAAAACAAAAAGAAATCAAACCTAAAGAAAGAAAGTAAAGAAACCTCGCTTCC
Col-0 ATCATACCAAAACAAAAAGAAATCAAACCTAAAGAAAGAAAGTAAAGAAACCTCGCTTCC
*****

#1 GATGCTGAAAAAGCCACTGAAACAAGTAATCTTAGGCAGCGGCGGAGAAAGCTTTTTTTA
#2 GATGCTGAAAAAGCCACTGAAACAAGTAATCTTAGGCAGCGGCGGAGAAAGCTTTTTTTA
#3 GATGCTGAAAAAGCCACTGAAACAAGTAATCTTAGGCAGCGGCGGAGAAAGCTTTTTTTA
#4 GATGCTGAAAAAGCCACTGAAACAAGTAATCTTAGGCAGCGGCGGAGAAAGCTTTTTTTA
#5 GATGCTGAAAAAGCCACTGAAACAAGTAATCTTAGGCAGCGGCGGAGAAAGCTTTTTTTA
#6 GATGCTGAAAAAGCCACTGAAACAAGTAATCTTAGGCAGCGGCGGAGAAAGCTTTTTTTA
#7 GATGCTGAAAAAGCCACTGAAACAAGTAATCTTAGGCAGCGGCGGAGAAAGCTTTTTTTA
#8 GATGCTGAAAAAGCCACTGAAACAAGTAATCTTAGGCAGCGGCGGAGAAAGCTTTTTTTA
#9 GATGCTGAAAAAGCCACTGAAACAAGTAATCTTAGGCAGCGGCGGAGAAAGCTTTTTTTA
#10 GATGCTGAAAAAGCCACTGAAACAAGTAATCTTAGGCAGCGGCGGAGAAAGCTTTTTTTA
Col-0 GATGCTGAAAAAGCCACTGAAACAAGTAATCTTAGGCAGCGGCGGAGAAAGCTTTTTTTA
*****

#1 TAGAGAACATAGAGCTTTTATTTTAAGAGAC-----CTTTCAGTAAAAAT
#2 TAGAGAACATAGAGCTTTTATTTTAAGAGAC-----CTTTCAGTAAAAAT
#3 TAGAGAACATAGAGCTTTTATTTTAAGAGAC-----CTTTCAGTAAAAAT
#4 TAGAGAACATAGAGCTTTTATTTTAAGAGAC-----CTTTCAGTAAAAAT
#5 TAGAGAACATAGAGCTTTTATTTTAAGAGAC-----CTTTCAGTAAAAAT
#6 TAGAGAACATAGAGCTTTTATTTTAAGAGAC-----CTTTCAGTAAAAAT
#7 TAGAGAACATAGAGCTTTTATTTTAAGAGAC-----CTTTCAGTAAAAAT
#8 TAGAGAACATAGAGCTTTTATTTTAAGAGAC-----CTTTCAGTAAAAAT
#9 TAGAGAACATAGAGCTTTTATTTTAAGAGAC-----CTTTCAGTAAAAAT
#10 TAGAGAACATAGAGCTTTTATTTTAAGAGAC-----CTTTCAGTAAAAAT
Col-0 TAGAGAACATAGAGCTTTTATTTTAAGAGACAGAAAATTTTTTATT-TTTCAGTAAAAAT
*****

#1 TAAGATTTTCAT
#2 TAAGATTTTCAT
#3 TAAGATTTTCAT
#4 TAAGATTTTCAT
#5 TAAGATTTTCAT
#6 TAAGATTTTCAT
#7 TAAGATTTTCAT
#8 TAAGATTTTCAT
#9 TAAGATTTTCAT
#10 TAAGATTTTCAT
Col-0 TAAGATTTTCAT
*****

```

Supplemental Figure 11.12: Sequence alignment of the 10 clones from circular 5'RACE.

A comparison of the reported Col-0 sequence with *NAT-IAA14* 5'RACE transcript sequence obtained after cloning in pZero[®]-2 and sequencing is depicted in (C). Blue nucleotides display the *NAT-IAA14* 5'end sequence. The additional cytosine (red) accrues through the usage of SuperScript III. The sequence alignment was performed by the program CLUSTALW.


```

#1      ATCATACCAAAACAAAAAGAAATCAAACATAAGAAA-----
#2      ATCATACCAAAACAAAAAGAAATCAAACATAAGAAA-----
#3      ATCATACCAAAACAAAAAGAAATCAAACATAAGAAAAGAAAGTAAAG-----
#4      ATCATACCAAAACAAAAAGAAATCAAACATAAGAAAAGAAAGTAAAG-----
#5      ATCATACCAAAACAAAAAGAAATCAAACATAAGAAAAGAAAGTAAAGAAACCTCGCTTCC
#6      ATCATACCAAAACAAAAAGAAATCAAACATAAGAAAAGAAAGTAAAGAAACCTCGCTTCC
Col-0   ATCATACCAAAACAAAAAGAAATCAAACATAAGAAAAGAAAGTAAAGAAACCTCGCTTCC
          *****

#1      -----
#2      -----
#3      -----
#4      -----
#5      GATGCTGAAAAAGCCACTGAAACAAGTAATCTTAGGCAGCGCGGAAA-----
#6      GATGCTGAAAAAGCCACTGAAACAAGTAATCTTAGGCAGCGCGGAAA-----
Col-0   GATGCTGAAAAAGCCACTGAAACAAGTAATCTTAGGCAGCGCGGAGAAAGCTTTTTTTA

#1      -----TTTTTTTTTTTTTTT
#2      -----TTTTTTTTTTTTTTT
#3      -----
#4      -----T
#5      -----
#6      -----
Col-0   TAGAGAACATAGAGCTTTTATTTTAAGAGACAGAAAATTTTTTATT-----

#1      TTTTTTTTTTTTTTTTTTTTTTTTTTTTTTTCAGTAAAAATTAATAATTCATTTATAAAAAATAT
#2      TTTTTTTTTTTTTTTTTTTTTTTTTTTTTTTCAGAAAAATTAATAATTCATTTAAAAAAAATAT
#3      --TTTTTTTTTTTTTTTTTTTTTTTTTTTTTTCAGTAAAAATTAATAATTCATTTATAAAAAATAT
#4      TTTTTTTTTTTTTTTTTTTTTTTTTTTTTTTCAGTAAAAATTAATAATTCATTTATAAAAAATAT
#5      -----TTTTTTTTTTTTTTCAGTAAAAATTAAGATTTTATATAAAAAATAT
#6      -----TTTTTTTTTTTTTTCAGTAAAAATTAAGATTTTATATAAAAAATAT
Col-0   -----TTTTTTTCAGTAAAAATTAAGATTTTATATAAAAAATAT
          ***** ***** ***** ***** **

#1      CATAAGGGGTAAAAATACATATGCCGGG
#2      CATAAGGGGTAAAAAACATATGCCGGG
#3      CATAAGGGGTAAAAATACATATGCCGGG
#4      CATAAGGGGTAAAAATACATATGCCGGG
#5      CATAAGGGGTAAAAATACATATGCCGGG
#6      CATAAGGGGTAAAAATACATATGCCGG-
Col-0   CATAAGGGGTAAAAATACATATGCCGGG
          ***** *****

```

Supplemental Figure 11.13: Sequence alignment of the six clones from circular 3'RACE.

Cloning in pZero[®]-2 and sequencing of the amplicons resulted in the annotated *NAT-IAA14* 3'end after comparison with the reported Col-0 sequence (C). The sequence of the annotated *NAT-IAA14* 3'end is shown in green. The 5'end starting site is shorter than the annotated transcriptional start site due to a potential degradation during the preparation. The thymine stretch (red) ranging from 5 to 34 nt suggests that *NAT-IAA14* is polyadenylated in *A. thaliana*. The program CLUSTALW was used for sequence alignment.

B) *NAT-IAA14prom* -GAAAATGAATAATTTAAGTGCAAGTGGTGAATTCCTAGATTCTCCCTCAATGCCACATT
nat-iaa14_2 TGAAAATGAATAATTTAAGTGCAAGTGGTGAATTCCTAGATTCTCCCTCAATGCCACATT

NAT-IAA14prom AAAGCAAGTTTGTTCACATGACATCTCAAAAAAATCCTATCAATAGTAGGGTTGAGGT
nat-iaa14_2 AAAGCAAGTTTGTTCACATGACATCTCAAAAAAATCCTATCAATAGTAGGGTTGAGGT

NAT-IAA14prom TAAAAATAAAGAGTTATAAACTGCGAAAGCATGTTTAGGAATTCACCTTATGCCATAC
nat-iaa14_2 TAAAAATAAAGAGTTATAAACTGCGAAAGCATGTTTAGGAATTCACCTTATGCCATAC

288 bp

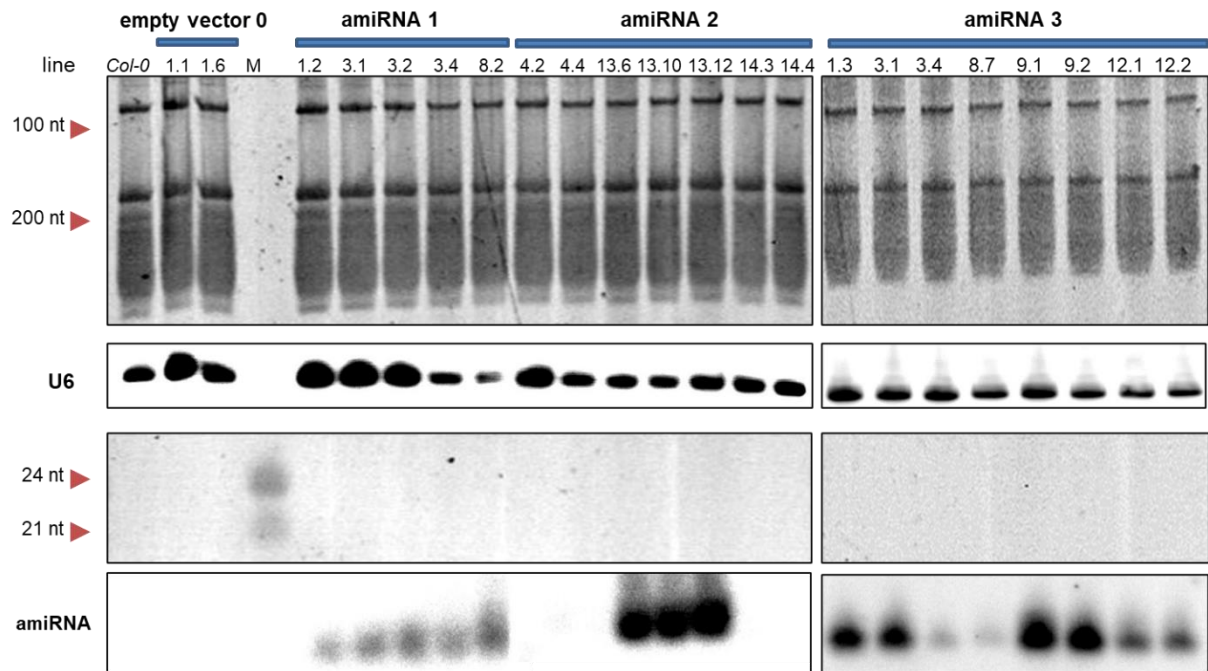
NAT-IAA14prom CAAAACCAACTAAAGAATAATGGTTTAGATATTCTGATGTTATGCCAAGCATTAGGGA
nat-iaa14_2 CAAAACCAACTAAAGAATAATGGTTTAGATATTCTGATGTTATGGTGTAAACAAATT
 *****|.:*: * .: * *: * .: *

NAT-IAA14prom GGAGAATAATTCGGAATCATTTCATCAATTATCCAACTATCATTCATTGTAGGAGTAAC
nat-iaa14_2 G----ACGCTTAGACAACCTAATAACACATTGCGGACGTTTTTAATGTACTGGGG-----
 * * .*. * .*. *: *: *: *: *: * . * .*: * .: * .*. *

NAT-IAA14prom TAGAATTCCTCAGTTCATTAATGGGAAATTAATAATAATTTTTAATTTATTGTGTCAAT
nat-iaa14_2 --TGGTTTTTCTTTTCACCAGTGAGACGG-----GCAACAGCTGATTGCCCTT
 .*. * *: * * * .*. * . * * : * . * * .: *

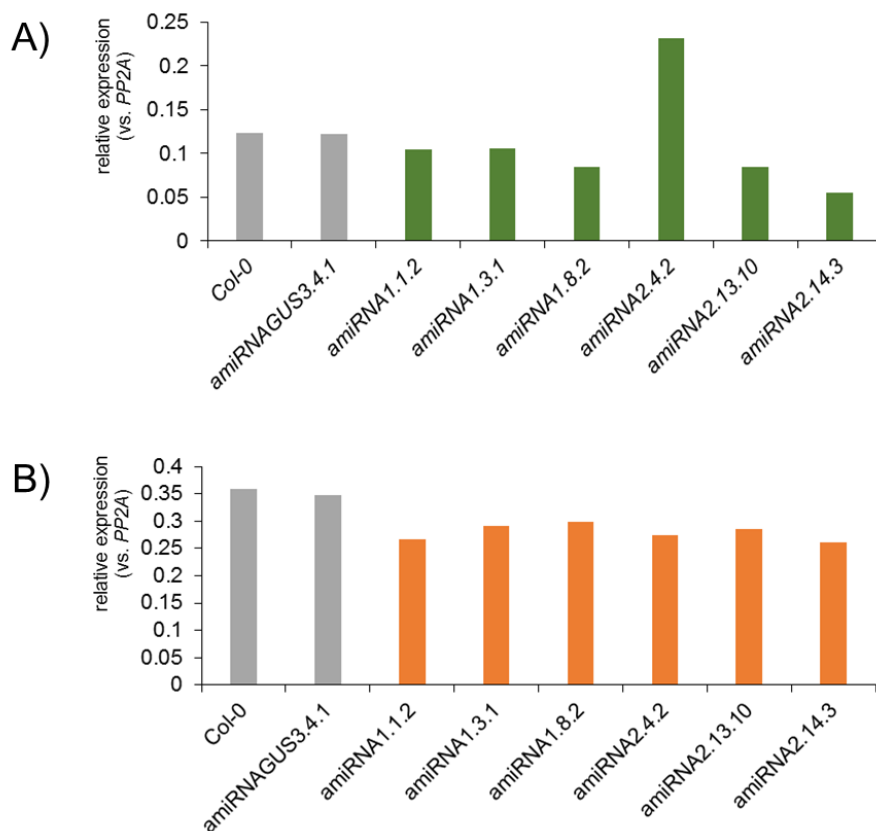
NAT-IAA14prom AACTAACTTTCTGTAAATATTA AAAAAGAAGGAAAAATGAGAGATTTCCAAACACTTC
nat-iaa14_2 CACCGCCTGGCCCTGAGAGAGTTGCAGCAAGCGGTCCACGCTGGTTTGCCCCAGCAGGCG
 .* .*. * * .*. * * * .: .*. * . * .: * . * .: * . * .*

NAT-IAA14prom AAAAACTACTTTTGATTT-----
nat-iaa14_2 AAAATCCTGTTTGATGGTGGTTCCG
 *****: * : * * * .: *



Supplemental Figure 11.16: Detection of amiRNAs targeting *NAT-IAA14* in homozygous *A. thaliana* transgenic lines.

Oligoprobes RR233, RR234, and RR235 labeled with [γ - 32 P]-ATP are used to detect the *amiRNA1*, 2 and 3, respectively. The first number of each transgenic line represents the corresponding *amiRNA* construct. *U6*, detected with oligoprobe RR85, is included as a control.



Supplemental Figure 11.17: *NAT-IAA14* and *IAA14* expression in transgenic amiRNA lines.

Transcript levels of *NAT-IAA14* (A) and *IAA14* (B) were determined by qRT-PCR in 14 d old Col-0 and amiRNA seedlings. qRT-PCR results were normalized by *PP2A* and values correspond to one experiment. The first number of each transgenic line represents the corresponding amiRNA construct.

```
Col-0          ATATTCTGATGTTATGCCAAGCATTTA[n]277CCTAAGATTACTTGTTCAGTGGCTTTT
cr_nat_iaa14_12.1 ATATTCTGATGTTATGCCAAGCATTTA[-]277CCTAAGATTACTTGTTCAGTGGCTTTT
*****
```

Supplemental Figure 11.18: Sequence alignment of the line *cr_nat-iaa14_12.1*.

The sequence comparison from *cr_nat-iaa14_12.1* with Col-0 is shown. Cleavage of gRNA2 and 3 at the *NAT-IAA14* gene region resulted in a 277 bp deletion. 208 bp are deleted at the 3' end of the *NAT-IAA14* promoter and 69 bp of the transcript at the 5' end. n (A, T, G, C) represents the nucleotides that were deleted [-] by the gRNA-mediated genome editing. The promoter is indicated in italics.

```
Col-0          GAGTCATTGAAAAACTTTTTCTACTTTGATG[n]1538-----CCTAAGATTACT
cr_nat_iaa14_7.14/46/54 GAGTCATTGAAAAACTTTTTCTACTTTGATG[-]1538AAAAACCTAAGATTACT
*****
```

Supplemental Figure 11.19: Sequence of the line *cr_nat-iaa14_7.14/46/54*.

Depicted is the alignment of the lines *cr_nat-iaa14_7.14*, *cr_nat-iaa14_7.46* and *cr_nat-iaa14_7.54* with Col-0. The gRNA1 and 3 mediated cleavages were leading to a deletion of 1538 bp (removing 1469 bp of the *NAT-IAA14* promoter 3' end and 69 bp at the *NAT-IAA14* 5' end). n (A, T, G, C) represents the nucleotides that were deleted [-] by the gRNA-mediated genome editing. The promoter is indicated in italics. Nucleotides added by the DNA repair mechanism are highlighted in red.

```

cr_nat-iaa14_40.3      CTAAAAAATTGTAGTGGGAATATAATTATAGCATCAAGCTAAAAAGAGTCATTGAAAAAC
Col-0                  CTAAAAAATTGTAGTGGGAATATAATTATAGCATCAAGCTAAAAAGAGTCATTGAAAAAC
cr_nat-iaa14_3.1      CTAAAAAATTGTAGTGGGAATATAATTATAGCATCAAGCTAAAAAGAGTCATTGAAAAAC
cr_nat-iaa14_8.8      CTAAAAAATTGTAGTGGGAATATAATTATAGCATCAAGCTAAAAAGAGTCATTGAAAAAC
cr_nat-iaa14_14.5     CTAAAAAATTGTAGTGGGAATATAATTATAGCATCAAGCTAAAAAGAGTCATTGAAAAAC
*****

cr_nat-iaa14_40.3      TTTTCTACTTTGATGCAGGGAACATGAGATGTAA- [-] 1883TTTACGGTAAGAAGAATAT
Col-0                  TTTTCTACTTTGATGCAGGGAACATGAGATGTAAAT[n] 1883TTTACGGTAAGAAGAATAT
cr_nat-iaa14_3.1      TTTTCTACTTTGATGCAGGGAACATGAGATGTAAAT[-] 1883-----
cr_nat-iaa14_8.8      TTTTCTACTTTGATGCAGGGAACATGAGATG---- [-] 1883-----
cr_nat-iaa14_14.5     TTTTCTACTTT-----[-] 1883----ACGGTAAGAAGAATAT
*****

cr_nat-iaa14_40.3      TGATTTTATTTTCTTTGAATGGATCTCTAATCTCAGATCTATATTTTGTTTTAATTTGGAT
Col-0                  TGATTTTATTTTCTTTGAATGGATCTCTAATCTCAGATCTATATTTTGTTTTAATTTGGAT
cr_nat-iaa14_3.1      -----
cr_nat-iaa14_8.8      -----
cr_nat-iaa14_14.5     TGATTTTATTTTCTTTGAATGGATCTCTAATCTCAGATCTATATTTTGTTTTAATTTGGAT

cr_nat-iaa14_40.3      TTAGAATTTGTATTAGATTTTTGAGTTCTTAAGTGATAAGTTTGGGAAGTTTGGATCAGT
Col-0                  TTAGAATTTGTATTAGATTTTTGAGTTCTTAAGTGATAAGTTTGGGAAGTTTGGATCAGT
cr_nat-iaa14_3.1      -----
cr_nat-iaa14_8.8      -----
cr_nat-iaa14_14.5     TTAGAATTTGTATTAGATTTTTGAGTTCTTAAGTGATAAGTTTGGGAAGTTTGGATCAGT

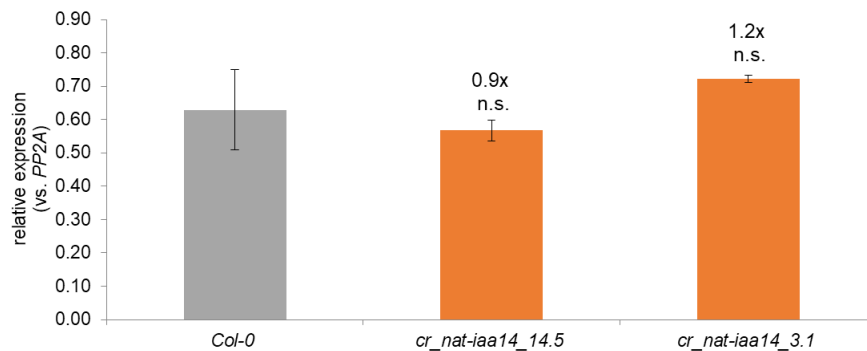
cr_nat-iaa14_40.3      TTTAATATGTTTTTTTTATTCTGGAATTTTTCCTTTTGTATATGTATTTGTCTCTAGAAA
Col-0                  TTTAATATGTTTTTTTTATTCTGGAATTTTTCCTTTTGTATATGTATTTGTCTCTAGAAA
cr_nat-iaa14_3.1      -----
cr_nat-iaa14_8.8      -----
cr_nat-iaa14_14.5     TTTAATATGTTTTTTTTATTCTGGAATTTTTCCTTTTGTATATGTATTTGTCTCTAGAAA

cr_nat-iaa14_40.3      ATCCGTTTTCTCGCCGGCTTAACTTCTGAACTGGTTATTTTCTTACCCGGCATAATGTATT
Col-0                  ATCCGTTTTCTCGCCGGCTTAACTTCTGAACTGGTTATTTTCTTACCCGGCATAATGTATT
cr_nat-iaa14_3.1      -----TAACTTCTGAACTGGTTATTTTCTTACCCGGCATAATGTATT
cr_nat-iaa14_8.8      -----TAA-TTCTGAACTGGTTATTTTCTTACCCGGCATAATGTATT
cr_nat-iaa14_14.5     ATCCGTTTTCTCGCCGGCTTAACTTCTGAACTGGTTATTTTCTTACCCGGCATAATGTATT
*****

```

Supplemental Figure 11.20: Sequence alignment of the lines *cr_nat-iaa14_40.3*, *cr_nat-iaa14_3.1*, *cr_nat-iaa14_8.8* and *cr_nat-iaa14_14.5* compared to the Col-0 sequence.

Cleavage of gRNA1 and 4 resulted in an 1884 bp (*cr_nat-iaa14_40.3*) and 1910 bp (*cr_nat-iaa14_14.5*) deletion, whereas the combination of gRNA1 and 5 led to a 2104 bp (*cr_nat-iaa14_3.1*) and 2109 bp (*cr_nat-iaa14_8.8*) deletion. n (A, T, G, C) represents the nucleotides that were deleted [-] by the gRNA-mediated genome editing. The promoter is indicated in italics.



Supplemental Figure 11.21: NAT-IAA14 knockout has no effect on IAA14 transcript levels in older plants.

The transcript level of NAT-IAA14 is shown in 29 day old Col-0 and *cr_iaa14_14.5* and *cr_iaa14_3.1* plants. qRT-PCR results were normalized by PP2A and values correspond to averages with SD from three experiments. (Student's t-test: * ≤ 0.05 ; n.s. = not significant)

```

Col-0          AGACATATATAGACAGCAAGAAGAGATATGAACCTTAAGGAGACGGAGCTTTGTCTTGGC
cr_iaa14_46.7 AGACATATATAGACAGCAAGAAGA-----CGGAGCTTTGTCTTGGC
cr_iaa14_46.6 AGACATATATAGAC-----AGACGGAGCTTTGTCTTGGC
cr_iaa14_46.8 AGACATATATAGAC-----AGACGGAGCTTTGTCTTGGC
cr_iaa14_46.9 AGACATATATAGAC-----AGACGGAGCTTTGTCTTGGC
*****
*****

```

Supplemental Figure 11.22: Sequence alignment of *cr_iaa14_46.7* and *cr_iaa14_46.6/8/9*.

The sequence alignment of *cr_iaa14_46.7* with a 19 bp deletion and *cr_iaa14_46.6*, *46.8* and *46.9* with a 30 bp deletion is depicted. The 5' UTR is indicated in gray. The CLUSTALW program was used for sequence alignment.


```

Col-0          ACATATTCTGATTTAAGACATATATAGACAGCAAGAAGAGATATGAACCTTAAGGAGACG
cr_iaa14_29.6 ACATATTCTGATTTAAGACATATATAGACAGCAAGAAGAGATATGAACCTTAAGG-----
cr_iaa14_8.5   ACATATTCTGATTTAAGACATATATAGACAGCAAGAAGAGATATGAACCTTAAGG-----
                *****

Col-0          GAGCTTTGTCTTGGCCTCCCCGGAGGCACTGAAACCGTTGAAAGTCCGGCCAAGTCGGGT
cr_iaa14_29.6 -----
cr_iaa14_8.5   -----

Col-0          GTTGGGAACAAGAGAGGCTTCTCCGAGACCGTTGATCTCAAACCTAATCTTCAATCTAAC
cr_iaa14_29.6 -----
cr_iaa14_8.5   -----

Col-0          AAACAAGGACATGTGGATCTCAACACTAATGGAGCTCCCAAGGAGAAGACCTTCCTTAAA
cr_iaa14_29.6 -----
cr_iaa14_8.5   -----

Col-0          GACCCTTCTAAGCCTCCTGCTAAGTAAGTCTATTTACACAATTCCTTAAGAAGAAGACC
cr_iaa14_29.6 -----
cr_iaa14_8.5   -----

Col-0          TTCCTTAAAAGGGAAGACTTTTTTTTTTTTTTTTTTTGAGATAAAAAGACTAATAGTTGATA
cr_iaa14_29.6 -----
cr_iaa14_8.5   -----

Col-0          TAAAAGTTCTTAAAATACATATATATGAAAGATGTAAGGATGCATAAGTAATAACGTTAT
cr_iaa14_29.6 -----
cr_iaa14_8.5   -----

Col-0          TGAATGTGTGTGTGTGTTTATATTCTATGCAGAGCACAAAGTGGTGGGTGGCCACCGG
cr_iaa14_29.6 -----
cr_iaa14_8.5   -----

Col-0          TGAGGAACTACCGGAAAAATGTTATGGCTAATCAGAAGAGCGGCGAAGCAGAGGAGGCAA
cr_iaa14_29.6 -----TTTCC-A
cr_iaa14_8.5   -----CAGAGGAGGCAA
                * *

Col-0          TGAGTAGTGGTGGAGGAACCGTCGCCTTTGTGAAGGTTTCCATGGATGGAGCTCCTTATC
cr_iaa14_29.6 TG-GTAGTGGTGGAGGAACCGTCGCCTTTGTGAAGGTTTCCATGGATGGAGCTCCTTATC
cr_iaa14_8.5   TGAGTAGTGGTGGAGGAACCGTCGCCTTTGTGAAGGTTTCCATGGATGGAGCTCCTTATC
                ** *****

```

Supplemental Figure 11.23: Sequence alignment of *cr_iaa14_29.6* and *cr_iaa14_8.5*.

The sequence comparison from *cr_iaa14_29.6* (485 bp deletion) and *cr_iaa14_8.5* (473 bp deletion) with Col-0 are shown in A). The 5' UTR is indicated in gray and the first intron of *IAA14* is indicated in italics. Nucleotides added or removed by the DNA repair mechanism are highlighted in red. The CLUSTALW program was used for sequence alignment.

```

                                domain I
Col-0      MNLKETTELCLGLPGGTETVESPAKSGVGNKRGFSETVDLKLNLQSNKQGHVDL
cr_iaa14_46.7 -----
cr_iaa14_8.5 MNLKET-----
cr_iaa14_29.6 MNLKEISMVVVEEPSPL*-----
cr_iaa14_46.6/8/9 MQTFAHNERIRSNWTCSSKSNGEVQEQIMNKKKRGQYALIFFWYCYDHFVLI*

                                domain II
Col-0      NTNGPKEKTFCLKDPSKPPAKAQVVGWPPVRNYRKNVNMANQKSGEAEEMSSGG
cr_iaa14_46.7 -----MANQKSGEAEEMSSGG
cr_iaa14_8.5 -----EEAMSSGG
cr_iaa14_29.6 -----
cr_iaa14_46.6/8/9 -----

                                domain III
Col-0      GTVAFVKVSMDGAPYLRKVDLKMYSYKDLSDALAKMFSSFTMGSYGAQGMID
cr_iaa14_46.7 GTVAFVKVSMDGAPYLKVDLKMYSYKDLSDALAKMFSSFTMGSYGAQGMID
cr_iaa14_8.5 GTVAFVKVSMDGAPYLKVDLKMYSYKDLSDALAKMFSSFTMGSYGAQGMID
cr_iaa14_29.6 -----
cr_iaa14_46.6/8/9 -----

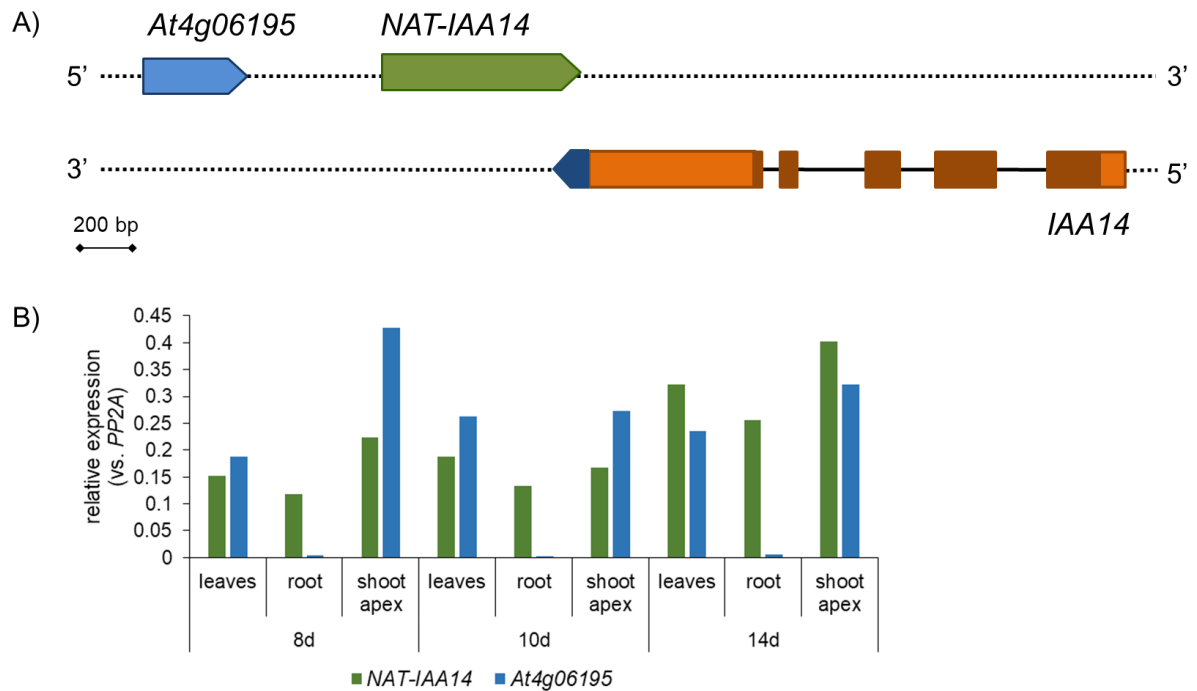
                                domain IV
Col-0      FMNESKVMDLLNSSEYVPSYEDKDGDWMLVGDVPWPMFVESCKRLRIMKGSEA
cr_iaa14_46.7 FMNESKVMDLLNSSEYVPSYEDKDGDWMLVGDVPWPMFVESCKRLRIMKGSEA
cr_iaa14_8.5 FMNESKVMDLLNSSEYVPSYEDKDGDWMLVGDVPWPMFVESCKRLRIMKGSEA
cr_iaa14_29.6 -----
cr_iaa14_46.6/8/9 -----

Col-0      IGLAPRAMEKFKNRS*
cr_iaa14_46.7 IGLAPRAMEKFKNRS*
cr_iaa14_8.5 IGLAPRAMEKFKNRS*
cr_iaa14_29.6 -----
cr_iaa14_46.6/8/9 -----

```

Supplemental Figure 11.24: Protein sequence alignment of *cr_iaa14* transgenic lines.

The protein sequence comparison of the *cr_iaa14* lines with Col-0 are shown and amino acids that differ from the original IAA14 sequence are highlighted in red. *In silico* translation suggests no functional IAA14 protein. The positions of the protein domains of IAA14 are indicated. Stop codons are shown as asterisk. The sequence alignment was performed by the CLUSTALW program.



Supplemental Figure 11.25: Expression pattern of the long non-coding RNA encoded by *At4g06195* compared to *NAT-IAA14* transcript levels in Col-0.

The genomic organization of the other RNA (blue, *At4g06195*), *NAT-IAA14* (green) and *IAA14* (brown: exons, orange: UTRs, dark-blue: 124 nt-longer 3'UTR) is shown in the schematic representation (A). The black line displays *IAA14* introns and the dotted line DNA strands. Leaves, roots and shoot apices were collected from 8 d, 10 d and 14 d old Col-0 seedlings grown in long-day conditions (B). qRT-PCR results of *NAT-IAA14* (green) and *At4g06195* (blue) were normalized by *PP2A* and values correspond to one representative experiment of two independent experiments.

11.2 Supplementary Tables

Supplementary Table 11.1: List of used primers

primer	Sequence (5'→3')	description
RR25	GCTGATTACAACATCCAGAAGG	<i>TUQG3</i> forward qPCR primer, <i>N. benthamiana</i>
RR26	TGCAACACAGCAAGCTTAACC	<i>TUQG3</i> reverse qPCR primer, <i>N. benthamiana</i>
RR69	GTTCCCCTCTTATCAAACCTTCACCC	<i>IAA14</i> forward PCR primer (5'UTR), CRISPR/Cas9 analysis (use with RR240)
RR70	GGGCACATTAGCATGAAGAGGAT	<i>IAA14</i> reverse PCR primer (annotated 3'end)/ forward primer probe_2 (RNase protection assay)
RR72	CCCGGCATATGTATTTTACCCC	<i>IAA14</i> reverse PCR primer (124 nt-longer 3'end), circular 5' and 3'RACE 2 nd PCR (use with RR202)
RR74	TTTCAGTAAAAATTAAGATTTTCAT	<i>NAT-IAA14</i> reverse PCR primer, CRISPR/Cas9 sequencing (use with RR625)
RR76	AATACGTTATTAATTCAGGACC	reverse primer RNA_1 (RNase protection assay)
RR79	AAGTTTTGGATCAGTTTTAATATG	<i>NAT-IAA14</i> forward PCR primer, circular 5' and 3'RACE 1 st PCR (use with RR148)
RR85	TCATCCTTGCGCAGGGGCCA	Oligo for <i>U6</i> detection
RR86	CACCATGAACCTTAAGGAGACGG	<i>IAA14</i> forward PCR primer (ATG), TOPO cloning
RR109	GGTTAGGGTGTTACTTTTTTCA	<i>prom_{NAT-IAA14}</i> forward PCR primer, CRISPR/Cas9 sequencing (use with RR227)
RR146	AGCCATAACATTTTTCCGGTAGTT	<i>IAA14</i> reverse PCR primer, circular 5'RACE 2 nd PCR and 3'RACE 2 nd PCR (use with RR228/RR464)
RR147	GGAAGCGAGGTTTCTTTACTTTCT	<i>NAT-IAA14</i> forward qPCR primer
RR148	GTAAAAACAAGCAGCAAATCCC	<i>NAT-IAA14</i> reverse qPCR primer, circular 5' and 3'RACE cDNA synthesis and 1 st PCR (use with RR79)
RR200	GTTCTCCACCACTACTCATTGCC	<i>IAA14</i> reverse PCR primer, circular 5' and 3'RACE 1 st PCR (use with RR241/RR224)
RR201	CCGCCGCTGCCTAAGATTA	<i>NAT-IAA14</i> forward PCR primer
RR202	ATCATACCAAACAAAAAGAAATCAAA	<i>NAT-IAA14</i> reverse PCR primer, circular 5' and 3'RACE 2 nd PCR (use with RR72)
RR224	CAAGAGCAATGGAGAAGTTCAAG	<i>IAA14</i> forward PCR primer, circular 3'RACE 1 st PCR (use with RR224)
RR225	TTTCCTTTGGGTCTTCGGGTGTTGG	forward primer probe_1 (RNase protection assay)
RR227	AAATTCAGGACCCATGAGAGGCG	<i>NAT-IAA14</i> reverse PCR primer (CRISPR/Cas9 sequencing (use with RR109)
RR228	CGTTTGCGCATAATGAAAGGATCC	<i>IAA14</i> reverse PCR primer, circular 5'RACE 2 nd PCR (use with RR146)
RR229	CTTGAATTCTCCATTGCTCTTGG	<i>IAA14</i> reverse qPCR primer (use with RR273)
RR233	GTGCAACGCCTTAGATGCATA	Oligo for amiRNA1 <i>NAT-IAA14</i> detection

RR234	ACGCGCCGGCTTAACTTCTGA	Oligo for amiRNA2 <i>NAT-IAA14</i> detection
RR235	GTGTAGTTCTGGTCGTTCCAA	Oligo for amiRNA3 <i>NAT-IAA14</i> detection
RR240	GATCCATCACTTTACTCTCGTTC	<i>IAA14</i> reverse PCR primer (CRISPR/Cas9 sequencing (use with RR69))
RR241	GAAGGTTTCCATGGATGGAGC	<i>IAA14</i> reverse PCR primer, circular 5'RACE 1 st PCR (use with RR200)
RR251	TGTAAAACGACGGCCAGT	M13 uni (-21) sequencing primer for colony PCR
RR252	CAGGAAACAGCTATGACC	M13 rev (-29) sequencing primer for colony PCR
RR267	CTCGACAAACATCGGCCAGGGGAC	<i>IAA14</i> reverse cDNA synthesis primer, circular 3'RACE
RR273	GTCCCCTGGCCGATGTTTGTGCGAG	<i>IAA14</i> forward qPCR primer (use with RR229)
RR277	GTGATCAATAAAGACATTACTTAGAC	reverse primer binding 70 nt downstream of the <i>NAT-IAA14</i> 3'end (RNase protection assay)
RR280	CTGTAAAATATTAATAAAGAAGGAAAA ATG	forward primer binding 68 nt upstream of the <i>NAT-IAA14</i> 5'end (RNase protection assay)
RR281	CCAACACCCGAAGACCCAAAGGAAA	forward <i>NAT-IAA14</i> PCR primer (RNase protection assay)
RR282	GAGTTTCCTCATTCTTCTTGCTTTC	forward <i>IAA14</i> PCR primer (4 th intron, RNase protection assay)
RR316	TTGGTGACAACAGGTCAAGCA	<i>GAPDH</i> (<i>At1g13440</i>) forward qPCR primer
RR317	GATTGCATTGAGCGACAAGTTT	<i>GAPDH</i> (<i>At1g13440</i>) reverse qPCR primer
RR319	GTAGGGATTCCATGCACTACAGC	<i>NAT-IAA14</i> reverse PCR primer
RR372	GGGGTAAAATACATATGCCGGG	<i>NAT-IAA14</i> reverse qPCR primer (CRISPR/Cas9 transgenic lines)
RR464	CTTTCAAATTCAGTCCATCCTCTTC	<i>IAA14</i> forward PCR primer, circular 3'RACE 2 nd PCR (use with RR146)
RR465	GTCTCTTAAAATAAAGCTCTATG	<i>NAT-IAA14</i> forward PCR primer (use with RR148)
RR478	TGCAACCTCCTCAAGTTCGATT	<i>UBC10</i> (<i>At5g25760</i>) forward qPCR primer, NMD gene for normalization
RR479	CAAGCAGGACTCCAAGCATTCTTCA	<i>UBC10</i> (<i>At5g25760</i>) reverse qPCR primer, NMD gene for normalization
RR480	GCTTTTTTATAGAGAACATAGAGC	<i>NAT-IAA14</i> reverse PCR primer (circular 3'RACE)
RR535	GGGTAATACGACTCACTATAGGTTTC CTTTGGGTCTTCGGGTGTTGG	forward primer RNA_1 (RNase protection assay)
RR536	GGGTAATACGACTCACTATAGGAATA CGTTATTAATTCAGGACC	reverse primer probe_1 (RNase protection assay)
RR537	GGGTAATACGACTCACTATAGGGGGC ACATTAGCATGAAGAGGAT	forward primer RNA_2 (RNase protection assay)
RR538	GTAATTGTGATAGTAAATCTATAG	reverse primer RNA_2 (RNase protection assay)
RR539	GGGTAATACGACTCACTATAGGGTAA TTGTGATAGTAAATCTATAG	reverse primer probe_2 (RNase protection assay)
RR563	TCTTCTTACCGTAAACGGCG	forward left primer T-DNA Insertion of <i>NAT-IAA14</i> (<i>SALK_113294</i>)

RR564	CGAAGCTGGAAAAGAGTTGTG	reverse right primer T-DNA Insertion of <i>NAT-IAA14</i> (SALK_113294, SALK_118398, SALK_012231)
RR565	AGACAAACCAACACCCGAAG	forward left primer T-DNA Insertion of <i>NAT-IAA14</i> (SALK_118398, SALK_012231)
RR574	CAAGTCGGTTCATCGCCAAATTGGG	<i>EXPANSIN L1</i> (At3g45970) forward qPCR primer (RNA stability assay)
RR575	GTATCCACCGTTACTACGAACCTG	<i>EXPANSIN L1</i> (At3g45970) reverse qPCR primer (RNA stability assay)
RR576	GGCGTAAGGTTGATTGGCTCAC	<i>EIF4A1</i> (At3g13920) forward qPCR primer (RNA stability assay)
RR577	GATGAGAACACGGGAGGAACCAG	<i>EIF4A1</i> (At3g13920) reverse qPCR primer (RNA stability assay)
RR625	GTGGCGTTGTGGATGCATGTGG	<i>promoter_{NAT-IAA14}</i> forward PCR primer, CRISPR/Cas9 sequencing (use with RR74)
RR641	TACAGCTAGTGCTTCTTCCATCG	other lncRNA (At4g06195) upstream <i>NAT-IAA14</i> forward qPCR primer
RR642	CGCTCTACTACAAAGTTCTCAATG	other lncRNA (At4g06195) upstream <i>NAT-IAA14</i> reverse qPCR primer
RR646	GCACACAAGCTATTTATTTGACACACC	Cas9 reverse PCR primer
RR656	GGTGAGATCGTGTGGGATAAGG	Cas9 forward PCR primer
RR668	TTGAAGACATCTCATACTAATCACTTT TGATTTGTCTCGAGATGTCTTCAA	Golden gate cloning for the linker region between <i>AlcA</i> promoter and <i>NAT-IAA14</i> , forward primer
RR669	TTGAAGACATCTCGAGACAAATCAAAA GTGATTAGTATGAGATGTCTTCAA	Golden gate cloning for the linker region between <i>AlcA</i> promoter and <i>NAT-IAA14</i> , reverse primer
RR670	TTGGTCTCAACATCTCAGGAGCTTTGA ATGGATCTCTAATCTCAGATCTATATT TTG	Golden gate cloning for <i>prom_{IAA14}::IAA14</i> construct, forward primer
RR702	TTGAAGACATCTCACTGAAAAACGCT CGAGATGTCTTCAA	Golden gate cloning for <i>NAT-IAA14</i> 3'end, forward primer
RR703	TTGAAGACATCTCGAGCGTTTTTTCAG TGAGATGTCTTCAA	Golden gate cloning for <i>NAT-IAA14</i> 3'end, reverse primer
RR709	ATGGTGAGCAAGGGCGAGG	<i>mCherry</i> forward qPCR primer (transient co-expression assay)
RR718	CCACCCTTGGTCACCTTCAG	<i>mCherry</i> reverse qPCR primer (transient co-expression assay)
RR785	TTGAAGACATCTCAGGAGAATCACTTT TGATTTGTCTCGAGATGTCTTCAA	Golden gate cloning for the linker region between vector and <i>NAT-IAA14</i> , forward primer
RR786	TTGAAGACATCTCGAGACAAATCAAAA GTGATTCTCCTGAGATGTCTTCAA	Golden gate cloning for the linker region between vector and <i>NAT-IAA14</i> , reverse primer
RR823	GTGATAAGTTTGGGAAGTTTTGG	<i>NAT-IAA14</i> forward qPCR primer (use with RR372)
DM195	AGCCAACTAGGACGGATCTGGT	<i>PP2A</i> forward qRT primer
DM196	GCTATCCGAACCTTCTGCCTCATTA	<i>PP2A</i> reverse qRT primer

12 Acknowledgements

This work would not have been possible without the invaluable support of so many people, to whom I would like to say a heartfelt thank you.

The completion of my dissertation would not have been possible without the support and nurturing of Dr. Selma Gago Zachert, who supervised me with great dedication. With her patience, perseverance, always new ideas and deep understanding about the topic, she provided me the knowledge, skills and confidence and prepared me excellently to excel in this field. I greatly appreciate the countless hours of discussion with her and I am forever thankful to have been her doctoral student.

Furthermore, I would like to thank Prof. Dr. Sven-Erik Behrens for the numerous suggestions and ideas to further advance my project. His support especially in my countless presentations helped to build up my confidence level. In addition, I would like to thank him for reviewing my PhD thesis.

I would also like to thank the whole department "Molecular Signal Processing" headed by Prof. Dr. Steffen Abel, whom I would like to thank for reviewing my doctoral thesis. Especially I would like to thank the members of our research group Dr. Ammar Mousa Jaber, Dr. Shiv Kumar Meena and Katja Baumann-Kaschig for the great working atmosphere and the stimulating and productive discussions. I would also like to thank the former group members Katja Seidel and Dr. Maria Pogoda for their pioneering work, which was essential for my doctoral thesis. I would like to extend my sincere thanks to the Bachelor students Alexis Bantle, Julia Beimdiek and Daniela Hübner for their contributions to my work.

Thanks should also go to the GRK 1591 for the mentoring and financial support. The scientific input from excellent researchers along with the retreats provided an ideal atmosphere to develop as a scientist. Special thanks to Prof. Dr. Ulla Bonas for being part of my thesis committee and for her constructive criticism on my project.

Last but not least I thank my family for their support, understanding, time and love without which it would not have been possible to complete this work. Above all, I would like to thank my husband Martin, who always motivated me to finish my thesis, helped me to focus on what really counts and gave me all the time I needed to do so. The greatest gift was our son Jonas, whom he took care of so lovingly while I was writing. Additionally, I would like to thank my parents for the opportunity and support during my biochemistry studies and doctorate. Many thanks also to my mother-in-law, who took care of our son so often during the pandemic so that I had time to write my doctoral thesis.

THANK YOU!

13 Curriculum vitae

Name: Susanne Engelmann, née Höpfner
Date of Birth: May 16, 1990
Birthplace: Karl-Marx-Stadt, now Chemnitz
Nationality: German

Education

11/2014 – 10/2020 Martin Luther University Halle-Wittenberg/ Leibniz Institute of Plant Biochemistry - Halle (Saale), Germany
PhD student

10/2012 – 09/2014 Martin Luther University Halle-Wittenberg - Halle (Saale), Germany
Master of Science (final grade 1.4), MA Biochemistry (120 LP)

10/2009 - 09/2012 Martin Luther University Halle-Wittenberg - Halle (Saale), Germany
Bachelor of Science (final grade 2.1), BA Biochemistry (180 LP)

Work experience

since 11/2020 IPDx Immunoprofiling Diagnostics GmbH – Leipzig, Germany
Research Scientist

07, 11 - 12/2013 Martin Luther University Halle-Wittenberg - Halle (Saale), Germany
Research Assistant

10/2011 - 11/2011 Martin Luther University Halle-Wittenberg - Halle (Saale), Germany
Research Assistant

Fellowships

11/2014 – 06/2019 Graduate Fellow – German Research Foundation (GRK1519)

Publication

Friedrich S, **Engelmann S**, Schmidt T, Szczepankiewicz G, Bergs S, Liebert UG, Kümmerer BM, Golbik R, Behrens SK: „*The Host Factor AUF1 p45 Supports Flavivirus Propagation by Triggering the RNA Switch Required for Viral Genome Cyclization*“ (J Virol. 2018 Feb 26;92(6):e01647-17. doi: 10.1128/JVI.01647-17)

Skills and Activities

05/2017 - 08/2017 Deutscher Akademischer Ausstauschdienst, Research Internships in Science and Engineering
Supervision of the internship of Alexis Bantle, University of South Carolina, Columbia, USA

Languages: German (Native), English

14 Statutory Declaration

Hiermit erkläre ich an Eides statt, dass ich mich mit der vorliegenden wissenschaftlichen Arbeit erstmals um die Erlangung des Doktorgrades bewerbe, die Arbeit selbständig und ohne fremde Hilfe verfasst, nur die angegebenen Quellen und Hilfsmittel genutzt und die den benutzten Werken wörtlich oder inhaltlich entnommenen Stellen als solche kenntlich gemacht habe.

Halle (Saale), den _____

Susanne Engelmann